Computational strategies in flame-spread modelling involving wooden surfaces

Carlsson, Jörgen

2003

Computational strategies in flame-spread modelling involving wooden surfaces

-An evaluation study

Jörgen Carlsson

Department of Fire Safety Engineering
Lund University, Sweden

Brandteknik
Lunds tekniska högskola
Lunds universitet

Report 1028, Lund 2003

Computational strategies in flame-spread modelling involving wooden surfaces
- An evaluation study

Jörgen Carlsson

Lund 2003

Computational strategies in flame-spread modelling – An evaluation study

Jörgen Carlsson

Report 1028
ISSN: 1402-3504
ISRN: LUTVDG/TVBB--1028--SE

Number of pages: 129
Illustrations: Jörgen Carlsson

Keywords
Computational Fluid Dynamics, CFD, flame spread, fire growth, fire modelling, pyrolysis modelling, computational methods

Sökord
CFD, flamspridning, brandtillväxt, brandmodellering, pyrolysmodellering

Abstract
Various approaches to flame-spread and fire-growth modelling are discussed and are evaluated using experimental results from different tests. Use of Computational Fluid Dynamics, CFD, in fire modelling is discussed and the performance of different CFD codes in wall flow modelling is analysed. Different pyrolysis models are discussed with respect to their major assumptions and the input data required.

Brandteknik
Lunds tekniska högskola
Lunds universitet
Box 118
221 00 Lund

brand@brand.lth.se
http://www.brand.lth.se

Telefon: 046 - 222 73 60
Telefax: 046 - 222 46 12

Department of Fire Safety Engineering
Lund University
P.O. Box 118
SE-221 00 Lund
Sweden

brand@brand.lth.se
http://www.brand.lth.se/english

Telephone: +46 46 222 73 60
Fax: +46 46 222 46 12

Summary

Flame spread is governed by heat transfer to a surface and the subsequent thermal response or behaviour of the material. The heat exposure that occurs results in the release of combustible pyrolysis gases. As heat accumulates within the material, the rate at which combustible gases are released eventually becomes sufficiently high to produce a flammable mixture in the boundary layer, which can either ignite spontaneously, if the temperature is high enough or be ignited by a pilot flame. This rather complex phenomenon, including the boundary layer interaction between a fluid and a solid phase and the thermal degradation of the material, has been studied in varying detail ever since the late 1960s, both experimental and theoretical work in this area having been presented frequently ever since.

Traditionally, most of the work on engineering flame-spread calculations considers empirical relationships in certain well-known scenarios and includes specific “tuning” parameters that need to be correlated for optimum performance in the scenario of interest to be achieved. Although models of this sort have played an important role in obtaining an understanding of the course of flame spread and can be useful for comparative purposes, it is difficult, if indeed possible at all, to use them in arbitrary end scenarios without prior knowledge of the results. Due to the lack of generality and flexibility of models of this type, they are not very useful as tools in fire safety engineering.

One well-known analytical stand-alone flame-spread model is considered in theoretical terms, the input parameters required being discussed. The model is employed in two different scenarios to demonstrate the basic techniques involved. From this study the model is shown to have significant dependencies on the input data.

The alternative to stand-alone analytical models seems to be one based upon Computational Fluid Dynamics, CFD. CFD techniques, basically described by a set of numerical approaches used in solving flow-governing partial differential equations, have long been used in research and in many engineering disciplines, several general-purpose codes being commercially available today. Also, a number of CFD codes have been developed and specifically adapted to the simulation of fire (or, perhaps more adequately, of buoyancy controlled turbulent reacting flows). The large number of control volumes needed and the complexity of the calculations make simulations using CFD a costly process in terms of time and computer power. In the final analysis, the capabilities and the accuracy attained in CFD modelling is a matter of what the modeller is prepared to sacrifice in terms of computational time.

Many factors contribute to making CFD simulation of fire a great challenge. Use of the popular k-ε turbulence closure model, for example, is known to create uncertainty in simulation results for a turbulent flow field, easily producing errors regarding the entrainment of air into the fire plume through overestimating the entrainment of air in horizontal flows and underestimating it in the vertical plume. Also, although approximating the boundary layer close to walls by use of semi-empirical wall-functions applied on the near-wall nodes makes it possible to avoid integrating the flow equations through the boundary layer it may nevertheless add uncertainty to the results. The validity of the wall functions for assessing buoyant reacting flows is also far from certain. In addition, since the output of the k-ε model controls the most commonly used combustion model, the Eddy Dissipation Concept, EDC, through the assumption that “mixed is burnt”, one cannot take

for granted that a simulation using these solution methods will behave perfectly in close proximity to the flame.

Despite its current flaws, Computational Fluid Dynamics opens up new possibilities to flame-spread modellers. Pyrolysis models describing the thermal response of a material exposed to some given net heat flux can be applied to each computational cell in the solid phase and be solved simultaneously so as to interact with the fluid flow. It should be emphasised that the material models that are coupled to different CFD codes do not necessarily involve more physics, nor greater computational complexity than the earlier stand-alone models, but they are all designed to take advantage of the output the general CFD program provides.

On the basis of systematic CFD simulations, it was shown that the heat flux from the flame and from hot fire gases is clearly dependent upon several computational assumptions, such as grid resolution and numerical scheme. On the other hand, predictions of gas temperature showed less sensitivity to variations in the computational conditions than heat-flux predictions did. It was also noted that different CFD codes based upon the same general principles and model equations showed appreciable variation in the results they provided.

Four different pyrolysis models of varying sophistication and complexity were discussed and evaluated. The models were first evaluated on stand-alone basis in terms of a level of heat flux specified by the user, the results being compared with corresponding Cone Calorimeter measurements. This procedure provides a measure of the consistency of the computational results as compared with experiments using cone fluxes of differing magnitude. It can also provide assistance in obtaining input data or determining how reasonable such data is before its being used in large scale modelling, in which the pyrolysis model is implemented in its original CFD environment. Simulations of two large-scale tests of differing geometry representing a challenge to the overall models, were likewise performed. It was concluded that none of the models were able to provide adequate and consistent predictions of the resulting flame spread and fire growth for the two scenarios. In comparing the measured and the computed incident heat flux it appeared that the of best-fit correlations with results obtained in the Cone Calorimeter involved certain inadequacies.

Sammanfattning (Summary in Swedish)

Flamspridning styrs av nettotransporten av värme mot brännbara ytor och den termiska reaktion från det exponerade materialet som följer. När ett brännbart material utsätts för en hög värmebelastning bryts det ned och avger brännbara gaser i en process som kallas pyrolys. Om värmepåverkan är tillräckligt hög kan en brännbar koncentration uppstå vid ytan och antändning kan ske, antingen genom en pilotlåga eller, om temperaturen i gaserna blir tillräckligt hög, genom självantändning. Processen med successiv värmetransport, termisk nedbrytning och antändning sammanfattar flamspridningens hörnstenar och har sedan mitten av förra seklet varit föremål för ett stort antal brandforskare som under åren producerat ett flertal både teoretiska och experimentella studier. Få, om några, av de modeller som föreslagits har emellertid använts utanför den ursprungliga forskningsmiljön.

Flera studier har riktat in sig på fristående flamspridningsmodeller avsedda att användas i ett ingenjörsmässigt sammanhang. Dessa modeller bygger traditionellt på ett antal empiriska samband som anpassas till något eller några enskilda scenarier. Tillämpning inom andra scenarier än det eller de som ursprungligen avsågs är här inte generellt möjlig även om viss parameteroptimering kan vara utförbar. Detta skulle emellertid kräva att resultatet var känt redan innan beräkningen. Även om denna typ av modeller har spelat en stor roll för att öka förståelsen för flamspridning och även om de har ett användningsområde inom vissa jämförande beräkningar är de på grund av bristen på flexibilitet och generaliserbarhet inte särskilt användbara inom ramen för brandteknisk dimensionering.

En välkänd fristående flamspridningsmodell av detta slag har studerats och diskuteras i rapporten. Nödvändig indata och hur denna kan erhållas diskuteras och två olika beräkningsexempel presenteras för att visa på de tekniker som används. Studien visar också på modellens känslighet med avseende på indata.

Flamspridningsberäkningar baserade på en lösning av flödesfältet med hjälp av en CFD kod, Computational Fluid Dynamics, framstår som det alternativ som erbjuder de bästa möjligheterna till att utföra generella flamspridningsberäkningar. CFD kan i princip beskrivas som ett antal numeriska metoder vilka används i syfte att lösa de partiella differentialekvationer som antas beskriva olika flöden. Flera kommersiella koder finns tillgängliga på marknaden och det finns även ett antal gratiskoder som utvecklats speciellt för att simulera konsekvenserna av brand. Beräkningarnas komplexitet tillsammans med det stora antal kontrollvolymer som krävs för storskalig användning av CFD gör metodiken kostnadskrävande i termer av tid och datorkraft. Simuleringarnas prediktiva förmåga är därför nära kopplat till vad modelleraren är beredd att investera i beräkningstid.

Ett flertal faktorer bidrar till att göra CFD-simuleringar av brand en stor utmaning. Flera av de mest populära modellerna är behäftade med osäkerheter som i många fall kan vara svåra att utvärdera. Den mest populära turbulensmodellen, k-ε, är bland annat känd för att ha problem med att korrekt simulera inflödet av luft i en brandplym. Modellens begränsade giltighet i gränsskiktet nära väggar innebär vidare att semiempiriska randvillkor måste tillämpas för att utvärdera det konvektiva flödet, vilket bidrar till osäkerheterna framförallt vad avser värmetransporten till ytan. Osäkerheterna från beräkningarna med k-ε modellen kommer också att påverka EDC-förbränningsmodellen (Eddy Dissipation Concept) genom antagandet att bränsle och syre inte kan existera samtidigt. Det finns därför ingen anledning

att förvänta sig att en CFD modell som bygger på dessa antaganden ger felfria resultat, framför allt inte i flamman och dess direkta närhet.

Oavsett de osäkerheter som för närvarande är en del av CFD simuleringen, öppnar beräkningskonceptet nya möjligheter för beräkning av flamspridning. Som en komplettering av flödesberäkningen kan olika modeller för termisk nedbrytning, pyrolysmodeller, länkas till varje kontrollvolym av en solidgrid (separat eller som en integrerad del av fluidgriden) och på så sätt interagera med gasflödet. Dessa pyrolysmodeller är inte nödvändigtvis mer sofistikerade än de tidigare fristående modellerna, men de har alla utvecklats för att dra fördel av den information som erhålls från CFD beräkningarna.

Systematiska CFD beräkningar har utförts för att utvärdera modellernas förmåga att göra beräkningar på värmeflöde mot en yta och temperaturer i brandplymen. Slutsatserna från denna utvärdering är att resultaten avseende värmeflöde, konvektion och strålning, påverkas märkbart av olika antaganden och indata såsom gridstorlek och val av numeriskt schema. Temperaturen i brandplymen visade däremot mindre känslighet när dessa beräkningsförhållanden ändrades. Det noteras också att olika CFD koder ger olika resultat i samma scenario.

Fyra olika pyrolysmodeller med olika grad av komplexitet diskuteras och utvärderas både fristående, mot resultat från konkalorimetern, och som en del av sin ursprungliga CFD miljö. Genom att pyrolysmodellen extraheras från CFD koden och används fristående kan resultat från konkalorimetern användas för att härleda materialspecifik indata till modellen och även utvärdera hur konsekvent antändning och effektutveckling beräknas för de olika värmeflöden som använts vid experimenten. Två olika fullskaleförsök simuleras med indata som härletts från konkalorimetern. Den allmänna slutsatsen från genomförda simuleringar är att ingen av de använda modellerna predikterar flamspridning och brandtillväxt konsekvent mellan de olika scenarierna.

Nomenclature

Attention should be directed briefly at a number of basic terms and concepts that are employed here. In referring to a "flame spread model" it is the overall, comprehensive model that is meant, including submodels for the calculation of fluid flow, combustion and different heat transfer mechanisms, as well as routines for modelling the thermal breakdown of the solid material. The latter are generally referred to as material or pyrolysis models.

Throughout the report, the term flame spread is associated with the continuous movement of an ignition front, or pyrolysis zone, over a surface plane whereas fire growth concerns the increase in heat release rate that arises as a consequence of the flame spread. Flame spread by scattering or the movement of burning solid material is not taken up here because of its random origin and occurrence.

The term "wall-adjacent node" has been used in connection with CFD calculations referring to the control volume closest to a wall surface.

The following nomenclature has been employed:

c_p	specific heat capacity at constant pressure,
h	enthalpy,
k	turbulent kinetic energy or conductivity,
k_a	gas absorption coefficient,
k_s	scattering coefficient,
l	turbulent mixing length,
m	mass,
p	pressure,
s	stoichiometric oxygen to fuel mass ratio,
t	time,
t_{0-}	moment just before time = 0,
t_{0+}	moment just after time = 0,
t_p	dummy variable of integration,
u, v, w	gas velocity in x- y- and z- direction respectively,
u_{char}	characteristic velocity,
u_i	gas velocity in x_i direction,
x, y, z	room co-ordinates,
x_{char}	characteristic length scale of flow,
y_{flame}	height of flame,
y_{py}	height of pyrolysis front,
$y_{py,0}$	initial height of pyrolysis front,
y^+	dimensionless distance between near wall node and wall surface which also could be viewed upon as a Reynolds number based on friction velocity

A	Arrhenius pre-exponential factor for a chemical reaction,
D	mass diffusion coefficient,
E	total emissive power,
E_a	activation energy,
E_g	emissive power for a gas with temperature T_g,
H_r	heat of reaction,
H_g	heat of gasification,
H_{py}	heat of pyrolysis,
I	radiant intensity,

K	constant in non-linear flame length correlation,
M_i	molar mass for species *i*,
P	shear stress term in equation in the k-ε turbulence model,
R	ideal gas constant,
R_f	flux Richardson number,
R_{fu}	rate of reaction,
T	temperature,
W	width of flame,
Y_α	mass fraction of species α,
β	Shvab-Zeldovic function or thermal expansion coefficient in the k-ε turbulence model,
Γ_ϕ	turbulent diffusivity for ϕ,
δ	Kronecker's delta also known as the identity tensor,
ε	viscous dissipation rate of turbulent kinetic energy or surface emissivity,
ξ	mixture fraction,
μ	dynamic viscosity,
μ_t	turbulent (or eddy) viscosity,
ν	kinematic viscosity,
ν_i	stoichiometric coefficient for species i,
ρ	density,
σ	Stefan Boltzmann constant,
σ_t	turbulent Prandtl number,
τ_{ij}	stress tensor due to surface forces (pressure and viscosity),
ϕ	symbol for an arbitrarily scalar,
Ω	arbitrarily volume in space,

Superscripts

$'$	Reynolds averaged fluctuating variable,
$''$	Favre averaged fluctuating variable,
$\cdot$	time derivate,
–	Reynolds, or time, average,
~	Favre, or density weighted, average.

Subscripts

α	arbitrary chemical species,
fu	fuel or fuel stream,
i, j, k	cartesian co-ordinator directions,
m	moisture,
ox	oxidant or oxidant stream,
pr	products,
py	pyrolysis,
t	turbulent,
vir	virgin material,
vol	volatiles
w	wood

Acknowledgements

I would like to express my appreciation to all my friends and colleagues at the Department of Fire Safety Engineering for their making an inspiring place to work, and special thanks to those who patiently helped me in my endless search for additional computer resources.

Special thanks to Dr. Phil Rubini for help on matters concerning Computational Fluid Dynamics, especially the CFD code Sofie, to Dr. Zhenghua Yan for all our discussions on fluid mechanics and flame spread and also for giving me insight into his interesting work and allowing me to use his CFD code, to Simo Hostikka for his valuable help with the CFD code FDS and the pyrolysis model within.

I am very much indebted to Birgit Östman, project coordinator at Trätek, for her continuous support and help.

Ulf Göransson and Dr. Björn Karlsson have both been valuable discussion partners on flame spread modelling.

The work has been supervised by Göran Holmstedt, who has provided me invaluable support and encouragement.

The study was carried out as part of the Nordic Wood project “Brandsäkra Trähus” with the financial support of Nordisk Industrifond, VINNOVA and the Swedish wood industry. Their support is gratefully acknowledged.

Table of Contents

1. Introduction

By tradition, building codes around the world tend to be very restrictive regarding the use of combustible building materials. Recent developments in Fire Safety Engineering, FSE, have led the way, however, to performance based fire regulations being introduced, in which the regulations do not prescribe the fire safety design in detail but provide qualitative objectives regarding the performance of a building in case of fire. This opens up possibilities for new design solutions, including the use of wood-framed buildings or visible wooden surfaces, such as interior linings or wooden facades. The performance based regulations require, however, that the new design be verified with respect to safety to life and property protection. The verification procedure for ensuring the fire safety of buildings on which there are visible wooden surfaces is an area in which FSE methodology fails, however. Thus far, no model has proved to be functional in connection with arbitrary end-use flame-spread and fire-growth scenarios[*].

1.1 Background

Numerical analysis of flame spread dates back to the work on the spread of laminar diffusion flames of John de Ris[2] in the late 1960s. In 1984, Fernandez-Pello[3] reviewed various existing theories on flame spread. He concluded that the controlling mechanisms were rather well understood and that detailed governing equations could be provided but that the problem of the mathematical formulation of arbitrary scenarios was still to be solved. Some eight years earlier, Williams[4], in his well-known paper on fire spread published in 1976, had pointed out that theoreticians "…often attempt to include all potentially important phenomena in their models of fire spread, believing that they cannot properly describe the process if something that contributes is neglected". He argued that there could be a merit in the opposite approach, namely that of studying limited scenarios and focusing one's attention to the most essential phenomena in specific cases. This line of argumentation can be seen as a recognition of the problem of complexity and a realisation of the fact that a detailed numerical analysis of flame spread in arbitrary end scenarios may first be possible at some time in the future. Long after Fernandez-Pello's review, Williams's paper, despite its being published prior to that, became the starting point for much research concerned with flame spread and fire growth. Unfortunately, this led to most of the physics of the problem being avoided and to case-specific models with only modest chances of further generalisation being developed. Yet the need of generalisation and of models being useful for solving engineering problems has made it necessary to, in the one way or the other, incorporate fundamental laws of nature into flame spread modelling. From user's point of view it is revealing to note that the models developed in more than thirty years of research have seldom if ever been applied beyond their research environment.[5]

The architects and building engineers who wish to make use of visible wooden surfaces have had little benefit from the newly established performance based regulations. The one way of verifying a new design involving visibly exposed wood is still to carry out full-scale testing of the specific setting or, under certain circumstances, treating the wood with different fire retardants. The use of sprinkler systems may or may not provide a sufficient level of safety.

[*] Concerning the use of calculation procedures in building fire safety design, the Swedish Building Regulations, BBR, (2001)[1] states that calculations "… shall be performed in accordance with a model which gives a satisfactory description of the problem at hand".

1.2 Objective and purpose

The aim of this report is to review the current state of the art in modelling fire and flame spread on solid surfaces, including heat transfer and thermal decomposition analysis. A number of existing flame spread models, namely one stand-alone analytical model and four pyrolysis models coupled with general or fire-specific CFD codes (Computational Fluid Dynamics), are discussed and are applied in different modelling situations so as to evaluate their predictive performance. The major design assumptions, methods of solution and capabilities are addressed. Although the materials of concern are primarily wooden products, the assumptions and modelling approaches involved are quite similar for a variety of different materials, composites included.

1.3 Overview of the dissertation

Chapter 2 provides a brief introduction to the natural appearance and properties of wood, providing certain insight into the complexity of the task of modelling the thermal decomposition of a combustible solid. In addition, certain modelling concepts and computational strategies are taken up so as to provide a background and a possible future to model development in flame spread calculations.

In Chapter 3 an analytical approach to flame-spread modelling is described in detail. On the basis of sample calculations, in which the model predictions are compared with experimental results, it is shown that its predictive capabilities are limited.

Chapter 4 provides an introduction to some of the methods of fire modelling based upon the use of Computational Fluid Dynamics, including calculation of reacting turbulent flow and heat transfer from flames and hot gases to solid objects.

Four different pyrolysis models developed to interact with the turbulent reacting flow as calculated using a CFD code are discussed in Chapter 5. The models involved are of differing complexity although developers have been devoted to user-friendliness and computational efficiency. A presentation of main features and assumptions of each model are given, along with a discussion of the input data required.

In Chapter 6 three experimental setups of differing size are employed chosen so that the models could be evaluated both on a stand-alone basis and integrated into their original CFD environment. This chapter also presents some numerical experiments carried out for investigating the CFD code's sensitivity to changes in the computational conditions and thus its capabilities of providing consistent predictions of the turbulent reacting flow and the resulting heat flux to wall surfaces.

At the end of Chapters 3 and 6 conclusions based on studying the different model approaches are summarised and certain practical considerations regarding the various model approaches and their use are taken up. Chapter 7 provides a brief summary of the conclusions drawn, possible fruitful avenues for future work being discussed.

2. Wood and its thermal degradation

Essentially, wood can be regarded as a composite consisting of hundreds of billions of cells in every cubic meter of solid material. Although the raw material is often heavily processed prior to use, the resulting products still possess the basic properties given by nature at the specific place of growth. Variations in the material properties may thus be observed, also within a given species. In addition, when a piece of wood is subjected to high temperatures, molecular changes that affect the material properties occur.[6] The modelling of such natural materials inevitably calls for major simplifications. This chapter is intended to provide an introduction to the subject of thermal degradation and flame-spread modelling on wooden surfaces.

2.1 Characteristics of wood

Different wood species can be identified broadly as being softwoods (conifers) or hardwoods (broad leaves). The terms softwood and hardwood are not really based on the stability or stiffness of the material but rather on its cellular composition and basic structure. The primary materials of which the cell walls are constructed are cellulose, hemicellulose and lignin. A fourth component, the extractives, include different organic or inorganic compounds such as acids, fats, oils, resins, waxes, silica or sugars that are not really part of the basic wood structure; in the tree they often have a maintenance function of some type. The major components of the wood matrix are given in Table 1[6].

Table 1 Major components of wood

Cell material	Softwood (mass%)	Hardwood (mass%)
Cellulose	40-45	45-50
Hemi-celluloses	25-30	21-35
Lignin	26-34	22-30
Extractives	0-5	0-10
Lumen (approx.)	65 vol%	55 vol%

Cellulose is a natural polymer consisting of linear chains of glucose, its chemical representation being $(C_6H_{10}O_5)_n$, the expression inside the parentheses being the monomer*. The young cell has only one thin wall, the primary wall. As the cell grows, the cellulose molecules arrange themselves, mostly in crystalline form, to produce fibrous structures called fibrils that form the cell walls, layer by layer, giving rise to three secondary walls.

It is cellulose, with its fibrous structure, that contributes most to the mechanical performance of wood, but it is also the constituent that contributes the most to the generation of flammable gases during a fire. At about 200 °C, cellulose starts to break down, producing a variety of volatiles and leaving behind a carbonaceous residue, char, which can undergo further

* From a kinetic modelling standpoint it can be of interest to note that a detailed reaction scheme for the combustion of methane, CH_4, in air includes at least 144 reverse reactions and 33 species[7]. Since the complexity of the overall combustion process increases with the size and structure of the molecules, the kinetics of cellulose combustion alone seem almost impossible to describe in detail.

oxidation according to rather complex reaction schemes. When the temperature of the wood material has reached approximately 450 °C, the volatilisation of cellulose is complete.[8,9]

The flexibility of wood is due to the presence of non-crystalline hemicellulose that acts as a filling within the cellulose, with its crystalline properties. Hemicellulose is a collective term for mixtures of carbohydrates, polysaccharides such as glucose, mannose, galactose, xylose, arabinose, 4-O-methylglucuronic acid, and galacturonic acid residues. The composition of the mixture differs between species, and between hardwoods and softwoods. Hemicelluloses are less thermally stable as a whole than cellulose, but produce lesser amounts of combustible gases.[6,9]

Lignin is a resinous material which acts as a sort of glue and as fibre reinforcement, holding the cellulose and hemicellulose together. It has a rather complicated structure consisting of networks of ring-shaped molecules of different kinds. The process of the volatilisation of lignin is somewhat different from that of cellulose and hemicellulose, being more prolonged in time and resulting in a larger fraction of residual char, as shown in Figure 1.

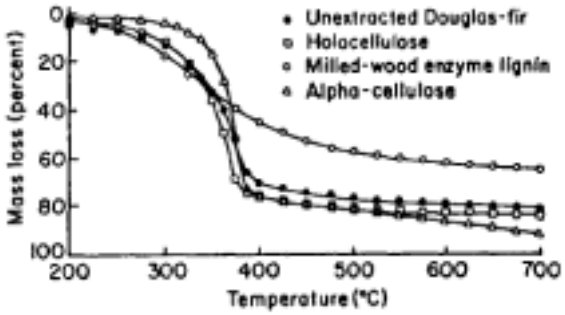

Figure 1. Mass loss of isolated wood components (Douglas fir) heated in nitrogen environment at 5 °C/min (from ref. 10).

The time scales for the heat transfer and the chemical decomposition of the different constituents are illustrated in Figure 2. The kinetic time is calculated from measurements based on thermogravimetric analysis, TGA. Two conclusions can be drawn from the figure. First, simplifying the pyrolysis kinetics to a one-step global reaction may be overly crude, three different pyrolysis reactions, one for each major component of the wood, possibly needing to be taken into account. Secondly, at high temperatures the thermal waves are rate-determining whereas at lower temperatures the kinetic time scale is comparable to the thermal time and may also be rate-determining.

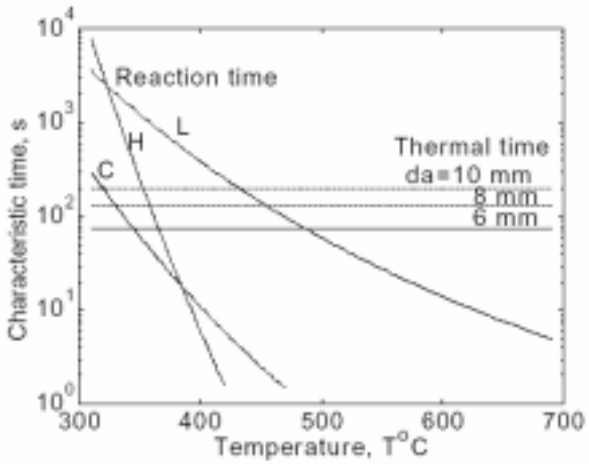

Figure 2. Illustration of the characteristic time scales of kinetic and thermal processes. C=Cellulose, H=Hemicellulose and L=Lignin (from ref. 11).

Wood is a hygroscopic material, meaning that it easily absorbs and retains moisture. The moisture content "strives" at attaining equilibrium with the relative humidity of the surrounding air. When the relative humidity of the air is 100 %, the moisture content reaches the saturation point of the fibres. At a moisture content below the fibre saturation point, normally about 25-35 percent by mass, the moisture is mostly present within the cell walls where water molecules bond to OH-groups in the lignin, hemicellulose and non-crystalline cellulose. At the fibre saturation point the cell walls are completely saturated, any further absorption being deposited in the cell cavities as free water. Because of the chemical bonds the bound water requires more energy to evaporate than free water (2260 kJ/kg)[12]. Thus, besides the primary constituents mentioned above, the water content also affects both the thermal and the mechanical properties of the wood such as dimensional changes, stability, heat and mass transfer, and pyrolysis.

2.2 Introduction to pyrolysis and flame spread modelling

Flame spread and fire growth are governed by the net heat transfer through the surface of a solid fuel* and the subsequent thermal response of the material that has been exposed. Thus, from a macro-scale standpoint, the rate of flame spread depends on such factors as the thermal properties of the material and the flame morphology and its properties. Williams[4] expressed this in an equation he termed "the fundamental equation of flame spread". It includes the solid material density (ρ), the difference between the enthalpy of the solid at the initial temperature and at the apparent ignition temperature ($\Delta h = h_{T_{ig}} - h_{T_0}$), the net heat flux ($\dot{q}$) and the spread rate ($v$). His equation can be summarised as

$$v \sim \frac{\dot{q}}{\rho \Delta h} \qquad [1]$$

* Although the report concerns mainly flame spread on wooden surfaces, the basic theory and modelling assumptions are the same as for flame spread on most solid materials, not applying to wood alone.

The fundamental equation of flame spread encompasses in this very general form the different types of flame spread although the more detailed chemistry and physics may differ considerably. The equation also points to the importance of the initial conditions, such as moisture content and preheating of the solid[13], both of which can be shown to have a decisive influence on flame spread and need to be taken into account in any modelling effort.

The modelling strategies that are needed differ depending on the thickness of the material. A thermally thin material can be considered to have a negligible temperature gradient (a low Biot's number), whereas a thermally thick material is sufficiently thick to show a distinct temperature distribution within the solid (a high Biot's number). In most practical situations, only thermally thick cases need to be addressed. Accordingly, only high-Bi modelling is examined in the present study.

When a wooden material is exposed to heat, it degrades, producing combustible gases, such as carbon monoxide, methane, ethane, ethylene and a range of different hydrocarbons. The thermal response of the fuel depends on its chemical composition, its basic structure and the presence of extractives. If the rate of pyrolysis is sufficiently high, the concentration of combustible gases in the boundary layer soon reaches the lower flammability limit, making it possible to ignite them by means of an ignition pilot, such as a small flame or a spark.

A key feature of all flame-spread modelling is the choice of criteria for ignition of the combustible gas. Whatever the criteria, the critical values for ignition must generally be derived by use of different experimental procedures. Kanury[14] has presented a summary of results obtained by several researchers proposing different criteria to predict the ignition of the pyrolysis gases. In flame-spread modelling, the most commonly employed modelling criterion for ignition is a constant "critical surface temperature". This has been used extensively, despite the fact that a fixed numerical value for a given material cannot readily be obtained on the basis of experimental data, due to there being distinct dependencies on the scenario, including the external heat flux and the moisture content. A very high heat flux results in a high ignition temperature. For "normal" heat fluxes of about 20-30 kW/m^2, however, the ignition temperature of untreated wooden products can generally be chosen as a constant with a value of about 300-350 °C.[15] In more complex pyrolysis models that have been developed which keep track of a moving pyrolysis front inside the solid, critical pyrolysis temperatures of approximately the same numerical values have likewise been employed[16].

A more physically oriented approach to ignition and flame spread modelling is to include chemical kinetics by use of an Arrhenius function for describing the continuous and temperature-dependent thermal decomposition of the solid fuel, $\frac{d\rho_i}{dt} \sim \rho_i A \exp\left(-\frac{E_a}{RT}\right)$. This has been used in several studies[17,18], some of which also divide decomposition of the material into several steps in accordance with the behaviour of its components, as examination of Figure 2 suggests to be a reasonable approach. The method suffers seriously however, from the lack of consistent experimental data on the pre exponential factors, A, the activation energies, E_a and the heat of pyrolysis.

Because of the complexity of the detailed kinetics involved the modeller is forced to make simplifications. The level of simplification chosen is a balance between such factors as the computational cost, the availability of the input data needed or the possibilities of obtaining it and the expected performance of the model as compared with other sub-models used in the

calculations. A commonly employed description of the pyrolysis of wood divides the process into the production of three different pyrolysis products - char, gas and tar - where “char” is the non-volatile carbonaceous residue, “gas” is a comprehensive name for the low-molecular-weight gaseous products that burn momentarily, and tar represents the high-molecular-weight gaseous products that condense at room temperature. A simple scheme can be written as

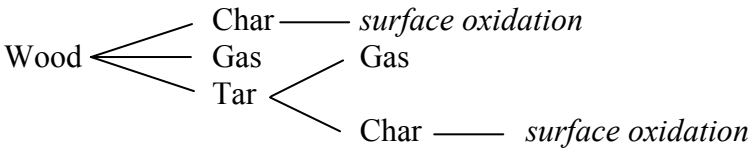

Figure 3. A simplified description of the pyrolysis process although perhaps too comprehensive to be used in practical engineering calculations of flame spread.

This scheme may nevertheless be too complicated and sophisticated to be used in any engineering flame-spread model. Although it does represent a simplified version of the pyrolysis process, further simplifications are needed to make the model useful for practical calculations. Because of the practical shortcomings of the more advanced modelling approaches, there have been recent attempts to simplify the numerical ignition schemes through linking the ignition criteria to properties that can easily be derived in small-scale experiments, such as with use of the Cone Calorimeter[19,20]. However, as will be discussed later, this test procedure contains a series of flaws that can have a decisive influence on the results, so that if these are used to perform large scale simulations, the results of the latter can be misleading.

The experimental and theoretical data available suggests lateral, or opposed-flow flame-spread, to be of little importance. The rate of spread is one or two orders of magnitude less than the upward, concurrent-flow, flame spread[21,22]. This is due to that the opposed-flow flame spread being governed by the diffusion of fuel from the flame zone through a quenching layer between the solid surface and the flame. It is also facilitated by the opposing velocity going to zero at the boundary layer close to the surface. In earlier work, the lateral flame spread was assumed to be governed by gas phase heat conduction, empirical correlations being derived by considering an energy balance at the leading edge of the flame, although the rate of the opposed-flow flame spread has been shown to be dependent to only a slight degree on the surface temperature gradient.[23]

In the chapters that follow different engineering flame-spread models are introduced and are examined in some detail, the basic principles and the underlying modelling assumptions of the models being discussed and certain sample calculations being compared with experimental data. A rather straightforward stand-alone thermal approach is considered first. Both analytical and numerical solutions to the flame-spread equation are discussed, a standard method for obtaining the required input parameters to the model being presented. Secondly, four different material models coupled to different CFD codes are reviewed and their capabilities tested.

3. An analytical model for flame-spread calculations

This chapter discusses a stand-alone modelling approach for upward flame-spread and fire-growth calculations. The flame spread is viewed as involving the movement of a pyrolysis front defined by a critical "ignition" temperature at which the material is considered to produce a sufficiently large amount of pyrolysis gases to support piloted ignition and sustain the spread of flame. The long-continued interest in this modelling approach, despite various limitations to it, is perhaps based on its being the seemingly simplest and most straightforward way of engineering flame spread calculation.

Generally speaking, the necessary input parameters are the thermal properties of the material, including its thermal conductivity k, its density ρ and specific heat capacity c_p, a constant ignition temperature and an expression (or a database) describing the material contribution to the rate of heat release at different points in time, i.e. the rate of pyrolysis.

The thermal response of the material can be related directly to bench scale tests, such as by means of the Cone Calorimeter[24], either in the form of a mathematical representation of the test output or by using the test results directly as a model input. Either way, the fundamental drawback of this approach is that the heat flux to the surface needs to be postulated in advance and then be kept constant over time.

Another testing device associated with early thermal modelling strategies is the LIFT[25,26] (Lateral Ignition and Flame-spread Test) apparatus. The use of tests based on it will be discussed.

In the following, the fundamental principles of physics and all the chemical kinetics are ignored, the material under consideration being assumed to be homogenous, thermally thick and with thermal properties that are constant in time, independent of temperature.

3.1 The derivation and solution of an upward flame spread correlation

Many approaches to thermal modelling of upward, concurrent-flow, flame spread have been proposed during the last few decades. Basically, all of these require that the flame morphology, especially the flame height as well as the heat transfer to the unaffected solid surfaces, can be sufficiently well estimated. The present section concerns the derivation and solution of a fairly simple one-dimensional thermal flame spread model. A general equation is derived and its solution, both using an analytical and a simple numerical approach, is discussed. The general approach to modelling here is shown in Figure 4.

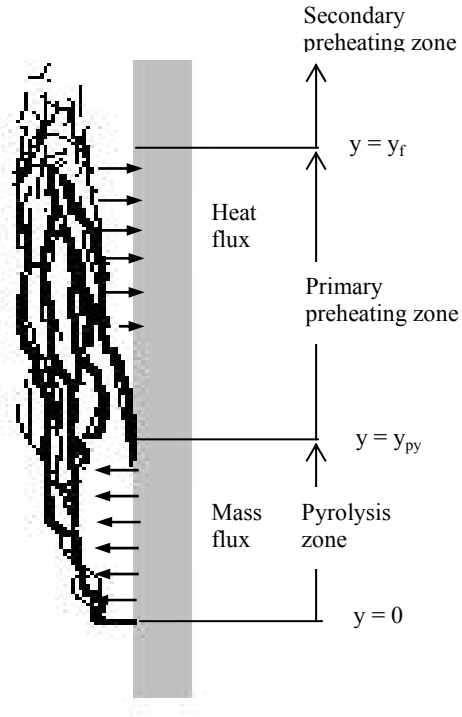

Figure 4. Diagram of upward, concurrent-flow, flame spread.

The vertical scale can be dealt with in different ways accounting for the subsequent burnout of fuel. For example, y = 0 at the bottom of the sample can be fixed and a burnout length be applied, one that moves upwards as the fuel is consumed. Another approach is to shift the entire scale as burnout occurs. A third option is to simply take no explicit account of the burnout, since it often exists implicitly in the mathematical, or numerical, representation of the pyrolysis history of the material in any case. This last method is used in the analysis that follows.

One assumes that in Figure 4 the heat flux from the flame and from the hot gases is at a constant level and considers only the primary heating zone, i.e. the region $y_p < y < y_f$. The rate of flame spread, defined as the continuous propagation of the pyrolysis front, can then be written as

$$V(t) = \frac{dy_p}{dt} = \frac{y_f - y_p}{t_{ig}} \qquad [2]$$

Saito, Quintiere and Williams (SQW)[27] used Equation [2] as a starting point for obtaining an expression of the rate of flame spread, extending the equation by deriving relationships for the flame height, y_f, and the height of the pyrolysis zone, y_p, in the manner shown below.

The flame height is assumed to depend on some power of the total rate of heat release:

$$y_f(t) = K\left(\dot{Q}_{tot}(t)\right)^n \qquad [3]$$

with an initial condition, present at the instant just after the primary ignition occur, being given by

$$y_f(t_{0+}) = K\left(\dot{Q}_b + y_{po} W \dot{Q}''(0)\right)^n \qquad [4]$$

where $\dot{Q}_b$ is the rate of heat release by the burner, W is an assumed constant width of the burning area as it propagates, a width assumed to be equal or to be closely related to the width of the burner. K is a positive constant.

$\dot{Q}''(0)$ represents the rate of heat release per unit area from the solid surface that ignites first, that is, the area covered by the initial burner flame.

The flame height differs somewhat for any given rate of heat release, the height depending upon the geometry of the scenario. The flame height is larger, for example, when the fuel is located in a corner than in the case of a free-burning scenario. This can be explained by a decrease in the rate of air supply to the combustion zone through the air flow being blocked by the walls, resulting in the flame being elongated upwards. For this reason the constant 'K' is employed, relating the flame height to the fire location and to the condition of the surroundings.

The height of the pyrolysis region as a function of time is assumed to follow the integral relationship

$$y_p(t) = y_{po} + \int_0^t V_p(t_p)\,dt_p \qquad [5]$$

the corresponding initial condition describing the situation when ignition first occurs and the material behind the burner flame begins to burn

$$y_f(t_{0-}) = y_{po} = K\dot{Q}_b^n \qquad [6]$$

The flame length at an arbitrarily point in time can be related to the height of the pyrolysis zone by use of the integral $\int_{y_{po}}^{y_p(t)} W\dot{Q}''(y,t)\,dy$, which can be rewritten as an integral evaluated from time 0+ to t so as to obtain $\int_0^t WV(t_p)\dot{Q}''(t-t_p)\,dt_p$. The time-parameter t_p is a dummy variable of integration introduced so as to make the equation continuous, allowing the rate of pyrolysis and the rate of heat release to be evaluated using different time scales. The resulting equation for flame height as a function of time becomes

$$y_f(t) = K\left(\dot{Q}_b + y_{po} W \dot{Q}''(t) + \int_0^t WV(t_p)\dot{Q}''(t-t_p)dt_p \right)^n \quad [7]$$

By substituting into Equation 2 the correlations between flame height and height of the pyrolysis zone that are obtained, one can rewrite this seemingly simple relation to end up with the following Volterra integral equation for the movement of the pyrolysis front[28]

$$V(t) = \frac{dy_p}{dt} = \frac{1}{t_{ig}}\left(y_f - y_p\right) =$$
$$= \frac{1}{t_{ig}}\left[K\left(\dot{Q}_b + y_{po} W \dot{Q}''(t) + \int_0^t WV(t_p)\dot{Q}''(t-t_p)dt_p \right)^n - \left(y_{po} + \int_0^t V(t_p)dt_p \right) \right] \quad [8]$$

The value of the flame-height exponent, n, has been subject to debate, however, the simple correlation that results when it is assumed that n = 1 having proved to give reasonable estimates of the flame height when compared with experimental data. This is fortunate since it allows an analytical solution to be obtained. [29]

3.1.1 An explicit solution

The SQW methodology was studied further by Karlsson and Thomas[30], who solved the Volterra equation, Equation [8], analytically using Laplace-transforms. This required certain additional assumptions and simplifications:

- The history of the transient rate of heat release from the burning solid material, as obtained from a bench scale test, such as through the use of the Cone Calorimeter, can be approximated by use of a fairly simple mathematical expression. The relationship here can conveniently be put in the form of $\dot{Q}''(t) = \dot{Q}''_{\max} \exp(-\lambda t)$, λ being a decay coefficient and t the length of time after ignition at which the rate of heat release is at a maximum, $\dot{Q}''_{\max}$. A still more convenient solution can be obtained through expressing the material behaviour as a constant average value, $\dot{Q}''(t) = \dot{Q}''_{ave}$ of prescribed duration. Figure 5 provides a comparison of these two approaches.

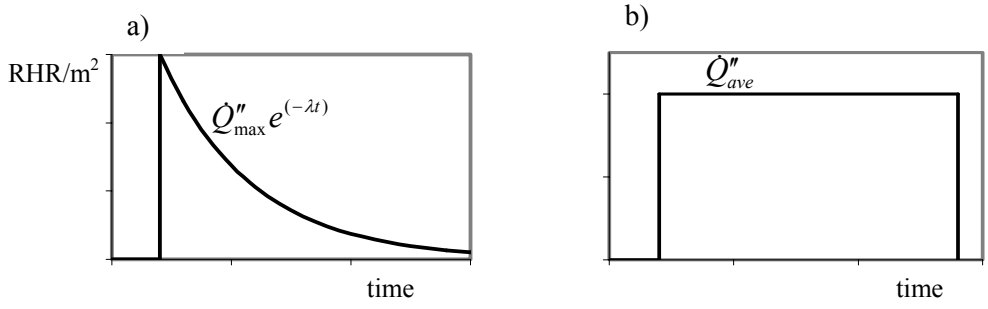

Figure 5. Mathematical representations of Cone Calorimeter data.

- The width of the propagating pyrolysis front over the sample can be assumed to be constant in time and space. A constant is usually chosen so as to correspond to the width of the initial fire (or burner).

  In some scenarios it can be convenient to express the flame-spread velocity in terms of area rather than of length-scales: $V(t) = \frac{A_f - A_p}{t_{ig}}$. This has been used for the calculation of flame spread under a ceiling. Karlsson[28] optimised an algorithm applied to the ISO 9705 Room Corner Test[31] in which there were combustible materials on the walls and ceiling. This resulted in an overall equation very similar to Equation [8]. If one assumes a rate of heat release of the form $\dot{Q}''(t) = \dot{Q}''_{\max} \exp(-\lambda t)$ and that the flame area is linearly dependent upon the momentary rate of heat release $\dot{Q}''(t)$, as written in the form $A_f = A_0 + K\dot{Q}_{ceiling}$, one obtains:

$$\frac{dA}{dt} = \frac{1}{t_{ig}}\left[A_0 + K\left(A_0\dot{Q}''_{\max} e^{-\lambda t} + \int_0^t \dot{Q}''_{\max} e^{-\lambda(t-t_p)} V(t_p)dt_p \right)^n - \left(A_0 + \int_0^t V(t_p)dt_p \right) \right] \quad [9]$$

  The term A_0 represents the initial area of pyrolysing material, calculated mathematically as $A_0 = K\left(\dot{Q}_b + A_w\dot{Q}''_{\max} e^{(-\lambda t)} - 150\right)$, where 150 is a model-tuning parameter representing the heat release rate, in kW, required for the flames to reach the ceiling in the Room Corner Test.

- The flame length is assumed to be linearly dependent upon the total rate of heat release the coefficient 'n' thus being given a value of unity so that $y_f = K\dot{Q}_{tot}$. The parameter K is expressed accordingly in units m/W or m^2/W, depending on how the width, W, is expressed in Equation [8]. If n is assigned any other value than unity, Equation [8] cannot be solved analytically.

- The initial fire is assumed to be constant.

- Preheating of the material in front of the flame tip is ignored. Mathematically, this can be expressed by use of a constant initial surface temperature T_0 above the pyrolysis zone.

Employing the assumptions above, using an exponential variation to represent the contribution of the material to the rate of heat release, $\dot{Q}''(t) = \dot{Q}''_{\max} \exp(-\lambda t)$, Thomas and Karlsson[30] solved Equation [8] analytically by use of Laplace transforms. The final solution involved the use of two different relationships giving rise to four possible solutions, each with a unique physical implication. The solutions and their physical interpretations are discussed below.

The complete solution and the computational steps employed in transforming the integral equation into an algebraic relationship is beyond the scope of this text. The interested reader should consult reference 30. Here only the final result of the procedure is discussed. The first overall relationship for the movement of the pyrolysis front after the Laplace transforms have been completed is written as

$$V(t) = \frac{C_1}{s_2 - s_1}\left(s_2 e^{s_2 t} - s_1 e^{s_1 t} \right) \quad [10]$$

In this equation $C_1 = \dfrac{K\dot{Q}''_{\max} y_{po} W}{t_{ig}}$ represents a "constant" for the specific scenario, the parameters s_1 and s_2 being the real roots of the quadratic equation

$$s^2 + \frac{1 - \mathrm{a} + \lambda t_{ig}}{t_{ig}} s + \frac{\lambda}{t_{ig}} = 0 \qquad [11]$$

such that $\mathrm{s}_{1,2} = -\dfrac{1}{2t_{ig}}\left(1 - \mathrm{a} + \lambda t_{ig}\right) \pm \sqrt{\Delta}$, where $\Delta = \dfrac{1}{4t_{ig}^{\,2}}\left(1 - \mathrm{a} + \lambda t_{ig}\right)^2 - \dfrac{\lambda}{t_{ig}}$ and "a" is a dimensionless rate of heat release defined as $\mathrm{a} = K\dot{Q}''_{\max}$.

If the roots of Equation [11] turn out to be complex, that is if the parameter Δ is negative, the solutions will still have physical implications. However, the resulting flame spread equation needs then to be rewritten in the form

$$\mathrm{V}(t) = \frac{\mathrm{C}_1 e^{\alpha t}}{\beta}\left[\alpha \sin(\beta t) + \beta \cos(\beta t)\right] \qquad [12]$$

where the roots s_1 and s_2 are of the type $\alpha \pm i\beta$, where $\alpha = -\dfrac{1}{2t_{ig}}\left(1 - \mathrm{a} + \lambda t_{ig}\right)$ and $\beta = \sqrt{|\Delta|}$, Δ being a negative number.

Together, Equations [10] and [12] yield four possible solutions, each having a different physical interpretation. Baroudi and Kokkala[32] provided an interesting graphical representation of the different solutions. Their diagram is reproduced in Figure 6, where regions I and IV are the real solutions to Equation [11], whereas II and III represent the complex solutions.

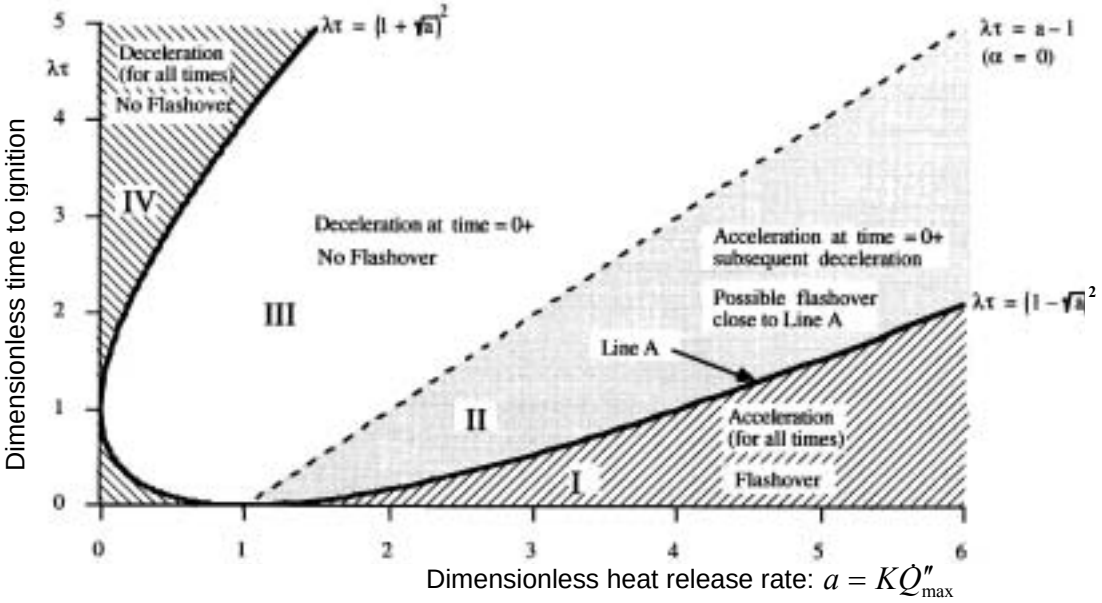

Figure 6. Graphical representations showing an interpretation of the flame spread equations in terms of accelerating or decelerating flame spread.

Due to their trigonometric representation, the solutions obtained for regions II and III will inevitably show oscillatory behaviour, varying between negative and positive peaks as illustrated in Figure 7. The validity of the relationship ceases when the solution crosses the abscissa for the first time, this representing extinction, as at point A in Figure 7. This numerical behaviour can be understood on the basis of Equation [12] in terms of which there is a limiting state for region II as described by

$$\lim_{t\to\infty} \quad V_{II}(t)_{t\to\infty} = \pm 0 \quad \text{(Oscillating with smaller and smaller amplitudes)} \qquad [13]$$

where for region III:

$$\lim_{t\to\infty} \quad V_{III}(t)_{t\to\infty} = \pm\infty \quad \text{(Oscillating with amplitudes of increasing size)} \qquad [14]$$

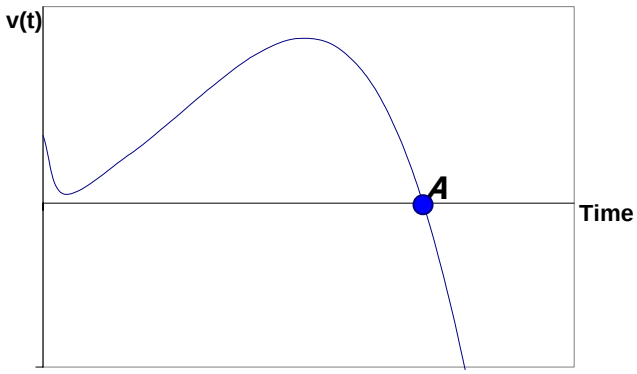

Figure 7. One possible solution to the flame-spread equation showing the oscillatory behaviour originating from its trigonometric representation. As can be seen, this scenario belongs to region III in Figure 6.

Representing the data from the Cone Calorimeter as an average rate of heat release, $\dot{Q}''_{ave}$, as shown in Figure 5b, results in a solution considerably easier to obtain and use. When Laplace transforms are applied, the equation for the rate of flame spread becomes

$$V(t) = \frac{K\dot{Q}_b}{t_{ig}} a e^{(a-1)\frac{t}{t_{ig}}} \qquad [15]$$

where $a = K\dot{Q}''_{ave}W$. If $a \geq 1$, the flame spread can be assumed to accelerate continuously.

3.1.2 Numerical solution

The main advantage in solving the flame spread equation, Equation [8], analytically is that this allows the physical implications of the solutions to be readily understood in a phenomenological sense. Accordingly, a graphical plot such as in Figure 6 can help clearify the phenomenon of flame spread.

One disadvantage of choosing an analytical solution is that the flexibility of the model becomes rather poor, the required mathematical representations, such as of the rate of heat release from the Cone Calorimeter, needing to be simplified by use of some mathematically convenient relationship, and the flame height needing to be expressed as a simple linear function of the total rate of heat release, in addition to the preheating of the material above the flame not easily being accounted for. These drawbacks can be at least partially avoided by using numerical techniques to solve Equation [8]. Several possible mathematical procedures are available, Kokkala, Baroudi and Parker[33], for example, using the Forward-Euler solution technique to solve the time integral and comparing their results with those of the analytical solution, found the fit to be excellent. Karlsson[34] also obtained a solution for flame spread by use of numerical techniques, the results corresponding well with those of the Room Corner Test for over 20 different wall-lining materials.

A very simple and straightforward numerical approach used to evaluate integrals is the so-called trapezoidal approximation method or trapezoidal rule. The basic assumption used in this approach is that the integral can be approximated by using a number of trapezoidal shapes. The smaller the shapes are the better the approximation generally is. Although this approach does not lay claim to be either efficient or very stable, it is rather useful and instructive when employed in an initial study. Figure 8 clarifies the basic conceptions involved.

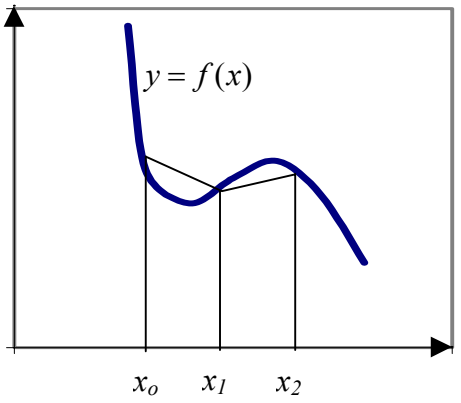

$$\Longrightarrow \int_{x_0}^{x_2} f(x)dx \approx \frac{x_2 - x_0}{2}\left[\frac{f(x_0)+f(x_1)}{2} + \frac{f(x_1)+f(x_2)}{2}\right]$$

Figure 8. Basic conception involved in the trapezoidal integration approach. ($x_1 - x_0 = x_2 - x_1$)

Using n equally thick trapezoidal shapes, a generalisation can be expressed as:

$$\int_{x_0}^{x_N} f(x)dx \approx \frac{x_2 - x_0}{2n}\left[f(x_0) + 2f(x_1) + 2f(x_2) + \ldots + 2f(x_{n-1}) + f(x_n)\right] \qquad [16]$$

Lee[35] used this approach to solve Equation [8] by replacing the two time integrals, $I_1(t)$ and $I_2(t)$ by a trapezoidal summation so that

$$V(t) = \frac{1}{t_{ig}}\left[KW\left(\frac{\dot{Q}_b}{W} + y_{po}\dot{Q}''(t) + \underbrace{\int_0^t V(t_p)\dot{Q}''(t-t_p)dt_p}_{I_1(t)}\right)^n - \left(y_{po} + \underbrace{\int_0^t V_p(t_p)dt_p}_{I_2(t)}\right)\right] \qquad [17]$$

Due to the nature of the algorithm, an iterative solution approach is needed. The normalised rate of flame spread with a maximum prescribed residual of ε is used as the convergence criterion.

$$\frac{V(t) - V(t_{last})}{V(t)} \leq \varepsilon \qquad [18]$$

The general procedure is to start with an estimated or a guessed value of V(t) and then calculate a new V(t) using Equation 17, comparing the result with the convergence criterion, Equation [18]. If the result does not fulfil the convergence criterion, one sets V(t)=new estimated (actually the old calculated) value, $V(t_{last})$, and runs the procedure again.

3.2 Obtaining input to the thermal flame spread model

The model equations require the user to provide certain input data, primarily model-specific coefficients and physical quantities, some of which have already been briefly introduced. These mainly experimentally-derived parameters include the following:

- ✓ The prevailing heat flux to the surface.
- ✓ The time to ignition at the prevailing incident heat flux.
- ✓ The ignition temperature T_{ig} .
- ✓ The maximum, or peak, rate of heat release, $\dot{Q}''_{\max}$.
- ✓ The decay coefficient, λ .
- ✓ The thermal properties of the solid material, evaluated in this context as the thermal inertia, $k\rho c$.
- ✓ The flame-height parameter, K.

In this section these parameters will be presented in some more detail and simple engineering methods for obtaining their numerical values will be introduced. It is important to recognize that one is largely dealing with empirical and lumped parameters and above all that calculations of this sort give approximate answers.

3.2.1 Heat flux from flames

A key feature in using the analytical model described above is that it is assumed to be possible to assign a constant heat flux, one that applies over the height of the flame in its entirety. The heat flux above the flames is assumed to be zero. Karlsson[28] used an assumed incident flux of 50 kW/m^2 when employing the model to calculate the rate of heat release in the Room Corner Test, ISO 9705. It is, however, difficult to provide any guidance on how to make this choice. The choice can clearly affect the outcome of calculations. Since it is likely to be influenced by such factors as the size and location of the initial fire and the characteristics of the fuel, the proper approach appears to be to carry out experiments beforehand specific to the scenario in question, or possibly to perform CFD calculations, although results obtained in similar experimental setups may provide some guidance.

The model input corresponds to of the rate of pyrolysis at a given incident heat flux. Since the input stems directly from experimental data, the net heat flux, including the additional heating contribution of the flames, originating from the sample, is implicitly accounted for by the assumption that the behaviour measured in the Cone Calorimeter is representative of the scenario in question. The total incident flux that Karlsson employed was high but not unreasonable.

The incident heat flux towards the surface of a sample is not likely to remain constant over the entire "flame height", however. To obtain a basic idea of how the heat flux varies over the flame height, one can assume the flame temperature to vary between a minimum of 700°C and a maximum of 1100°C, the resulting variation in radiative power being $\left(\frac{1373}{973}\right)^4$, which is approximately a factor 4.

3.2.2 Time to ignition and ignition temperature

Parameters and phenomena such as the temperature rise at the surface of the solid, the minimum ignition heat flux, $\dot{q}''_{0,ig}$, and the time to ignition, t_{ig}, can be estimated by use of Fourier's second law, often referred to as the general heat transfer equation, together with the concept of ignition temperature. Using a somewhat simplified one-dimensional analysis, one can write the equation as

$$\frac{\partial}{\partial x}\left(k\frac{\partial T}{\partial x}\right) = \rho c \frac{\partial T}{\partial t} \qquad [19]$$

assuming an initial condition of $T(x,0) = T_0$ and the boundary condition at the surface of the unburned solid written as

$$\dot{q}''(0,t) = -k\left.\frac{dT}{dx}\right|_{x=0} = \alpha \dot{q}''_e - h_{conv}(T - T_0) - \varepsilon\sigma\left(T^4 - T_0^4\right) \approx \dot{q}''_e - h(T - T_0) \qquad [20]$$

In the last step, the absorptivity α is assigned a value of unity and the heat losses are bracketed into a simple, yet highly non-linear relationship.

The material is also regarded as being thermally thick, which gives the following boundary condition for the rear surface of it:

$$T(\infty,t) = T_0 \qquad [21]$$

The minimum heat flux, $\dot{q}''_{0,ig}$, for piloted ignition can then be expressed directly, using Equation [20]. At this limiting flux, the external heat transfer and the heat losses from the surface, which are at or just below the critical ignition temperature, are equal, no heat being conducted into the solid, the net flux being zero. In mathematical terms,

$$q''_{0,ig} = h\left(T_{ig} - T_0\right) \qquad [22]$$

Equation [22] is frequently used to obtain estimates of the ignition temperature, the rather crude assumption being made that the heat transfer coefficient can be assigned a constant value, the limiting heat flux being derived from the experimental data.

If a constant heat exposure, $\dot{q}''_e$, and a temperature-independent constant heat transfer coefficient, h (which actually has a T^3 dependence) are assumed the temperature distribution in a thermally thick solid can be simplified by use of Equations [19] and [20], Laplace-transforms being used to obtain an ordinary second order differential equation. Using the initial and boundary conditions as given above and solving for the general case, one obtains[36]

$$T(x,t) = T_0 + \frac{\dot{q}''_e}{h}\left[\operatorname{erfc}\left(\frac{\mathrm{x}}{2\sqrt{\alpha t}} \right) - \exp\left(\frac{hx}{k} + \frac{h^2 t}{k\rho c} \right) \operatorname{erfc}\left(\frac{x}{2\sqrt{\alpha t}} + \sqrt{\frac{h^2 t}{k\rho c}} \right) \right] \qquad [23]$$

which for the special case x = 0, that is for the surface temperature, reduces to

$$T(0,t) - T_0 = \frac{\dot{q}''_e}{h}\left[1 - \exp\left(\frac{h^2 t}{k\rho c} \right) \operatorname{erfc}\left(\sqrt{\frac{h^2 t}{k\rho c}} \right) \right] \qquad [24]$$

where erfc X is the complementary error function defined as

$$\operatorname{erfc} X = 1 - \operatorname{erf} X = \frac{2}{\sqrt{\pi}} \int_X^\infty \exp\left(-t^2\right) dt \qquad [25]$$

Equation [24] is rather arduous to derive, and apply to an engineering problem or to calculations concerning part of a larger analytical relationship. If the surface heat losses are totally ignored, however, the correlation called for becomes much more practical in terms of analytical treatment:

$$T(0,t) - T_0 = 2\dot{q}''_e \sqrt{\frac{t}{\pi k\rho c}} \qquad [26]$$

By considering the concept of ignition temperature at the surface and rearranging Equation [26], a simple, though frequently used relationship for the time to ignition can be obtained:

$$t_{ig} = \frac{\pi \mathrm{k}\rho\mathrm{c}\left(\mathrm{T_{ig}} - \mathrm{T_0}\right)^2}{4\dot{\mathrm{q}}''^{\,2}_{\mathrm{e}}} \qquad [27]$$

Not surprisingly, this relationship suffers from the assumption that surface cooling due to convection and re-radiation can be ignored. Figure 9 shows the effect on the rise in surface temperature of the choice of differing degrees of cooling on a flat plate exposed to a constant external radiative flux of 30 kW/m^2. The surrounding fluid temperature is assumed to remain at the ambient temperature. The time required for an increase of 300 degrees in the surface temperature Equation [26] (involving no surface cooling) provides and that of the numerical solution to Equations [19] and [20] (involving surface cooling as a function of temperature) provides differ by a factor of more than two.

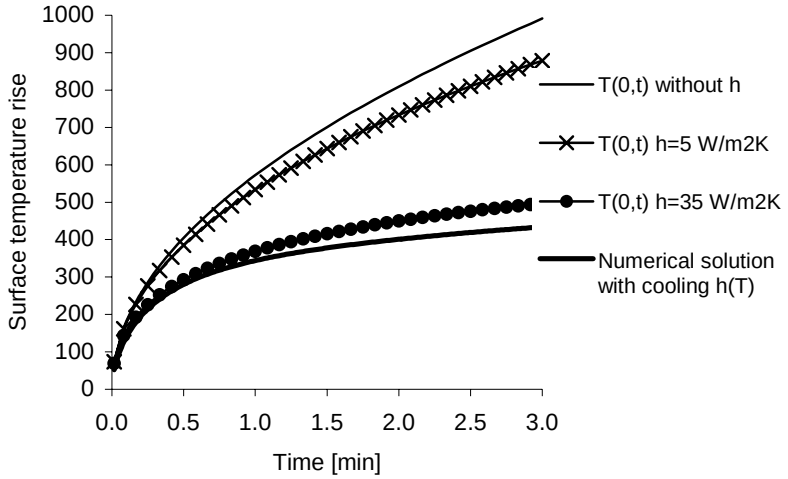

Figure 9. The effect of surface cooling in solving the heat transfer equation. In the numerical solution, cooling varies as a function of temperature but the result can be realistically approximated using Equation [24] with h=43 W/m^{2}K. In practise, cooling originates primarily from surface re-radiation.

3.2.4 Rate of pyrolysis representation

The contribution of a burning material to the total rate of heat release is estimated here using data from the Cone Calorimeter. If Equation [8] is solved using numerical methods, RHR data can be taken directly from the test results. For an analytical solution, however, the data has to be represented by a mathematical relationship. Karlsson[28] determined the curve-fitted exponential temporal RHR-decay, $\dot{Q}''_{\max} e^{-\lambda t}$, for various materials. Data for some of these are given in Table 2. The expression employed can be expected to be representative of the initial behaviour of charring materials that create an insulating carbonaceous layer as they burn, which effectively limits the heat transfer into the solid and the resulting rate of pyrolysis.

Table 2. $\dot{Q}''_{\max}$, λ and time to ignition as obtained using the Cone Calorimeter at a heat flux of 50 kWm^{-2}. There are two different parameters in the table that both represent time to ignition, t_{ig} being the time to ignition as obtained from the test data and τ being the value calculated according to Equation [27].

Material name	$\dot{Q}''_{\max}$ [kW/m^2]	λ [s^{-1}]	t_{ig} [s]	τ [s]
Insulation fibreboard	184	0.0090	12	20
Medium density fibreboard	208	0.0027	28	48
Particle board	204	0.0030	34	57
Wood panel, spruce	168	0.0075	21	36

The decay coefficient λ is determined using a best fit to the decaying phase during testing. It is calculated from

$$\lambda = \text{average of} \left(\frac{\ln\left[\frac{\dot{Q}''_{cone}(t)}{\dot{Q}''_{\max}} \right]}{t} \right) \qquad [28]$$

Here $\dot{Q}''_{cone}(t)$ represents the time-dependent rate of heat release from the Cone Calorimeter. A hint of the implications of an approximation of this kind is provided in Figure 10 for "Medium density fibreboard", MDF, and untreated spruce.

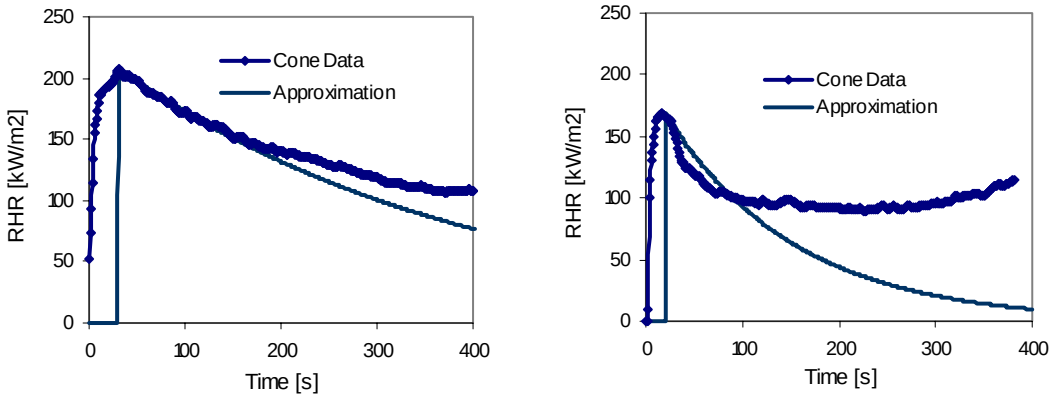

Figure 10 Data from the Cone Calorimeter at 50 kW/m^2 compared with an approximation using the $\dot{Q}''_{\max} e^{-\lambda t}$ relationship and the parameter values shown in Table 2. Left: MDF, Right: wooden (spruce) panel

3.2.5 Estimating the thermal properties, *kρc*

In this section a method for deriving the thermal inertia, or $k\rho c$, from experimental data using the LIFT apparatus[26] will be discussed. The fundamental assumption is that a direct proportionality exists between the ratio of the minimum ignition heat flux, $\dot{q}''_{0,ig}$, to the external heat flux, $\dot{q}''_e$, and the square root of the time to ignition at that external flux, expressed mathematically as

$$\frac{\dot{q}''_{0,ig}}{\dot{q}''_e} = b\sqrt{t_{ig,e}} \qquad [29]$$

The coefficient b can be obtained by plotting the ratio $\frac{\dot{q}''_{0,ig}}{\dot{q}''_e}$ versus $\sqrt{t_{ig,e}}$ and fitting a straight line from the origin up to the point where $\frac{\dot{q}''_{0,ig}}{\dot{q}''_e} = 1$.

Using the definition

$$\frac{\dot{q}''_{0,ig}}{\dot{q}''_e} = \begin{bmatrix} b\sqrt{t_{ig,e}} & \text{if } t \le t' \\ 1 & \text{if } t \ge t' \end{bmatrix} \equiv F(t) \qquad [30]$$

where t' represents the characteristic equilibrium time at which $\frac{\dot{q}''_{0,ig}}{\dot{q}''_e} = 1$, Quintiere and Harkleroad[37] derived the proportionality coefficient, b, as function of the apparent thermal inertia, defined as the product of the material conductivity, the density and the specific heat capacity, $k\rho c$.

$$k\rho c = \frac{4h^2}{\pi b^2} \qquad [31]$$

Note that this product is generally considered not to represent a lumped parameter but to have a clear dependency on temperature. In addition, the parameter includes moisture effects and, most importantly, parts of the chemistry of the ignition process.

Illustrative example:
This example is intended to explain the methodology used in deriving the thermal inertia of a material on the basis of a series of small-scale tests. The procedure provides useful insight into the methods used to determine different input data in flame spread modelling of this kind.

Assume that a number of ignition tests were performed using the LIFT apparatus. The minimum ignition heat flux was determined to be 16.3 kW/m^2, data from the subsequent tests being presented in Table 3. From the data obtained, one can derive approximations of both the thermal inertia, $k\rho c$, and the surface ignition temperature at the minimum heat flux.

Table 3 Time to ignition for different external heat fluxes, as determined by experimental data obtained for a non-specified material in the LIFT apparatus.

Flux kW/m^2	Flux ratio	Time to ignition [s]
17.1	0.95	1074
20.9	0.78	339
25.1	0.65	197
30.0	0.54	105
40.0	0.41	47
46.1	0.35	36
51.8	0.31	27
58.2	0.28	21

Since at the minimum ignition heat flux, $\dot{q}''_{0,ig}$, the surface temperature, T_{ig}, corresponds to the equilibrium temperature, it can be estimated from $\dot{q}''_{0,ig}$ and Figure 11, in this example, T_{ig}≈390 °C at 16.3 kW/m^2.

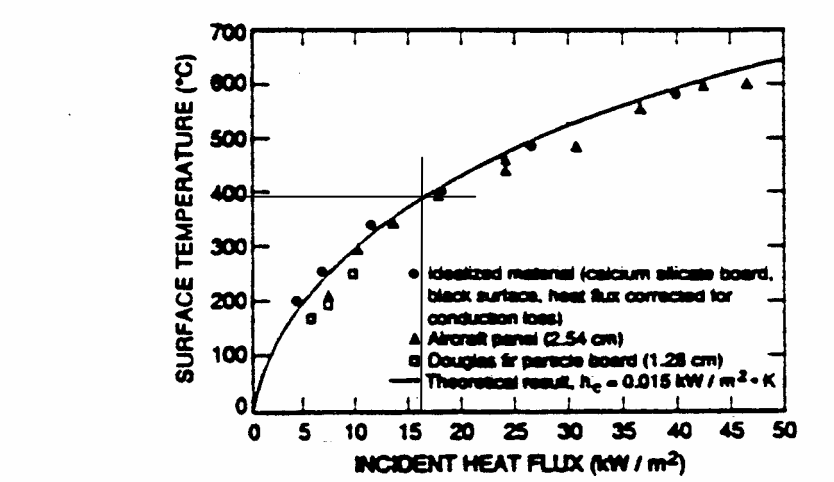

Figure 11. Equilibrium surface temperature plotted against external heat flux (diagram from ref. 26).

An approximate value for the total heat transfer coefficient at the ignition temperature can be calculated from Equation [22] which, if an ambient temperature of 20 °C is assumed gives

$$h \approx \frac{16.3*10^3}{390-20} = 44.05 \ \text{kWm}^{-2}\text{K}^{-1}$$

In Figure 12 the heat flux ratio is plotted against the square root of the time to ignition. The slope of the first linear part of the graph gives the b-value.

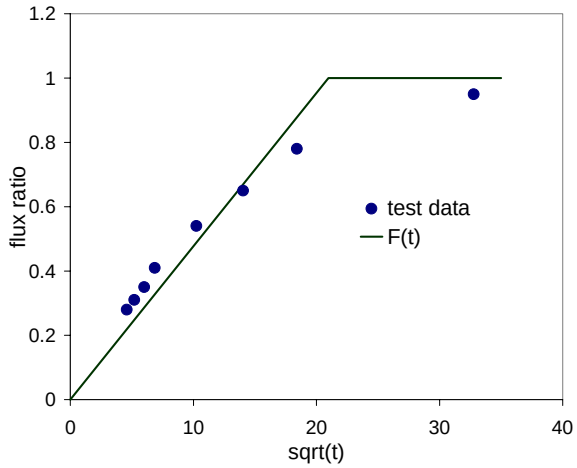

Figure 12. Derivation of the F(t) function by means of a best-fit analysis.

The slope is calculated as b=0.048 $s^{-½}$. This allows the thermal inertia to be estimated using Equation 38:

$$k\rho c = \frac{4*44.05^2}{\pi*0.048^2} = 1.09*10^6 \ \ \text{W}^2\text{sm}^{-4}\text{K}^{-2} \quad \text{(a rather high value)}$$

3.2.6 Estimates of the flame height parameter, *K*

The course of flame spread can differ considerably depending on the surroundings in the flame-spread situation, the location of the initial fire, the position of the combustible materials, the presence of a ceiling etc. Phenomena such as the limited air entrainment into the fire plume and re-radiation from adjacent surfaces, from a ceiling or from a gas layer can contribute considerably to the increase in flame height and in the rate of flame spread. To account for these effects, an additional help-parameter, *K*, is introduced. Its numerical value is derived directly from experiments using a particular configuration.

Strictly speaking, it is not possible to describe the flame height in terms of a constant, since it instead is a parameter characterised by its highly fluctuating nature. Due to the random appearance of a turbulent flame, it is quite impossible to provide definite numerical values concerning flame heights. Accordingly, a value corresponding to the point of 50 percent intermittency is often used to describe the apparent "effective" height of a flame. In Table 4, values that have been used earlier for a variety of materials[38,39] are presented. Although the appropriate units for *K* depend on how the flame spread equation is written, the values shown in Table 4 has been used just as well for units of m^2/kW as for units of m/kW.

Table 4 Preliminary suggestions concerning the flame location parameter.

Scenario	Approximate values for K
Flame spread up a vertical wall	0.01
Flame spread in a corner	0.015
Flame spread under a ceiling	0.02

3.4 Sample calculations

The aim of this section is to further study the Karlsson-model using a hands-on approach. That which follows is intended to serve not as a validation analysis but rather as a guide to the central parts of the model. Two different scenarios are considered, the results for each are compared with experimental data. The first scenario is that of a study of upward flame spread, reported in an experiment carried out by Blomqvist and van Hees[40]. The second is a room fire as described by ISO 9705[31,41], the Room Corner Test.

3.4.1 Upward flame spread on a PMMA surface

The analytical methodology described in this chapter deals basically with the six scenarios shown in Table 5. Although the equations can be applied to a somewhat broader range of flame spread situations than employed here, numerical solutions are generally required, additional assumptions and further tuning of the model likewise being needed.

Table 5 Scenarios relevant of the analytical flame spread calculation procedure.

Scenario	HRR representation	Ignition source
Wall	Exponential decay	Line burner
Corner	Exponential decay	Square burner
Ceiling	Exponential decay	Flame area A_0
Wall	Average heat release	Line burner
Corner	Average heat release	Square burner
Ceiling	Average heat release	Flame area A_0

The time-dependent parameters to be solved are the rate of flame spread (flame spread velocity), $V(t)$, the height of the pyrolysis front, $y_p(t)$, and the total rate of heat release during flame spread, $\dot{Q}''_{total}(t)$.

This first scenario considers a straightforward case in which a burner ignites the bottom end of a flat vertical board. The flame height parameter is given the value of K=0.01 m/kW. The board, made of PMMA* is 3.0 meters in height and 0.3 meters wide. The ignition source (a propane burner) burns at an approximate heat release rate of 20 kW, presumably resulting in an average heat flux of about 35 kW/m^2, occurring uniformly over the height of the flame. This is the first approximation in using the model, a best guess of the prevailing heat flux stemming from the flames.

The time to ignition for the PMMA board is estimated using Equation [27]. Using the thermal properties and ignition temperature of the board according to Quintiere[22], $k\rho c = 1.02\ \mathrm{kW^2 s/m^4 K^2}$ and T_{ig}= 378°C, respectively, results in a calculated time to ignition of

$$\tau = \frac{\pi k\rho c\left(T_{ig} - T_0\right)^2}{4\dot{q}''^{\,2}_e} = \frac{\pi * 1.02 * \left(378 - 20\right)^2}{4 * 35^2} = 84\ \mathrm{s}$$

The contribution of the board material to the rate of heat release is evaluated using Cone Calorimeter test data, from an incident cone flux of 35 kW/m^2, to obtain an average value, as shown in Figure 13. It is believed that $\dot{Q}''_{ave}$ = 430 kW/m^2 provides a reasonable estimation of the heat release during the first minutes of the test.

* Polymethylmethacrylate, chemical formula: $(C_5H_8O_2)_n$

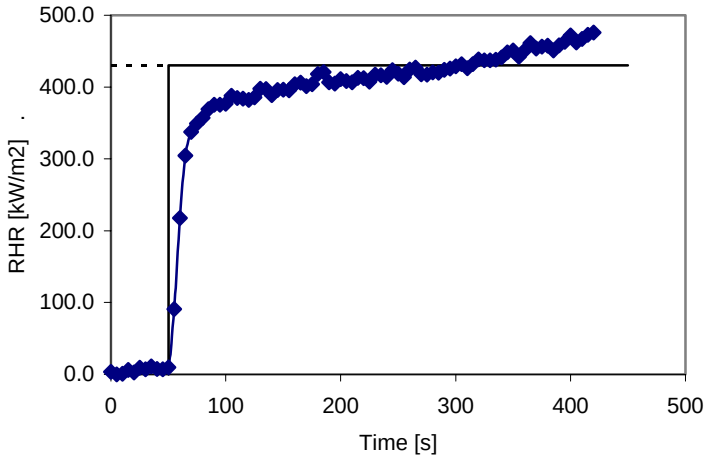

Figure 13. Representation of the rate of heat release using an average value from a Cone Calorimeter test at 35 kW/m^2.

Equation [15] can be used to solve for the flame spread velocity. First, one can note that the flame spread can be expected to accelerate continuously since

$$a = K\dot{Q}''_{ave}W = 0.01*430*0.30 = 1.29 > 1$$

$$V(t) = \frac{K\dot{Q}_b}{\tau} a e^{(a-1)\frac{t}{\tau}} = \frac{0.01*20}{84} *1.29* e^{(1.29-1)\frac{t}{\tau}} = 0.0031* e^{0.00345t}$$

The resulting flame spread velocity is plotted in Figure 14.

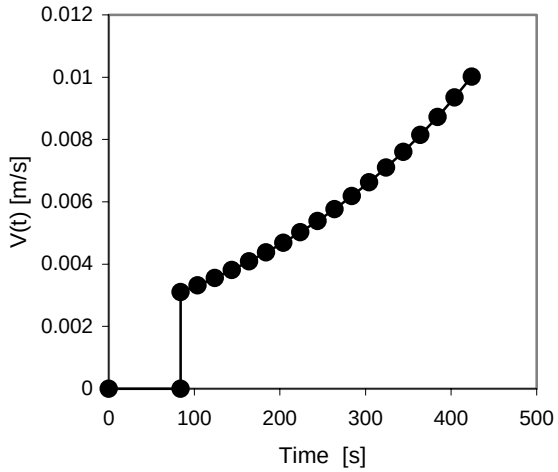

Figure 14. Velocity of the pyrolysis front as a function of time.

The height of the pyrolysis front as a function of the time from ignition can be evaluated by integrating the velocity as given above. This gives

$y_p(t) = y_{p0} + \int_0^t V(t_p)dt_p$ which can be solved in a rather straightforward way to obtain

$$y_p(t) = K\dot{Q}_b + \frac{K\dot{Q}_b a}{(a-1)}\left(e^{(a-1)\frac{t}{\tau}} - 1\right) = 0.20 + 0.89\left(e^{0.00345t} - 1\right)$$

A comparison of the resulting time dependence with the experimental data[40] is shown in Figure 15. From these results it is evident that the speed of the pyrolysis front, as shown in Figure 14, is predicted quite well, whereas the height of the pyrolysis zone is underestimated.

From the basic equations employed it is also clear that lowering the ignition temperature would not make Figure 15 look any better, even though ignition would start earlier, since it also would increase the exponent in the equation for the pyrolysis front.

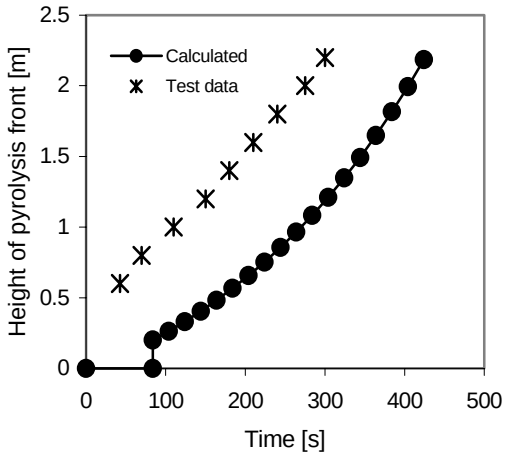

Figure 15. Height of the pyrolysis front as function of the time from the start of the test.

The time dependent total rate of heat release following this fire scenario can be described by the relation

$$\dot{Q}''_{tot}(t) = \dot{Q}_b + y_{p0}\dot{Q}''_{ave}W + \dot{Q}''_{ave}W\int_0^t V(t_p)dt_p$$

Integrating and solving this equation yields

$$\dot{Q}''_{tot}(t) = \dot{Q}_b + y_{p0}\dot{Q}''_{ave}W + \frac{K\dot{Q}_b a}{a-1}\dot{Q}''_{ave}W\left(e^{(a-1)t/\tau} - 1\right)$$

or

$\dot{Q}''_{tot}(t) = 20 + 26 + 115\left(e^{0.00345t} - 1\right)$ resulting in the relationship described in Figure 16, where it is assumed that the total width of the sample is burning, the pyrolysis zone being described as a top-hat profile.

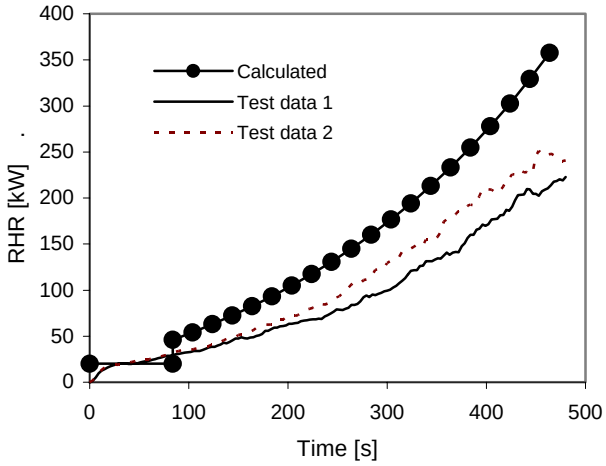

Figure 16. Total rate of heat release as compared with experimental data. In the calculation, the board is ignited after 84 s from the start of the test.

One can note that the calculated results overestimate the rate of heat release somewhat, as can be seen in Figure 16, but that they underestimate appreciably the position of the pyrolysis front, Figure 15. This indicates that the RHR per unit area from the material have been overestimated. However, since the slopes of the experimental and calculated curves in the two figures are similar, other explanations may be plausible. Clearly the entire width of the sample does not ignite instantaneously, instead the heat exposure and thus the rate of pyrolysis being higher in the centre of the sample, which also result in the formation of a rounded off cone shape of the pyrolysis front rather than the presumed top-hat profile. Another explanation for the discrepancies referred to may be that the experimental reports on the height of the pyrolysis front are somewhat incorrect. Making precise and objective visual observations is very difficult.

Karlsson[28], in his sample calculations of fire growth in the Room Corner Test, used a constant incident heat flux of 50 kW/m^2, which provided close agreement to experimental data. From Figure 17 it is evident that the choice of heat exposure is a rather sensitive parameter.

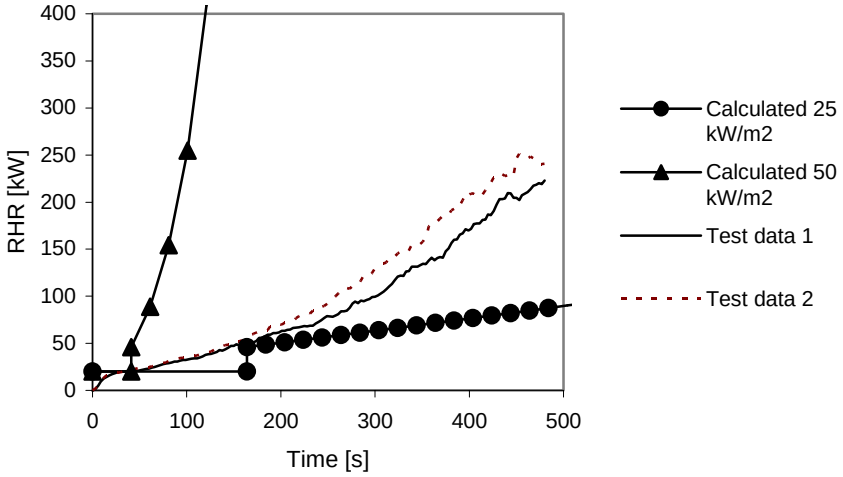

Figure 17. Sensitivity analysis of the model with respect to incident heat flux.

3.4.2 The Room Corner Test, untreated spruce lining

In this scenario the flame-spread procedure is used in its entirety, using the equations for calculating the RHR-time history of a fire in an enclosure, the Room Corner configuration, having a quadratically shaped initial fire source 0.17 meter long on each side and of 100 kW power, located in the back corner of the room as seen from the door opening. A diagram of the room showing its inner dimensions in mm is presented in Figure 18. The enclosure have an untreated wooden lining (spruce) fixed onto the ceiling and onto three walls, the wall on which the front door is located being non-combustible. The following input data were obtained from the literature:

Table 6 Input data for the flame spread equations[24,34]

Parameter [units]	Numerical value
$k\rho c$ [kW^{2}s/m^{4}K^2]	0.489
$\dot{q}''_{0,ig}$ [kW/m2]	19.5
$\dot{Q}''_{\max}$ [kW/m^2]	168*
λ [s^{-1}]	0.0075*
τ [s]	36*
$\lambda\tau$ [-]	0.27*

Since the width of the burner flame is normally somewhat less than the total width of the burner, which is 0.17 meters, the effective width of the flame may need to be corrected somewhat. However, making "free estimates" of this type would be a very questionable approach in practise. For the flame-width approximation to be a good one, one would need to see the actual experiment before making the estimate. Further research would be needed to establish a link between the width of the burner and the width used in the calculations. For this reason, the calculations below involve use of the original burner width, using no modification.

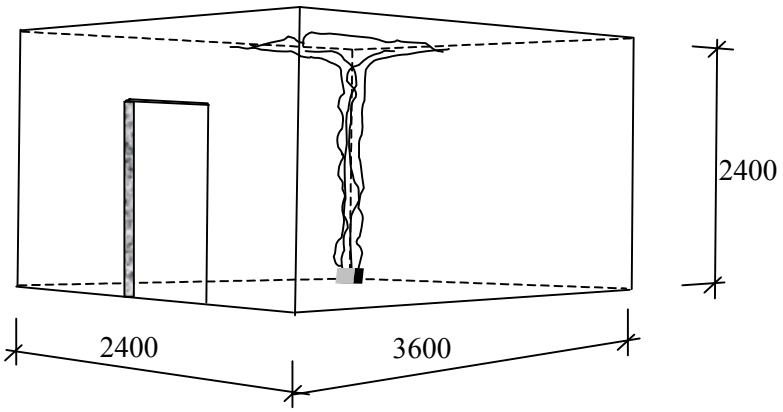

Figure 18. Sketch of the enclosure. The ceiling and the walls (except for the door-wall) have a wooden lining.

* These values are derived on the basis of an incident heat flux of 50 kW/m^2 in the Cone Calorimeter.

The fire growth is largely governed by the flame spread under the ceiling. The solid material behind the initial burner flame is assumed to ignite instantaneously after a period of time corresponding to the time to ignition. Flame spread on the wall surfaces is not further considered, however, the area between the ceiling and the initial flame tip being omitted in the fire growth calculations. The contribution of the side walls is neglected in the calculations because of the difficulties in calculating the heat exposure, doing so basically needs computerised numerical methods.

The course of the flame spread can thus be divided into three distinct periods of time and the events associated with them:

1→2: the initial fire (burner)
2→3: the wall surfaces behind the burner flame being ignited
3→ flashover: the flame front propagating under the ceiling.

This course of events can be represented mathematically by use of the equations given below[39]:

1. time<τ $\dot{Q}_{tot}(t) = \dot{Q}_b$ [32]

2. τ<time<2*τ $\dot{Q}_{tot}(t) = \dot{Q}_b + \dot{Q}''_{\max} A_{wall} e^{-\lambda(t-\tau)}$ [33]

3. time>2*τ $\dot{Q}_{tot}(t) = \dot{Q}_b + \dot{Q}''_{\max} A_{wall} e^{-\lambda(t-\tau)} + \dot{Q}_{ceiling}\left(t - 2\tau\right)$ [34]

where A_{wall} is the area of the wall behind the initial burner flame, the RHR contribution of the lining material of the ceiling being calculated using

$$\dot{Q}_{ceiling}(t) = A_0 \dot{Q}''_{\max} e^{-\lambda t} + \int_0^t \dot{Q}''_{\max} e^{-\lambda(t-t_p)} V(t_p) dt_p \quad [35]$$

$$A_0 = K\left(\dot{Q}_b + A_{wall}\dot{Q}''_{\max} e^{(-\lambda t)} - 150\right) \quad [36]$$

Figure 19 shows the moment when the ceiling has been ignited, at the time $t = 2*\tau$.

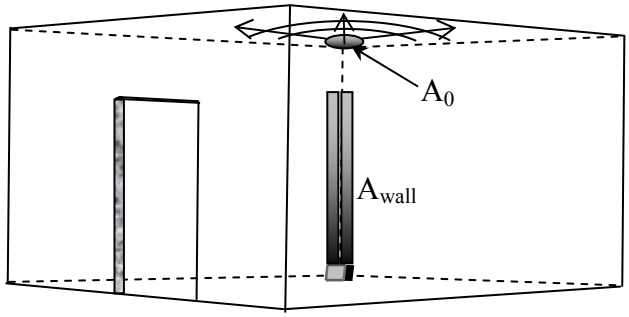

Figure 19. The burning pattern upon ignition of the ceiling. Transient flame spread takes place under the ceiling only, the combustible sidewalls thus being practically ignored in the calculations.

In Equation [36], the terms within the brackets can be interpreted as the rate of heat release emanating from the flames that reach beyond the ceiling. The value "150" is a constant provided by Karlsson[28]. It denotes the RHR required for the flames to reach the ceiling. Since the heat release from the wall lining decreases over time, the exposed ceiling area, A_0, also decreases continuously from a maximum value. Thus, the choice of initial burning area under the ceiling may be subject to some debate. In the present calculations the smallest area, one corresponding to $A_0 = A_0(2\tau)$, is employed.

Whereas the first two periods, 1 and 2, are rather straightforward to deal with mathematically, the third period requires special attention. Equation [35] contains a convolution integral that cannot be solved directly but is suitably converted to a solvable set of equations, using Laplace transforms. Such an operation results in the following two analytical equations which are complementary:

For $\left(1-\sqrt{K\dot{Q}''_{\max}}\right) < \lambda\tau < \left(1+\sqrt{K\dot{Q}''_{\max}}\right)$

$$\dot{Q}_{ceiling}(t) = A_0\dot{Q}''_{\max}e^{-\lambda t} + \frac{C_1}{s_2 - s_1}\left[\frac{s_2\dot{Q}''_{\max}\left(e^{s_2 t} - e^{-\lambda t}\right)}{s_2 + \lambda} - \frac{s_1\dot{Q}''_{\max}\left(e^{s_1 t} - e^{-\lambda t}\right)}{s_1 + \lambda}\right] \quad [37]$$

and for $\left(1-\sqrt{K\dot{Q}''_{\max}}\right)^2 < \lambda\tau < \left(1+\sqrt{K\dot{Q}''_{\max}}\right)^2$

$$\dot{Q}_{ceiling}(t) = A_0\dot{Q}''_{\max}e^{-\lambda t} + C_1C_2\dot{Q}''_{\max}\left[e^{K\dot{Q}''_{\max}t}\left(\cos(\beta t) + \frac{C_3}{\beta}\sin(\beta t)\right) - e^{-\lambda t}\right] \quad [38]$$

The constants C_1-C_3 are short for the following relationships:

$$C_1 = \frac{K\dot{Q}''_{\max}A_0}{\tau}$$

$$C_2 = \left[\frac{1}{\lambda}\left(\alpha^2 + \beta^2\right) + 2\alpha + \lambda \right]^{-1}$$

$$C_3 = \frac{1}{\lambda}\left(\alpha^2 + \beta^2\right) + \alpha$$

s_1-s_2 being the roots obtained using Equation [11].

In practice, this calculation should not be performed in any other way than by use of a computer program, even a simple spreadsheet being satisfactory enough for this purpose. Below, one time step, t = 80 seconds, is evaluated by use of hand calculations.

Calculating the roots of Equation 11, $s^2 + \frac{1-\mathrm{a}+\lambda\tau}{\tau}s + \frac{\lambda}{\tau} = 0$ results in

$$\mathrm{s}_{1,2} = -\frac{1}{2\tau}\left(1-\mathrm{a}+\lambda\tau\right) \pm \sqrt{\Delta} \quad \text{, with } \Delta = \frac{1}{4\tau^2}\left(1-\mathrm{a}+\lambda\tau\right)^2 - \frac{\lambda}{\tau}$$

hence,

$\mathrm{s}_1 = 0.0038$
$\mathrm{s}_2 = 0.0542$

The initial burning area of the ceiling, A_0, is estimated as

$$A_0 = 0.02\left(100 + \underbrace{2*0.17*1.96}_{A_{wall}} * 168 * e^{-0.0075*(36*2)} - 150\right) = 0.306 \ \mathrm{m}^2$$

Here the burning of the sidewalls, along a distance corresponding to the burner-flame height is set to 1.96 meters. A value obtained using the relation $L_f = 3.0D\left[\frac{\dot{Q}}{\rho_\infty c_p T_\infty D^{5/2} g^{1/2}}\right]^{2/3}$, describing the flame height of continuous flames, as reported by Hasemi and Tokunaga[42]. Their correlation for the highest flame tip in a scenario was obtained using a factor of 4.3 instead of 3.0 in the flame-height equation. This yields a flame height of $L_f = 2.6$ meters[*]. The value $\rho_\infty c_p$ is obtained using the values for air at the reference temperature, T_∞, D being taken as an equivalent diameter based on the burner area.

The RHR contribution from the lining material in the ceiling can be calculated on the basis of Equation [37], using a constant C_1, evaluated as

[*] This value is similar, but still somewhat lower than that used by Karlsson[28], the flame height at 150 kW ending up at 2.57 meters. A justification for choosing the lower value is that a very high incident heat flux has been assumed, 50 kW/m^2.

$C_1 = \frac{0.02*168*0.306}{36} = 0.0286$, which then gives

$$\dot{Q}_{ceiling}(80-2*36) = 0.2*168e^{-0.0075*8} +$$
$$+\frac{0.0286}{0.0542-0.0038}\left[\frac{0.0542*168\left(e^{0.0542*8}-e^{-0.0075*8}\right)}{0.0542+0.0075}-\frac{0.0038*168\left(e^{0.0038*8}-e^{-0.0075*8}\right)}{0.0038+0.0075}\right] = 96 \text{ kW}$$

To sum up, the total rate of heat release 80 seconds after burner ignition can be calculated according to Equation [34] as the sum of the three fire sources: burner, walls and ceiling linings

$$\dot{Q}_{tot}(80) = 100 + 168*0.67e^{-0.0075(80-36)} + 96 = 276 \text{ kW}$$

Evaluating other time-steps allows one to construct a graph, akin to the one presented in Figure 21, which represents a summation of three different heat release sources, as shown in Figure 20.

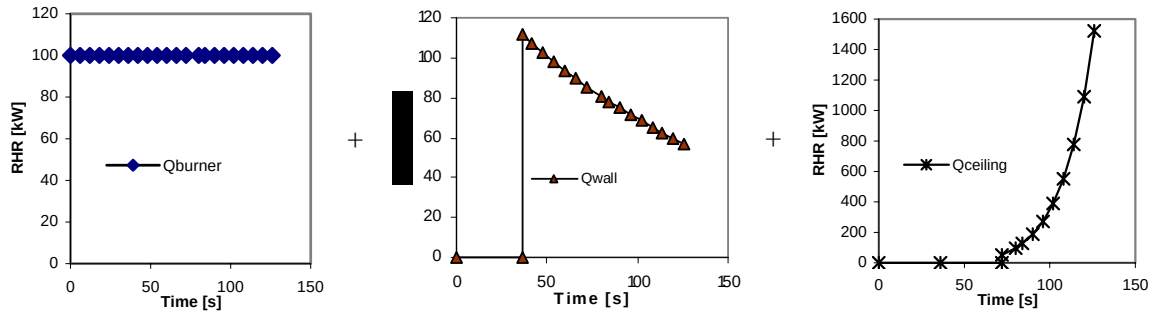

Figure 20 Contribution to the heat release rate of the different components. A comparison between the summation and the experimental data is shown in Figure 21.

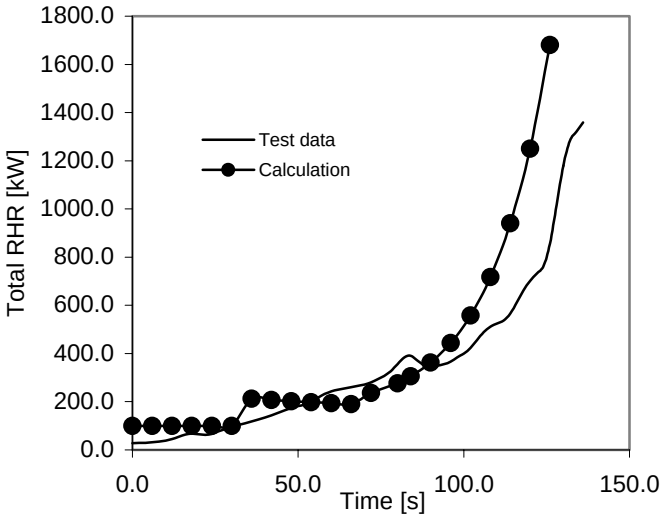

Figure 21 Fire growth in the combustible lining of a room as calculated using Equation [32]-[34].

In the example above, the incident heat flux is assumed to be constant at 50 kW/m^2 on surfaces that are directly exposed to flames. Both measurements and numerical modelling indicate that normally the heat flux is not constant over the flame height and is not as high as 50 kW/m^2. The effect of using an excess heat flux can be counteracted somewhat, however, by neglecting all preheating beyond the flame tip and excluding the majority of the side walls from the calculation*.

3.5 Conclusions and practical considerations

Karlsson[28] used the analytical upward-flame-spread modelling methodology discussed earlier in this section, evaluating the results for a variety of different materials. He conducted rather thorough investigations, optimising the model for two enclosure-fire scenarios, using the Room Corner Test. The first scenario had a combustible lining fixed to the ceiling and to three walls of the fire compartment, whereas in the second scenario the combustible lining materials were attached to three walls only. The final results correlated well with the experimental data, except for a few materials, such as the melamine-faced particleboard and the expanded polystyrene.

Several researchers have used identical or similar methodologies and solved a set of simplified flame-spread equations using different numerical approaches. The model presented here has been modified somewhat, for example so as to account more directly for the burnout of the combustible material. Different versions of it have also been implemented in zone models. Nevertheless, due to the model's underlying assumptions, it is rather non-flexible, scenario-dependent and sensitive to input, most of the input being treated as representing lumped parameters despite the fact that in practice they can demonstrate highly non-linear dependencies. This makes it rather difficult to apply the model outside the scenarios for which it has been developed. Basically, one should not do so.

Nevertheless, the model may well prove to be a valuable, as yet untried tool for studying the basic course of flame spread. Estimates for different materials of whether flame spread will be accelerative at all times, or sometime decelerate as well, can be obtained along with qualitative approximations of the heat release by a burning lining material and the rate of flame spread on it. Nonetheless, the numerical result obtained should be handled with great care. Some scenarios can be evaluated directly, using the analytical relationships found here and a simple spreadsheet. Since this may become rather awkward in the long run, however, a simple computer program can be required to perform the calculations needed.

Because of the negative aspects of this modelling approach, its limitations and the uncertainties connected with it, as well as the development of more flexible material models coupled to a general computer program for solving problems connected with the turbulent, reacting flow, rather little is to be expected from further development.

* It should be emphasised that since the model equations used and discussed here were specifically developed for this scenario, the choice of input data is not entirely an open issue.

4 Computational Fluid Dynamics

CFD (Computational Fluid Dynamics) is essentially a group of solution methods used to solve a set of non-linear partial differential equations derived from basic laws of nature, including the conservation of mass, momentum, energy and chemical species. The resulting equations describing the fluid flow are known as the Navier-Stokes equations. Thus far, CFD concern the exact mathematical description of a fluid flow. However, since the governing equations for a turbulent reacting flow include phenomena that are too complex to be solved directly, a number of simplified submodels need to be added to complement the original transport equations, including models to predict turbulence, combustion, radiation and wall effects. This is where the calculations abandon exactness and leave it to the engineer to attempt to imitate reality in the best possible way.

4.1 Numerical methods

By use of the Cartesian tensor notation*, the transport equations governing fluid flow can be summarised, for an arbitrarily dependent variable ϕ, as follows[43]:

$$\frac{\partial}{\partial t}(\rho\phi)+\frac{\partial}{\partial x_i}(\rho u_i\phi)=\frac{\partial}{\partial x_j}\left(\Gamma_{ij}\frac{\partial\phi}{\partial x_i}\right)+S_\phi \qquad [39]$$

This equation can be expressed in words as

[accumulation (or change in time) of ϕ] + [convective transport of ϕ]
= [diffusion of ϕ] + [production or destruction of ϕ]

The general procedure is to transform the continuous problem, as described by Equation [39], into a discrete problem by splitting the computational domain into a number of small elements or control volumes and discretising the differential equations on these volumes to obtain a solvable set of algebraic equations. These equations are commonly expressed in the form

$$a_P\phi_P=\sum_{NB}a_{NB}\phi_{NB}+b \qquad [40]$$

where a is a constant, b represents the source term, P is the current node and NB denotes the adjacent grid nodes.

* The tensor notation is very useful since it allows the entire three-dimensional equation to be presented although in a condensed way. Examples: $\text{grad}\ \phi=\frac{\partial\phi}{\partial x}+\frac{\partial\phi}{\partial y}+\frac{\partial\phi}{\partial z}=\frac{\partial\phi}{\partial x_i}$ or $\text{div U}=\frac{\partial u}{\partial x}+\frac{\partial v}{\partial y}+\frac{\partial w}{\partial z}=\frac{\partial u_i}{\partial x_i}$. The basic nomenclature used in defining a scalar as a zero-rank tensor and a vector as a first-rank tensor, involves calling a second-rank tensor simply a tensor.

In fact, Equation [39] has basically no analytical solution, at least not for practical problems. However, the numerical solution, using here the "finite volume method", can be derived using rather simple means of approximation. Employing a one-dimensional example, as shown in Figure 22, and integrating Equation [39] over the control volume confined by the points *w* (west face) and *e* (east face) yields a spatially discretised equation for the nodal value, P, in the form:

$$\frac{\partial}{\partial t}(\rho\phi\Delta x)+\left[\rho u\phi\right]_e-\left[\rho u\phi\right]_w=\left[\Gamma A\frac{\partial\phi}{\partial x}\right]_e-\left[\Gamma A\frac{\partial\phi}{\partial x}\right]_w+\overline{S}_\phi\Delta x \qquad [41]$$

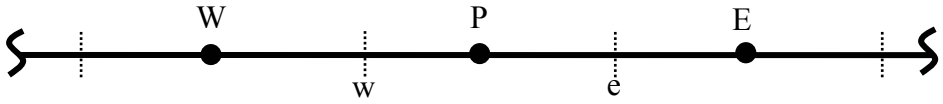

Figure 22 An illustration of a one-dimensional grid. The grid spacing does not have to be uniform, completely uniform grids, in fact, being rarely encountered.

The basic idea of using the finite volume formulation (as well as the finite difference method) is that this allows the dependent variables to be calculated and stored in the grid points[*]. The task of finding the face values of the convective term, as well as the diffusivity coefficient and the gradient of the dependent variable over the cell face then becomes an issue of interpolation between nodal values and their faces. Several interpolation schemes of varying accuracy and complexity have been presented. The tendency followed by the CFD community has been to give priority to simplicity, stability and speed before accuracy, approximations being first and second order accurate thus still being those most widely used.

Since in Equation [41] the rate-of-change term still includes the time derivative, the equation needs to be integrated over a time step, Δt. The two most widely recognised approaches in accounting for the time dependence here are the fully explicit and the fully implicit method, the former using only those values of the variables that were obtained from the previous, or "old", time step and the latter using only values from the new time step ($t+\Delta t$). The Crank-Nicolson method is a scheme that weights the old (earlier time-step) and the new (present time-step) values equally. Which method is best to use depends on the time scale the modeller needs to resolve.

If the transient flow equations have been discretised using the explicit method, the resulting equations are not coupled in space. Since all variables are known from the last time step, the equations can be solved analytically making the solution a very fast one. However, the usefulness of this approach is limited by the need of satisfying a numerical stability criterion effectively putting a tough constraint on the length of the time step:

[*] Although this is true for the scalar variables, it does not apply to the velocity components (the momentum equations), which are calculated and saved at the cell faces. This is known as a "staggered grid" solution.

$$\Delta t < \frac{1}{\frac{2\Gamma}{\rho(\Delta x)^2} + \frac{u}{\Delta x}} \qquad [42]^*$$

The implication of this criterion is that a particle, or fluid package, entering one side of the control volume is not allowed to exit on the other side during that same time step. If diffusion is negligible, this simplifies to $\Delta t < \frac{\Delta x}{u} = \frac{1}{C}$, where C is known as the Courant number.

On the other hand, using an implicit approach in discretising the time derivative provides an unconditionally stable solution, irrespective of the length of the time step. Thus, if the time scale of a phenomenon is large, the implicit method seems to be the way to proceed. The drawback of the method is that all the variables (fluxes and source terms) are evaluated on the basis of unknown variable values. This makes it necessary to solve a large number of, coupled, equations iteratively for each time step.

The discretisation process provides a number of linear algebraic equations of the same type as Equation [40], which can be represented in the form of large matrices for each variable. However, provided that the discrete equations for a grid point do not contain dependencies with other cells than those that are its direct neighbours[†], all the non-zero coefficients in a 1-D matrix for a align quite nicely in three diagonals. This behaviour makes Gaussian elimination particularly simple and fast to perform. The most common solution technique, which makes use of the appealing form of the matrices, is the TDMA (TriDiagonal Matrix Algorithm) also known as the Thomas algorithm. This approach turns out, in fact, to be a procedure that provides a direct solution to the one-dimensional case. If the problem involves two or three dimensions, however, the TDMA must be used in a line-by-line fashion in an iterative procedure.

4.2 Modelling the effects of turbulence

In nearly all fire scenarios of interest, the gas flow is turbulent by nature, characterised by random, highly fluctuating rotational movements in three dimensions. This seemingly chaotic flow consists of vortices, or eddies, on scales of differing length, the largest eddies generated by instabilities in the main flow being broken down into smaller and smaller scales in a process known as the "turbulent energy cascade". The size, or scale, of the largest eddies is generally referred to as the integral length scale. It is related to the geometry and the boundary conditions of the scenario. The smallest structures that can be sustained in the turbulent flow field, on the other hand, are given by limitations which originate from viscous dissipation. These are called Kolmogorov micro-scale eddies. At this length scale, the turbulent cascade ends and energy from all the remaining (Kolmogorov) eddies are dissipated as heat.

[*] This equation describes the stability criterion employing the upwind interpolation scheme.
[†] This is dependent upon the interpolation scheme employed. If such schemes as the central differencing, hybrid or power-law are used, this is a valid limitation.

The conservation equations that describe the turbulent flow, including the energy transfer from the larger to the smaller scales, can be modelled exactly on a very fine grid. This involves the 3d-Navier Stokes equations being solved directly the effects caused by turbulence being included. This is achieved by use of a methodology termed Direct Numerical Simulation, DNS[*]. In order to calculate all of the turbulent motion DNS must resolve all the time and length scales of the flow. This means that the control volumes must be of the same order of size as the Kolmogorov length scale[†]. The immense computational resources required make this approach quite impossible to use for all but very small problems of low Reynolds number.

To capture the effects of the turbulence in a flow field, the engineer is thus referred instead to one of several modelling techniques available, varying in their degrees of sophistication. The most popular (and time saving) approach is to regard the turbulent flow as being composed by a random fluctuation superimposed on a mean, averaged flow, such as

ϕ (instantaneous value) $= \tilde{\phi}$ (mean component) $+ \phi''$ (fluctuating component).

Using this decomposition of the flow into turbulent fluctuation and mean flow allows the governing equations to be rewritten so as to describe the main averaged flow, this being the part of the equations that can be solved directly, using additional terms for the fluctuating part that needs to be modelled, see Equation [43]. This approach is known as Reynolds Averaged Navier-Stokes simulation, RANS, and the added terms, describing the influence of the turbulence on the dependent variables, being known as Reynolds stresses (the second term in the parentheses on the right hand side of Equation [43]).

$$\frac{\partial}{\partial t}\left(\bar{\rho}\tilde{\phi}\right)+\frac{\partial}{\partial x_i}\left(\bar{\rho}\,\tilde{u}_i\tilde{\phi}\right)=\frac{\partial}{\partial x_j}\left(\bar{\rho}\Gamma_{ij}\frac{\partial\tilde{\phi}}{\partial x_i}-\bar{\rho}\,\overline{u_i''\phi''}\right)+\bar{S} \qquad [43]$$

4.2.1 The standard k-ε turbulence model

One of the most widely used RANS turbulence models is the standard k-ε model, originating from the work of Jones and Launder[44]. In this model, two additional transport equations, one for the kinetic energy of the local fluctuating motion, $k=\frac{1}{2}\overline{u_i'u_i'}$, and the other for the rate of

[*] This would imply that the turbulent motion is not entirely chaotic and random but still follows the basic laws of nature as described by the Navier-Stokes equations. Put differently, DNS may not be an exact description of the turbulent flow itself but is a direct numerical simulation of the Navier-Stokes equations and the related initial and boundary conditions. Thus, if the NS equations provide an exact description of the turbulence, DNS does so as well.

[†] To obtain an understanding of the length and time scales, consider the DNS of an air stream of normal ambient temperature flowing at a velocity of 10 m/s. The Kolmogorov length scale can be approximated by $\eta \sim l^{1/4}(u/\upsilon)^{-3/4}$, where l is the integral length, in the present example say l = 0.1 m, resulting in a Kolmogorov scale of the order of 10^{-5} m and the time scale of 10^{-6} s. This can be compared with what is used in the much simpler Reynolds averaged simulation of a large-scale fire in which computer resources often set a limit at about 0.1 meter and multiples thereof.

dissipation of the kinetic energy in the turbulent flow, $\varepsilon = \nu \overline{\frac{\partial u_i'}{\partial x_k} \frac{\partial u_i'}{\partial x_k}}$, are derived and solved to determine the local "turbulent viscosity", $\mu_t(x, y, z, t)$, which is used to relate the effects of the turbulent fluctuations of a dependent variable to its mean gradient.

Using Cartesian tensor notation, the additional transport equations for turbulent kinetic energy and its dissipation rate as used in standard high-Reynolds k-ε modelling are written as[44]

$$\frac{\partial(\bar{\rho}k)}{\partial t} + \frac{\partial(\bar{\rho}\tilde{u}_i k)}{\partial x_i} = \frac{\partial}{\partial x_j}\left(\mu_{lam}\frac{\partial k}{\partial x_i} + \frac{\mu_t}{\sigma_k}\frac{\partial k}{\partial x_i}\right) + P + G - \bar{\rho}\varepsilon \qquad [44]$$

$$\frac{\partial(\bar{\rho}\varepsilon)}{\partial t} + \frac{\partial(\bar{\rho}\tilde{u}_i \varepsilon)}{\partial x_i} = \frac{\partial}{\partial x_j}\left(\mu_{lam}\frac{\partial \varepsilon}{\partial x_i} + \frac{\mu_t}{\sigma_\varepsilon}\frac{\partial \varepsilon}{\partial x_i}\right) + c_{\varepsilon 1}\frac{\varepsilon}{k}(P+G)(1+c_{\varepsilon 3}R_f) - c_{\varepsilon 2}\bar{\rho}\frac{\varepsilon^2}{k} \qquad [45]^*$$

The terms, taken from left to right, describe the scalar rate of change, followed by transport through convection and transport through diffusion, the terms P and G representing turbulence production through turbulent shear stresses and buoyancy, the last terms concerning the destruction (dissipation) of k and ε, respectively. These equations are valid for flows of high Reynolds number. Their counterparts in low Reynolds-number modelling are very similar, but contain damping factors to counteract the advantage of the viscous stresses over the turbulent Reynolds stresses when Re is small, for example, in the boundary layer near the wall.

$P = -\overline{u_i'' u_j''}\frac{\partial \tilde{u}_i}{\partial x_j} \rightarrow (\text{Boussinesq}) = \mu_t\left(\frac{\partial \tilde{u}_i}{\partial x_j} + \frac{\partial \tilde{u}_j}{\partial x_i}\right)\frac{\partial \tilde{u}_i}{\partial x_j}$,

$G = -\beta g \overline{u_i'' T''} \rightarrow (\text{Boussinesq}) = \beta g \frac{\mu_t}{\sigma_k}\frac{\partial \tilde{T}}{\partial x_i}$, β is a thermal expansion factor calculated as $\beta = -\frac{1}{\bar{\rho}}\frac{\partial \bar{\rho}}{\partial \tilde{T}}$,

R_f is the flux Richardson number relating the rate of energy change due to buoyancy and to shear stresses, originally written as $R_f = -\frac{G}{P}$. However, since the buoyancy forces act only in the vertical direction, the term $c_{\varepsilon 3}R_f$ should vary depending on the direction of the shear flow. A modified Richardson number proposed by Rodi (1978)[46] distinguishes between horizontal shear layers, in which the lateral velocity component is in the direction of gravity

* This equation is a model equation, one not derived from first principles. The relation between the turbulent kinetic energy, its dissipation rate and a turbulent mixing length, $\varepsilon = \frac{k^{3/2}}{l}$, is based purely on dimensional arguments.

$$R_f = -\frac{G}{G+P}$$

and vertical shear layers, in which the lateral velocity vector is normal to gravity

$$R_f = 0$$

The resulting equation system, which describes the averaged turbulent flow, can be closed by using an eddy viscosity concept to relate the Reynolds stresses to the turbulent viscosity and the gradient of the mean flow as shown in Equations [46] and [47]*.

$$-\overline{\rho u_i'' u_j''} = \mu_t \left(\frac{\partial \tilde{u}_i}{\partial x_j} + \frac{\partial \tilde{u}_j}{\partial x_i} \right) - \frac{2}{3} \delta_{ij} \overline{\rho} k \quad \text{(Reynolds stress tensor)} \qquad [46]$$

$$-\overline{\rho} \widetilde{u_j'' \phi''} = \Gamma_t \frac{\partial \tilde{\phi}}{\partial x_j} \quad \text{(Turbulent scalar flux; } \phi \text{ denotes for example enthalpy or species concentration)} \qquad [47]$$

where $\Gamma_t = \frac{\mu_t}{\sigma_t}$ is the turbulent diffusivity for ϕ, and σ_t is the turbulent Prandtl or Schmidt number.

The turbulent viscosity, μ_t, is assumed to be isotropic in nature, i.e. to take on the same value for all $\overline{u_i' u_j'}$:

$\mu_t = c_\mu \overline{\rho} \frac{k^2}{\varepsilon}$, where c_μ is a model constant. [48]

This variable can be used then to close the equation system created by Eq. [44]-[47]. The isotropy assumption inherent in the Boussinesq hypothesis may provide unsatisfactory results, especially in the case of complex 3d-scenarios such as swirling flows. Consequently, several models referred to as anisotropic eddy-viscosity models have been proposed for eliminating the shortcomings of the original formulation. None of these have found wide-spread use.

A total of six empirical or "tuning" constants are included in the standard Re k-ε model. Although their numerical values should not be taken to be universally applicable, they have been shown to provide reasonable predictions also for strong buoyant flows.[47]

* This is similar to the procedure used in calculating the internal friction in a laminar flow, by use of the laminar viscosity and the flow gradient, $\tau = \mu_{lam} \frac{\partial u}{\partial x}$. Yet the turbulent viscosity is several orders of magnitude larger than the laminar viscosity of a gas, effectively making a fully turbulent flow comparable to the (laminar) viscosity of olive oil (at room temperature). In addition, the turbulent viscosity is a property of the flow, whereas the laminar viscosity is determined by the molecular composition of the fluid and thus is a property of the fluid itself. A similar comparison can be made of molecular diffusion to its turbulent counterpart in scalar transport.

σ_k=1.0, σ_ε=1.3, $c_{\varepsilon 1}$=1.44, $c_{\varepsilon 2}$=1.92, $c_{\varepsilon 3}$=0.8*, c_μ=0.09

The application of the standard k-ε model to a buoyant plume encounters problems in predicting the spreading rate of a vertical plume which controls the entrainment of air. Comparisons with experiments have shown there to be under-prediction by as much as 30 percent in a free buoyant plume[48], which strongly affects the predictions of temperature and velocity. This is particularly important for the flame spread models since the plume-centreline temperature and velocity both can be expected to be overpredicted thus affecting the resulting heat exposure. Further, from comparisons of ceiling-jet temperatures between computations and measurement, one finds that the k-ε model generally tends to overpredicts the horizontal entrainment.

Both SMAFS[49] and SOFIE[50] CFD codes include the *k-ε* turbulence model modified so as to include additional terms concerning buoyancy production and gradient diffusion†.

4.2.2 A note on LES

Another turbulence modelling technique that is now gaining increasing interest on the part of CFD community, fire safety applications included, is the Large Eddy Simulation approach, LES. Unlike the Reynolds averaging methodology, with its focus on the statistical properties of the flow, LES divides the turbulent flow field by length scale, employing a "filter" to remove the smallest structures, called the subgrid-scale components, from the general transport equations. The computational grid is made sufficiently small to resolve a range of scales, from the large geometry-dependent vortices down to some point within the turbulence inertial subrange. These scales are calculated explicitly from the Navier-Stokes equations. The effects of the smaller scales, which are essentially unaffected by the geometry, are modelled using a Sub-Grid Scale, SGS, model[51]. Whereas the RANS-based CFD codes are unable to elucidate the random motions associated with turbulence and its rotational vortices, the LES methodology is capable of providing a description of the instantaneous overall movements of the fluid.

In connection with LES, it can also be appropriate to introduce the Taylor microscale, which is a scale of intermediate length on the eddy scale continuum, its being located somewhere within the inertial subrange in between the integral and the Kolmogorov scales. This intermediate scale is generally assumed to provide an adequate estimate of the resolution required in a Large Eddy Simulation of turbulence. Using this approach, the number of grid points required to properly resolve a three-dimensional flow-field by use of LES can be estimated as[52]

* This value can be used, provided that the modified flux Richardson number approach according to Rodi[46] is employed. Otherwise, the value of $c_{\varepsilon 3}$ should vary between zero and unity, depending on which flow components are considered.

† Recently, LES capabilities were included in SMAFS, both codes also including several modelling approaches, such as k-ω and low-Re models.

$$N_{ls} \sim \left(\frac{Integral\ scale}{Taylor\ microscale} \right)^3 \sim Re^{3/2}$$

Within a short period of time, the CFD code FDS[53], Fire Dynamics Simulator, has gained considerable popularity among fire modellers worldwide. The code is based on the LES approach. It can be questioned, however, whether the simulations presented in this study, as well as in most practical applications of the model, are truly LES, since the grid resolution is far too large to capture any of the inertial subrange. The very large domains normally dealt with in fire safety applications make the use of extremely large control volumes understandable despite its being possible to question the generality of such calculations. The subgrid scale stress tensor, present in the momentum equation in the LES equations, is modelled by use of the widespread eddy viscosity based analysis proposed by Smagorinsky.[54,55]

4.2.3 Modelling the effects of wall flows

The buoyancy driven turbulent flow is slowed down in a boundary layer near the walls due to wall friction. This induces steep gradients in terms of turbulent viscosity and velocity, since the instantaneous velocity components are zero at the solid boundaries[*]. Temperature and enthalpy gradients are also generated, due to the difference between the solid- and gas-phase temperatures. To capture these gradients in a numerical simulation, the transport equations would need to be integrated through the entire wall boundary layer, including the laminar viscous sub-layer closest to the wall[†]. Very small control volumes are required for this task, so small that the cost in computational time is too great for most practical scenarios.

In the standard k-ε turbulence model, the influence of the solid boundaries on the fluid flow is commonly approximated by use of different semi-empirical correlations called wall functions. These are applied to the first fluid grid node adjacent to the wall surface, effectively providing the boundary conditions for the flow and turbulence equations and eliminating the task of integrating the equations all the way down to the wall.

One widely used approach serving as a complement to the k-ε model is the "law of the wall"[56] approach. The relationship is summarised in Figure 23 and is described mathematically in Equation [49].

$$u^+ = f\left(y^+\right) \qquad [49]$$

[*] This is referred to as a no-slip condition, referring simply to the condition that *u, v and w* = 0 at the wall surface or more generally, that (*u,v,w*) = wall-boundary velocity.

[†] It can be shown, however, that the high-Re k-ε model equations are not valid within this part of the boundary layer in which molecular viscosity plays a dominant role. This is a major argument against this model and for alternative turbulence models, such as the low-Re k-ε and the k-ω models (which will be considered later).

where u^+ is a dimensionless velocity related to the wall shear stress and the density of the fluid flow, $u^+ = u\left(\frac{\tau_s}{\rho}\right)^{-1/2} = \frac{u}{u^*}$, $u^* = \sqrt{\frac{\tau_s}{\rho}}$ is termed the friction velocity and y^+ is the dimensionless distance between the surface interface and the wall-adjacent node defined by

$$y^+ = \frac{u^* y}{\upsilon} \qquad [50]$$

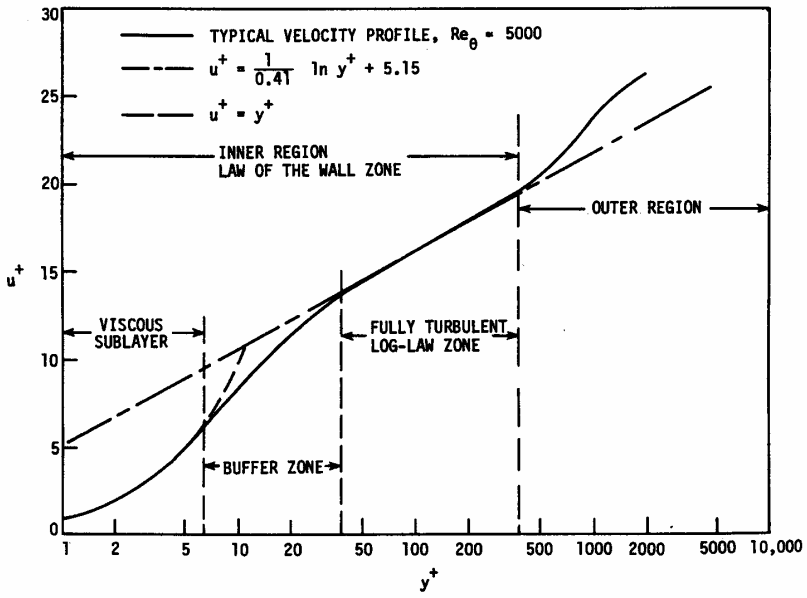

Figure 23. Typical velocity profile in a turbulent boundary layer (from ref 57).

At short distances from the wall, wall friction is dominated by viscous shear forces, measurements in the boundary layer suggesting the linear relationship

$$u^+ = y^+ \qquad [51]$$

The scale of the viscous sublayer closest to the wall is dependent upon the roughness of the wall surface. For a smooth surface, $y^+ < 11.63$ is usually employed as a limiting distance. The grid node to which the wall functions are applied is normally presumed to lie somewhere within the log layer, typically in the range of $30 < y^+ < 500$. The velocity, known to follow the law of the wall, its being assumed that there is no mass transfer or pressure gradient through the boundary layer, can be written as

$$u^+ = \frac{1}{\kappa}\ln\left(Ey^+\right) \qquad [52]$$

where κ is the von Karman constant, derived experimentally to be about 0.42, and E represents the effects exerted by the roughness of the surface. For smooth surfaces, the value of E is taken to be about 9.8, although the data for practical materials is scarce.

If it can be assumed that the turbulent flow is in local equilibrium and that the turbulence production is equal to the dissipation in the point where the wall functions are being applied (in the log law region), the wall shear stress can be shown to be a function of the fluid density and of the local turbulent kinetic energy:

$$\tau_s = \mu_t \frac{\partial u}{\partial y} = \frac{c_\mu^{1/4} \rho k^{1/2} u}{u^+} \qquad [53]$$

Inserting this relationship into the equations for non-dimensional velocity and the wall-to-fluid node distance, one obtains

$$y^+ = \frac{\rho k^{1/2} C_\mu^{1/4} y}{\mu} \qquad [54]$$

In flame-spread modelling, pyrolysis gases may leave the transpiring wall boundary and add a mass flow across the boundary layer. This calls for special adaptations of the wall functions and the addition of the dimensionless mass flow rate, $m^+ = \frac{\dot{m}_s''}{\sqrt{\tau_s \rho}}$.

The non-dimensional equations employed in wall function boundary-layer modelling involving a finite mass loss from the wall surface are reproduced below[49].

The laminar flow wall functions for mass injection into the boundary layer are

$$u^+ = \frac{\exp\left(m^+ y^+\right) - 1}{m^+} \quad \text{velocity} \qquad [55]$$

$$\varphi^+ = \frac{\exp\left(\sigma_{\mathrm{Sc/Pr},l} m^+ y^+\right) - 1}{m^+} \quad \text{scalar variable such as } \mathrm{h}^+ \text{ (enthalpy) or } \mathrm{Y}^+ \text{ (species)} \qquad [56]$$

Without mass injection, the equations reduce to

$$u^+ = y^+ \qquad [57]$$

$$\varphi^+ = \sigma_{\mathrm{Sc/Pr},l} y^+ \qquad [58]$$

The turbulent flow wall functions involving mass injection are written as

$$u^+ = \frac{1}{\kappa} \ln\left(E y^+\right) + \frac{1}{4\kappa^2} m^+ \left(\ln\left(E y^+\right)\right)^2 \qquad [59]$$

$$\varphi^+ = \frac{\exp\left[\sigma_t \left(\ln\left(1 + m^+ u^+\right) + m^+ P\right)\right] - 1}{m^+} \qquad [60]$$

Without mass injection, the equations become

$$u^+ = \frac{u}{c_\mu^{1/4} k^{1/2}} \quad [61]$$

$$\varphi^+ = \sigma_t \left(u^+ + P \right) \quad [62]$$

In the equations above, σ_t and $\sigma_{Pr,l}$ represent the turbulent and the laminar Prandtl number respectively, and σ_{Sc} is the Schmidt number. The parameter P is a function of the ratio $\sigma_{laminar} / \sigma_{turbulent}$, called the pee-function. It is actually an integration constant. Unfortunately, when mass injection into the boundary layer is present, the pee-function also shows a certain dependence on m^+ and u^+. The same applies for E, which is a constant when m^+ is zero, but at finite m^+ has a dependence on both the shear stress and the rate of mass injection in a way that has not been fully investigated. [58]

If the first grid node is within the log-layer and the wall functions referred to above are applicable, the wall shear stress is calculated from Equation [53] and the convective heat transfer coefficient from

$$h_{conv,coeff} = \frac{\rho u^* c_{p,fluid}}{h^+} = \frac{\rho c_\mu^{1/4} k^{1/2} c_{p,fluid}}{h^+} \quad [63]$$

The resulting convective heat transfer to the wall surface is calculated using

$$\dot{q}''_{conv} = h_{conv,coeff} \left(T_P - T_{wall\ surface} \right) \quad [64]$$

A wall function approach for evaluating the wall effects can also be used in LES analysis, although this is usually not necessary, since a grid size less than or equal to the Taylor microscale would resolve the boundary layer in any case. In contrast, the CFD code FDS does not employ this concept but uses other empirical correlations for the wall flow. Convective heat transfer to the wall, for example, is calculated using the largest value for the free and the forced convection respectively,[55]

$$\dot{q}''_{convective} = \Delta T * \max \left[C \left| \Delta T \right|^{1/3}, 0.037 \frac{k \, \mathrm{Pr}^{1/3}}{L^{0.2}} \left(\frac{|\mathbf{u}|}{\nu} \right)^{0.8} \right] \quad [65]$$

4.2.4 Alternative turbulence models for RANS simulation

Ever since the early days of CFD the validity of the wall functions presented above has been discussed. For fire and flame-spread applications, complexities such as mass injection and chemical reactions in the boundary layer, buoyancy and pressure gradients add significantly to the uncertainty regarding the predictive capabilities of the general CFD models. However, the advantages in this approach, of its simplicity and of the task of the integration of the model equations though the boundary layer being avoided, have been reason enough to make it the preferred one in industrial, and to some extent, in applied research CFD.

Still, if a very accurate representation of the boundary layer flow and heat transfer is required, the wall function approach may not be the most advantageous method. A number of alternative turbulence models have been presented during the few last decades. These include, for example, variations of the k-ω model, the two-layer model and the low-Reynolds number k-ε model that are presented briefly below.

- **The k-ω model** is a two-equation turbulence model, involving the partial differential equations for the turbulent kinetic energy, k, and the specific dissipation rate, ω. How ω is defined and the relation between the eddy viscosity, μ_t, and k- ω differ somewhat from one model developer to another. Wilcox[56] has shown the predictive capabilities with use of the following equations to be good:

$$\frac{\partial(\bar{\rho}k)}{\partial t}+\frac{\partial(\bar{\rho}\tilde{u}_i k)}{\partial x_i}=\frac{\partial}{\partial x_j}\left(\mu_{lam}\frac{\partial k}{\partial x_i}+\frac{\mu_t}{\sigma_k}\frac{\partial k}{\partial x_i}\right)+\tau_{ij}\frac{\partial \tilde{u}_j}{\partial x_i}-\beta^*\bar{\rho}k\omega \qquad [66]$$

$$\frac{\partial(\bar{\rho}\omega)}{\partial t}+\frac{\partial(\bar{\rho}\tilde{u}_i \omega)}{\partial x_i}=\alpha\frac{\omega}{k}\tau_{ij}\frac{\partial \tilde{u}_j}{\partial x_i}-\beta\omega^2+\frac{\partial}{\partial x_i}\left(\mu_{lam}\frac{\partial \omega}{\partial x_i}+\frac{\mu_t}{\sigma_\omega}\frac{\partial \omega}{\partial x_i}\right) \qquad [67]$$

$$\mu_t=\bar{\rho}\frac{k}{\omega} \qquad [68]$$

  where α, β, β^*, σ_k, σ_ω are all semi-empirical closure coefficients (tuning parameters) and τ_{ij} is the Reynolds stress tensor. The length scale can be evaluated from $l=\frac{k^{1/2}}{\omega}$.

  A great advantage in using ω instead of ε as the determining equation for the turbulence scale is that the asymptotic behaviour of ω in the boundary layer is known in greater detail than the behaviour of ε, and that its boundary layer balance can be represented with high accuracy. Its capabilities in predicting boundary layer flows (with or without significant pressure gradients) are surpassed somewhat by the need for a fine grid close to the wall.

- **The two-layer model** combines the normal high-Re k-ε model with a one-equation model (for the turbulent kinetic energy).[59] The approach is to separate the boundary layer into two parts, the standard equations being used in the outer region and the one-equation model, together with algebraic expressions for the length scale (used for determining the dissipation rate and the turbulent viscosity), in the inner region, where the molecular viscosity is important. Norris and Reynolds[60] used the following algebraic relationships for the turbulent viscosity and dissipation rate respectively:

$$\mu_t=c_\mu\rho k^{1/2}l_\mu \qquad [69]$$

$$\varepsilon=\frac{k^{3/2}}{l_\varepsilon} \qquad [70]$$

where $l_\mu = \kappa c_\mu^{-3/4} y\left[1-\exp\left(-\frac{\rho k^{1/2} y}{A_\mu}\right)\right]$ and $l_\varepsilon = \frac{\kappa c_\mu^{-3/4} y}{1+\frac{5.3\mu}{k^{1/2} y}}$. A_μ = 50.5 is a damping constant and c_μ = 0.09 is the same constant as in the standard k- ε model.

- **Low-Reynolds k-ε number models** have been developed because of the non-universality of the empirical wall functions. The approach is to integrate the transport equations for all dependent variables (including k and ε) all the way through the boundary layer. In order to reduce the effects from the turbulent viscosity*, damping functions $f_\mu, f_{\varepsilon 1}$ and $f_{\varepsilon 2}$ are applied to the coefficients $c_\mu, c_{\varepsilon 1}$ and $c_{\varepsilon 2}$. The same terms as before are still found in the Equations [44], [45] and [48] but new coefficients $c_\mu f_\mu, c_{\varepsilon 1} f_{\varepsilon 1}$ and $c_{\varepsilon 2} f_{\varepsilon 2}$ being added.

  One of the most successful Low-Re models is that of Lam and Bremhorst[61], which employs the following damping functions:

$$f_\mu = \left(1-e^{-0.0165\frac{k^{1/2} y}{\nu}}\right)^2 \left(1+20.5\frac{\nu\varepsilon}{k^2}\right) \quad [71]$$

$$f_{\varepsilon 1} = 1+\left(\frac{0.05}{f_\mu}\right)^3 \quad [72]$$

$$f_{\varepsilon 2} = 1-e^{-\left(\frac{k^2}{\nu\varepsilon}\right)^2} \quad [73]$$

  Very close to the wall, f_μ is small and $f_{\varepsilon 1}$ is large, $f_{\varepsilon 2}$ also tending to zero since the exponent tends to zero. In the fully turbulent flow, however, all three functions take on a value close to unity and the equations reduce to those of the standard k-ε model.

4.4 Modelling chemical reactions (combustion)

Chemical kinetics has its own time and length scales, the phenomenon generally being much too complex and computationally expensive to be included, even in reduced form, in practical CFD simulations†. Instead, in most fire modelling codes, combustion is calculated from the mixing rates of fuel and oxidant. Chemical reactions between fuel and oxygen are taken to follow a single one-step stoichiometric reaction.

* An artificial way of reducing the (over)predicted turbulent stresses.

† The detailed reaction mechanisms are unknown in the case of most practical fuels. Yet even if all the details of these chain reactions were known, their implementation into a global model would be of little interest because of the computational cost.

$$\nu_{fu}\mathrm{Fu} + \nu_{ox}\mathrm{Ox} \rightarrow \nu_{pr}\mathrm{Pr}$$

The reaction is assumed to proceed infinitely fast, meaning that all mixtures of oxygen and fuel react instantaneously as they mix. Since the time scale of chemical reactions is much smaller than that of the general conservation equations, the assumption of fast chemistry does not normally place any restrictions on the calculations that are typical, i.e. well-ventilated fires. The methodology does fail, however, under special circumstances such as in ignition or extinction calculations as well as calculations involving species with "slow" chemistry, such as NO_x, carbon monoxide and soot.[62]

The Eddy Breakup model, first proposed for turbulent premixed flames by Spading in a 1971 paper[63], is one of the most widely used combustion models. It was later modified by Magnussen and Hjertager[64] into the so-called Eddy Dissipation Concept, EDC, in which the local rate of the chemical reactions is related to the turbulent mixing of fuel and oxidant through the breaking up of eddies. The primary model equation is reproduced in Equation [74], which evaluates the reaction rate on the basis of the lowest of the (turbulent) time mean mass fractions of either fuel or oxygen. The chemical reaction itself is regarded as being instantaneous. Clearly, the success of a combustion model of this sort is closely related to the performance of the turbulence model.

$$R_{fu} = -\bar{\rho}\frac{\varepsilon}{k}\min\left[A\bar{Y}_{fu} \quad , \; A\frac{\bar{Y}_{ox}}{s} \quad \right] \qquad [74]$$

where $A = 4$ is an empirical model constant, $\bar{Y}$ is the local mean mass concentration and $s = \frac{\nu_{ox}M_{ox}}{\nu_{fu}M_{fu}}$ is the stoichiometric coefficient of oxygen in the reaction equation describing the complete fuel conversion to CO_2 and H_2O of one kg of fuel.

In using this approach the reaction chemistry has been left aside and the combustion problem has been simplified to the computation of the mixing of fuel and oxygen, basically an extension of turbulence modelling. The analysis is further simplified by assuming that the diffusivities (Γ in Eq [47]) are equal for all the scalars, which implies that the mixing process is the same for all species. It is then natural enough to introduce a conserved scalar* in combustion modelling, generally by using the mixture fraction, ξ, relating the oxidant to the mass concentration of the fuel:

$$\xi = \frac{\beta - \beta_{ox}}{\beta_{fu} - \beta_{ox}} \qquad [75]$$

where $\beta = Y_{fu} - \frac{Y_{ox}}{s}$ is called a Shvab-Zeldovic function[65], the functions $\beta_{fu} = \left(Y_{fu} - \frac{Y_{ox}}{s} \right)_{fu}$ and $\beta_{ox} = \left(Y_{fu} - \frac{Y_{ox}}{s} \right)_{ox}$ representing the relation between the mass fraction of the fuel and the

* A conserved scalar remains unchanged during the reaction, simply following the fluid motion, its transport equation thus having no source term.

oxidiser in the original fuel-inflow stream and in the air (or oxidant) stream, respectively. If the fuel stream consists only of fuel and the air stream consists of oxygen, but not of fuel, Equation [75] can be written in terms of mass fractions as

$$\xi = \frac{\left(Y_{fu} - \frac{Y_{ox}}{s}\right)_{mix} + \frac{Y_{ox}^{\infty}}{s}}{Y_{fu}^{\infty} + \frac{Y_{ox}^{\infty}}{s}} \qquad [76]$$

where ∞ represent the composition in the initial stream. In fire applications Y_{ox}^{∞} would typically correspond to the ambient mass concentration (=0.23) and $Y_{fu}^{\infty} = 1$.

As can be seen from Equation [75] or [76], the mixture fraction varies from 1 in the fuel stream to 0 in the air stream. It is assumed that the chemistry is infinitely fast, meaning that "mixed is burnt", the fuel and the oxidant being unable to coexist. The following relationships can be derived:

$$Y_{fu} = 0 \qquad \text{if } Y_{ox} > 0$$
$$Y_{ox} = 0 \qquad \text{if } Y_{fu} > 0$$

The reaction occurs then in a flamesheet in which the mixture of fuel and oxygen mass fractions take stoichiometric proportions:

$$\xi_{st} = \frac{Y_{ox}^{\infty}}{sY_{fu}^{\infty} + Y_{ox}^{\infty}} \qquad [77]$$

Since the Eddy Dissipation Concept takes no account of the reaction limitations set by the recirculation of fire gases and by the low oxygen concentrations in a post-flashover room, these models become less suited for the simulation of ventilation-controlled enclosure fires. Equation [74] can be extended to include the effects such as that of chemical kinetics, using an Arrhenius relation, and concentration of products, which is related to the temperature of the product gases.

The flamelet approach to combustion modelling is a more sophisticated simulation methodology, one that has been shown to generate promising predictions. The basic rationale is to view the turbulent flame as being composed of a large number of small laminar diffusion flames, called flamelets. The characteristics of these flamelets can be measured, providing unique state relationships for enthalpy, soot, chemical species, etc., as function of the mixture fraction coordinate as well as the scalar dissipation rate. Alternatively, these state relationships can be calculated using detailed chemical models containing a large number of reactions. Species concentrations and other information can be tabulated and stored in flamelet library databases, which are called upon during a simulation. The statistical fluctuation of the conserved scalar can be calculated using LES, the approach employed in using RANS codes being the use of a probability density function, PDF. A clear advantage of this model is that the chemistry in the combustion model is now separated from the calculations of turbulence. This makes the predictive capabilities of the chemical species concentration and the soot superior to those of the simpler models. Detailed chemical models

requiring reasonable computational resources can thus be applied to the CFD simulation of the general flow field.

FDS uses a rather simple method based on oxygen consumption calorimetry for estimating the local rate of heat release. The oxygen consumption is calculated from the mixture fraction and the corresponding rate of heat release can then be calculated from[55]

$$\dot{q}''' = \dot{m}'''_{O_2} \Delta H_{c,O_2} \qquad [78]$$

In addition, a scheme is employed for relating flame extinction to the temperature and the oxygen concentration. In principle, this appears to be useful in simulating under-ventilated fires, where most CFD codes fail to predict burning behaviour accurately.*

4.5 Modelling thermal radiation

Heat transfer through thermal radiation is of great importance in almost all fires of practical interest. From a modelling standpoint, radiative heat transfer exerts its numerical influence through the energy conservation equation, where it appears as a source term that needs to be modelled. Several modelling approaches have been suggested for dealing with this source term. In most CFD models, including SMAFS and SOFIE, radiation is modelled by use of the discrete transfer radiation model (DTRM) first proposed by Lockwood and Shaw[66], which solves the radiation transfer equation along a prescribed number of directions. These are generally thought of as 'radiation rays', starting from (the centre of) every surface element at the boundary and crossing through the fluid phase until it reaches another solid boundary. For FDS, a Finite Volume approach† has been adopted in solving the RTE using a default of about 100 discrete angles, much the same way as the governing flow equations are solved. In the text below, only the DTRM will be discussed.

Whatever discretisation method that is employed a major issue in thermal radiation modelling is that of how to obtain the properties of the participating media, soot and combustion gases. The presence of soot is an important but very difficult phenomenon to implement in CFD calculations. In most practical modelling cases, it is accounted for, rather crudely, by assuming a constant soot conversion factor to be related to the fuel inflow. The modelling of the optical properties of gases is also a rather tricky process; various approximations frequently employed are the Weighted Sum of Gray Gases, WSGG, approximation or Modaks simple model[67] for mixtures of soot, carbon dioxide and water vapour. Other more sophisticated methods such as wide-band or narrow-band models, which solve an RTE for different spectral bands, have been put into practice in several codes but these approaches are generally considered too expensive in terms of computer resources. FDS uses a narrow-band model, RADCAL[68], for calculation of the mean absorption coefficient, which is tabulated in advance of the computation as a function of the mixture fraction and the temperature.

* Although it can thus not be said that the method used makes FDS capable of handling under-ventilated fires, it is likely that also this crude model makes the specific code perform better than it would have otherwise.

† This approach includes the usual deficiencies of the FV method, such as that of numerical diffusion. The ray effect described later, however, does not occur when the calculation approach is employed.

Assuming that all soot particles are small compared with the thermal radiation wavelength, any scattering effects caused by the soot can be ignored and the radiation transfer equation be reduced to Equation [79].[66,69]

$$\frac{dI}{ds} = k_a \left(\frac{\sigma T^4}{\pi} - I \right) \qquad [79]$$

This equation can be integrated directly, assuming that the gas temperature is constant within the control volume, to yield the recurrence relation

$$I_{n+1} = I_n e^{-k_a \Delta s} + \frac{\sigma T^4}{\pi} \left(1 - e^{-k_a \Delta s} \right) \qquad [80]$$

The terms I_n and I_{n+1} denote successive radiative intensities along a 'ray' separated by the distance Δs, which is the ray-travelling distance through the control volume, k_a being the total absorption coefficient of the gas. Both the temperature and the absorption coefficient are assumed to be constant over the distance Δs, and similarly the intensities are considered to be uniform over the discretised solid angle $\delta\Omega$. Since the temperature is raised to the fourth power, calculations of radiation are rather sensitive to even rather small errors in the overall calculations.

The net energy exchange between the rays and the computational cell is calculated as $S_h = \sum_{all\ rays} \left(I_{n+1} - I_n \right) \delta A \delta\Omega$. This is used as a source term in the energy equation described by Equation [39]. δA is the area of the surface element projected in a direction normal to the incident ray.

The energy balance at a boundary surface is written as $q_w^+ = \left(1 - \varepsilon_w \right) q_w^- + \frac{\sigma T_w^4}{\pi}$, where q_w^+ denotes the heat flux leaving the surface and q_w^- denotes the flux arriving to the surface, calculated as $\sum_{all\ rays} I_j (\vec{\Omega}_j \cdot \vec{n}) \delta\Omega_j$.

The use of the DT radiation model is generally accompanied by various degree of ray-effects[70], to what extent depending on how many rays are used in the radiation simulation and on the size of the control volumes, that is, how well the prescribed rays cover the domain of interest. This phenomenon is also related to the characteristics of the fluid phase through which the different rays travel. Rays from boundary cells that travel through the flames return a higher radiative flux to the surface than those that do not. A graphical 2-d illustration of this shortcoming of the DTRM is shown in Figure 24, the black circle there representing a local heat source of high temperature. Assume that four rays, evenly distributed over the semi-circle, are launched from each of the boundary cells. It is obvious, when Equation [80] is applied along these ray paths in evaluating the incident flux to the boundary cells, that rays launched both from grid points A and B capture the heat source whereas the same heat source is completely invisible to rays originating from points C and D. Thus, since all rays launched from boundary cells C and D totally miss the heat source, the resulting heat fluxes are lower

than those if their neighbours A and B. The solution to this weakness of the model is to increase the number of nodes in the calculation domain or to increase the number of rays launched from the boundary surfaces.

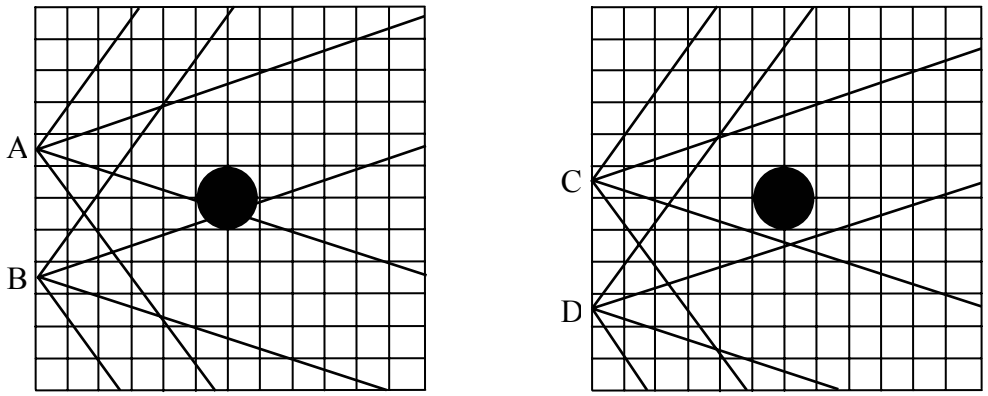

Figure 24. Two-dimensional illustration of the cause of the ray effect.

5. Flame spread modelling based on CFD methodology

Since CFD techniques allow variables to be calculated locally in a very fine mesh, there is no need of making the very rough and uncertain assumptions regarding flame height and heat flux pattern made by the analytical thermal model discussed in Chapter 3. The very complex gas-phase problem is conveniently solved by use of the general CFD code, and essential parameters such as heat transfer predictions and turbulence parameters can be used directly as input to the pyrolysis model in calculating the thermal response of a heat-exposed material.

The CFD techniques also open up possibilities for more sophisticated material models, designed for calculating the transient heat distribution within a solid material and the subsequent thermal degradation of the solid, resulting in a mass flow of pyrolysis products from the solid surface being injected into the turbulent reacting flow. CFD simulations do not normally provide numerically perfect or exact solutions, however. This is due to the need of making a number of modelling assumptions to account for different phenomena too complex to be solved for directly, so as to make simulation practically possible. Thus, basically all the submodels that ultimately form the overall CFD code contain approximations and simplifications of the phenomenon under consideration and since the flame-spread model is essentially at the end of the modelling chain, it suffers from the uncertainties of all the preceding computational steps.

In this chapter, the ideas basic to four different material models, each employed as an integrated part of a general CFD code, are discussed. The models performances are evaluated and computations being compared with results from different test scenarios in Chapter 6. The CFD codes used in the present study are Fire Dynamics Simulation version 2.2, FDS, Smoke Movement and Flame Spread version 5, SMAFS, and Simulation of Fires In Enclosures version 3.3, SOFIE.

5.1. Introduction

Combining the CFD simulation of a turbulent reacting wall flow with a material model for transient heating and pyrolysis opens up possibilities for more flexible overall flame spread models capable of dealing with the physics involved, models of a more fundamental sort than the thermal modelling approach presented earlier. The calculation procedure can be regarded as a four step coupled scheme, as shown in Figure 25.

The derivation of models describing the thermal response of a solid material requires that certain simplifications be made, consistent with the degree of complexity and sophistication aimed at. From an engineering standpoint, efforts directed at the development of complex models may need to be restrained somewhat in order for the models developed to be useful in practice. Simplifications are needed and will probably remain so until the input data that more complex models would require becomes generally available. The additional computer power needed to support the calculations called for by employing additional rate laws, however, being small.

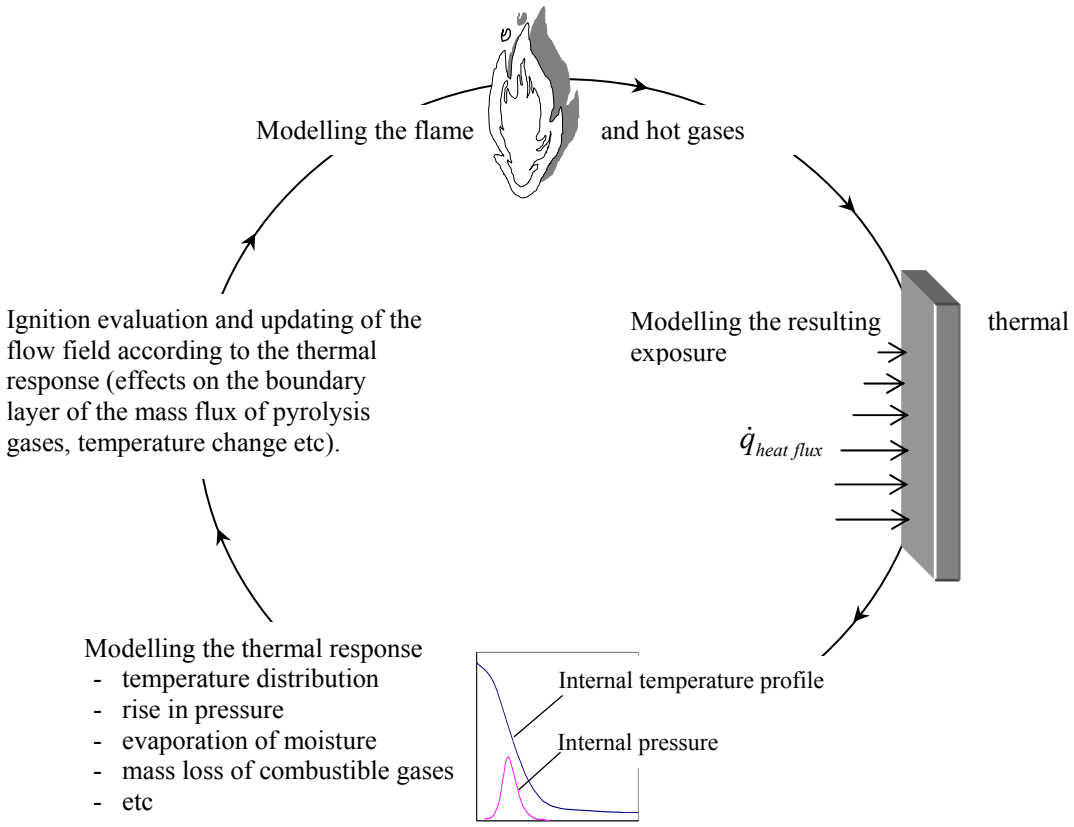

Figure 25. The flame spread calculation scheme.

Common simplifications include the use of one-dimensional heat transfer within the solid and the rear surface of the solid as well as its edges assumed to be impervious to both heat and mass transfer. The pyrolysis gases are also assumed to flow through the residual char without any resistance. In fact, the mass transport (and hence the transport of momentum) within the material is almost always ignored due to the complexity and computational cost of solving the momentum equation within the material. In addition, the chemical kinetics of pyrolysis, if account of at all, is assumed to follow a single step Arrhenius rate law with an order of unity.

Deriving the input parameters of a pyrolysis model often involves the use of a small-scale test such as the Cone Calorimeter as a reference scenario and evaluating different sets of input data to the model using it in a stand-alone mode, choosing values then representing the best fit to the experimental data. A major difficulty in trying to translate model predictions from small-scale simulations using a stand-alone model is that the modeller needs to assign an additional heat flux due to the flames after the onset of ignition rather than calculating it by use of the fluid dynamics and the rate of burning. It is not likely that this flame flux will remain constant throughout the test since both the total rate of heat release and the flame emissivity are likely to vary over time. In a large-scale simulation, this additional heat flux is calculated locally by use of the submodels in the CFD code.

In the present study, four different pyrolysis models of varying degrees of sophistication and originating from three different CFD codes are used to evaluate the potential of flame-spread modelling by use of the most popular CFD techniques presently employed. The fundamental

structure and key assumptions of the models are presented in the sections that follow. Since all of these pyrolysis models are incorporated into a CFD code, no further assumptions are required for the gas phase effects since the necessary properties are provided by the modelling of the gas flow and the turbulent combustion. Few of the general models that are available, however, distinguish between different fuels when applying the combustion model. The burner source and the combustible pyrolysis gases need to be involved in the same chemical reaction.

5.2 Yan pyrolysis model

In 1996 Yan and Holmstedt[71,72] presented a general pyrolysis model embedded in a CFD code, using it to predict flame spread on a vertical PMMA slab (non-charring) and on a particle board (charring material). Their results agreed well with the experimental data on the fire growth and the gas temperatures.

The pyrolysis model is essentially based on a solution of the general heat transfer equation, discretised on a separate solid grid using the central differencing approximation. The solid grid is applied within the material and is aligned in accordance with the cells in the gas phase grid. In order to resolve the scales of pyrolysis, the solid-grid control volumes are divided further into a number of very small elements, which follows the movement of the pyrolysis front into the material.

The CFD code SMAFS thus allows the solid and the fluid phase to be treated separately, making it possible to implement and solve rather complex material models on the separate computational mesh without threatening the overall stability or computational speed of the simulation. Also, this CFD code is the only one used in this study which supports the use of different reactions in the combustion model.

The mass continuity and the energy equation are employed for describing the solid phase. The momentum equation is made nonessential by ignoring mass transport and pressure generation inside the solid material. Combining the continuity and energy equation for the solid material, Yan and Holmstedt[71] were able to propose the simplified set of equations for pyrolysis reproduced below.

Heating phase:

$$\rho c_p \frac{\partial(T)}{\partial t} = \frac{\partial}{\partial x}\left(k \frac{\partial T}{\partial x} \right) \quad \text{if } T < T_{py} \text{ or } \rho = \rho_{char} \qquad [81]$$

Pyrolysis phase:

$$\dot{m}''' H_{py} = \frac{\partial}{\partial x}\left(k \frac{\partial T}{\partial x} \right) \quad \text{if } T \geq T_{py} \text{ and } \rho > \rho_{char} \qquad [82]$$

The model also contains a simple procedure to account for the effects of moisture, which can be included into Equation [81] in the form of a water heating and an evaporation term,

respectively. No account is taken for pressure generation or moisture transport within the material, however.

T_{py} is a critical pyrolysis temperature prescribed by the user and $\dot{m}''' = -\frac{\partial \rho}{\partial t} = \frac{\partial \dot{m}''}{\partial x} \geq 0$ is the mass loss rate per unit volume.

The reaction kinetics of pyrolysis is replaced here by the pyrolysis temperature and a constant heat of pyrolysis, using the definition $H_{py} \equiv H_{vol,T_{py}} - H_{s,T_{py}} = H_{vol,T_{py}} - \left(H_{s,T_0} + \int_{T_0}^{T_{py}} c_p dT \right)$, which can be interpreted as the difference in enthalpy between the volatile pyrolysates and the virgin solid at the pyrolysis temperature. The integral in the parentheses on the right hand side represents the energy required for preheating.

The movement of the pyrolysis front into the solid is tracked using a moving subgrid involving very small control volumes* superimposed upon the standard control volumes inside the solid. The central assumptions of the model are that pyrolysis occurs only when the temperature has reached the pyrolysis temperature and that during pyrolysis the temperature gradient in the material is small, all energy being used for pyrolysis and no further heating of the material occur until only char remains. Thus, the local temperature is considered to be constant throughout the pyrolysis process, adjusted by the endothermic pyrolysis reaction. This result in a kind of stepwise pyrolysis unlike the more continuum-like process obtained by use of an Arrhenius formulation of the material thermal response. In this connection, Yan and Holmstedt argue that the Arrhenius physics for most combustible solids can be ignored, since the pyrolysis process is endothermic nature and the activation energy is so high that the reaction is essentially determined by heat transfer in the solid and through it. Thus, the rate of pyrolysis can be assumed to be very small in areas where the material temperature is below the critical pyrolysis temperature.

5.2.1 General description of the input data

The material model that Yan developed requires a number of input variables, several of which may be rather tricky to assign an absolute number or a set of numbers to, whereas others can be derived directly from small-scale tests. The material matrix is simplified and treated as a single solid body, thus ignoring in effect the changes in thermal properties as the virgin material is converted into a residual char. This can nevertheless be taken account of in principle by specifying a temperature dependence of the specific heat capacity and of the thermal conductivity.

A standard procedure for deriving values for the input parameters is to seek appropriate advice from the literature and to try then to fit the modelling output to measurements made in the Cone Calorimeter for different heat fluxes, adjustments being made to the relevant parameters to obtain a best fit. The primary input variables are described below, a comprehensive sensitivity analysis of the most important inputs being presented in Appendix A.

* In this study these small elements are of the order 10^{-5} meter in size.

Solid-phase input

- ✓ *Char Density* in kgm^{-3} can be measured quite easily after a test. Typically, the density of the char represents about 10%-20% of the virgin density, its value being dependent upon the incident heat flux.

- ✓ *Virgin density* in kgm^{-3} is generally known for any given material but can be easily measured.

- ✓ *Specific heat capacity* in $Jkg^{-1}K^{-1}$ is roughly constant for a variety of wood-based products. A reasonably accurate value or at least a rather narrow range of values that can be useful in a Cone Calorimeter best-fit procedure, can be found in the literature. The data for the model can be provided in the form of a fourth-degree polynomial. Again, the virgin material and the residual char are treated as a single solid body, the heat capacity of the volatiles that move through the material matrix, not being included directly in the model but needing to be accounted for in the value for solid heat capacity.

- ✓ *Thermal conductivity*, in $Wm^{-1}K^{-1}$ is a parameter that is rather difficult to measure, its magnitude depending on the material temperature, the moisture content and the degree of charring. This parameter is also used to account for cracks and fissures in the charring layer, which increase the heat transfer to the inside of the material primarily through thermal radiation rather than heat conduction. In the original model, which is used here, the conductivity of the virgin solid material and of the carbonaceous residual are not kept separate. A polynomial temperature dependence can be constructed using values obtained from the literature or by producing a best fit to Cone Calorimeter. Yan[71], however, used a constant value for this parameter, demonstrating the apparent lack of reliable experimental data for practical use here.

- ✓ *Pyrolysis temperature*, given in Kelvin, is used for determining the onset of pyrolysis. It is given as a constant, its value being quite similar to the 'ignition temperature', which historically has been the ignition criterion most frequently employed in flame-spread modelling, its value ranging from about 300 to 350 °C[15]. Whether or not this is the best ignition criterion can be questioned, however, since its value is likely to vary dependent upon for example the moisture content and the incident heat flux. As can be seen in Appendix A this parameter has a major impact on the model performance.

- ✓ *Heat of pyrolysis*, Jkg^{-1}, which is also a product of simplification, would have a different meaning if an Arrhenius function were employed. It can be regarded as being a model tuning parameter which is why no experimental data is found in the literature. Hence, the modeller's only recourse is to use a best-fit procedure involving output of Cone Calorimeter tests for different heat fluxes. In the model, the rate of pyrolysis is restrained by either the energy available for pyrolysis or the virgin mass that remains.

- ✓ *Moisture content* is given as the mass fraction of the water the wood contains in relation to the mass of wood when oven-dried. The numerical value of this can be estimated if the temperature and relative humidity of the surroundings are known[73]. A fair guess would be a moisture content of about 10 percent for indoor linings.

- ✓ *Surface emissivity* needs to be assigned a constant value, a fair guess for sooty surfaces being one of close to unity, a value of 0.9-0.95 often being suggested in the literature.

Gas phase input

- ✓ *Characteristics of the fuel,* such as its specific heat, viscosity and molecular weight, as well as the chemical composition (molecular structure) of the pyrolysis gases (governing basically the stoichiometric reaction). These are not really a part of the pyrolysis model but are needed for the CFD solution of the reacting flow field. Another important fuel characteristic is the heat of combustion, which is discussed below.

- ✓ *Heat of combustion* of the pyrolysis gases, in Jkg^{-1} can be obtained from measurements in the Cone Calorimeter. Its value changes to some degree with such factors as heat flux and moisture content. This parameter refers to the chemical or effective heat of combustion, for which Moghtaderi[74] provides the following approximate equation for wooden materials: $\Delta H_{c,eff} = 0.075\dot{q}''_e - 2.70\frac{\rho_{moisture}}{\rho_{dry}} + 10.27$. The model input, in contrast, is a constant value.

- ✓ *Flame flux* in W/m^2, is required for using the pyrolysis model in a stand-alone mode. Its influence on the predicted rate of heat release is evaluated in Appendix A. In the present study, the flame flux is assigned a transient value based on using 10% of the calculated rate of heat release and a maximum flux over the fuel surface of 20 kW/m^2. An estimate of the maximum radiative flame flux can easily be obtained using $\dot{q}''_f = F_{1-2}\varepsilon_{\text{flame}}\sigma T^4_{\text{flame}}$, where $\varepsilon_{\text{flame}} = \left(1-\exp\left(-\kappa_s L\right)\right) + \varepsilon_g \exp\left(-\kappa_s L\right)$ is the total emissivity of the flame, $F_{1\text{-}2}$ is the view factor, κ_s is the absorption coefficient of soot, ε_g is the total emissivity of the water vapour and carbon dioxide, and L is the physical path lenght[75].

5.3 Qaccumulative pyrolysis model, SOFIE

A simple approach to incorporating flame spread capabilities into the CFD code SOFIE was presented recently by Rubini and co-workers[19]. They term their model the 'Qaccumulative flame spread model'. The rate of pyrolysis is governed using a heat of gasification approach, the more detailed studies of heat transfer through the wall, solid heating and thermal response being disregarded.

Ignition of the virgin solid is assumed to be dependent upon a certain critical value of the accumulated energy, $E_{critical}$ having been reached, expressed in terms of a modified incident heat flux over time:

$$E_{critical} = \int_0^{t_{ignition}} \dot{q}dt = \sum_0^{t_{ignition}} \max\left(\dot{q}_{total} - \dot{q}_{\min},\ 0.0\right)\Delta t \qquad [83]$$

This allows the ignition criterion and the accumulation of energy to be regarded as a substitute for heat conduction in the solid and the subsequent heating of it. The parameter q_{total} represents the total radiative and convective incident heat flux to the solid surface, q_{min} being a user-defined critical incident heat flux below which no ignition can occur. The latter parameter is introduced to prevent ignition from occuring on surfaces that have reached $E_{critical}$ but on which the heat flux is too low to sustain ignition, and also to account for the heat lost by conduction into the solid. An undesirable effect of its presence is that preheating, or in this case, the accumulation of heat, and thus the subsequent flame spread and fire growth, may be underpredicted on surfaces at locations remote from the initial fire.

It is assumed that once the critical energy has been reached the solid fuel to releases pyrolysis gases at a rate determined by the total incident heat flux and the heat of gasification.

$$\frac{dm}{dt} = \frac{\dot{q}_{net}}{H_g} \Delta A_{face} \qquad [84]$$

where ΔA_{face} is the face area of the computational cell and H_g is the local heat of gasification, which for thermally thick, vaporising materials in a steady state can be determined from the definition

$$H_g \equiv \frac{\dot{q}_{net}}{\dot{m}_{total}} = \frac{h_c \left(T_{surr} - T_{wall} \right) + R_{flux}}{\dot{m}_{total}} \qquad [85]$$

Because of the formation of an insulating char layer, all charring materials show a significant change in the rate of pyrolysis. In this model, the heat sink created by the char is modelled by introducing an additional modifying parameter into Equation [84], which relates the initial mass flux to the accumulated energy in the material. The depth of charring is approximated linearly, using the total mass loss from the cell face, the virgin density and the final char density.

Since at present, the CFD code SOFIE does not allow for heat transfer through a transpiring wall, the modeller needs to the make use of isothermal boundary conditions on the combustible wall surfaces and to make some best guess regarding the constant temperature to be employed. This affects the net heat transfer to the boundaries, both the convective and the radiative part of it, constituting as such a deliberate error which is added to the already rather subtle flame-spread calculations. However, more seriously, it affects the usefulness of the model as a tool in such calculations, related to fire safety engineering, as smoke movement, gas temperatures and incident heat flux to either escaping persons, firefighting personal or combustible objects in the vicinity of the fire.

5.3.1 General description of the input data

Although the intention of developing a practical engineering model with as few detailed solid phase input variables as possible could be seen as worthwhile some of the required input data becomes somewhat artificial or non-standard since the model is primarily empirical in

character. The model suffers most, however, from the use of isothermal boundary conditions on the transpiring walls rather than fuzzy input parameters.

Solid-phase input

- ✓ *Heat of gasification* in J/kg, concerns the thermal response of a material when subjected to a given heat exposure. The parameter is not really constant throughout the pyrolysis process even if a constant value may be motivated for thermally thick materials[76]. In the present version of SOFIE (v.3.3 April '01) a constant value for the heat of gasification is given, the early mass loss rate is made variable, however, using a modifier between 1 and 0.4 in size related to the accumulated energy in the material. This makes the mass loss profile a crude imitation of the mass loss output from the performance of a charring material in the Cone Calorimeter. Many simple pyrolysis models use the heat of gasification as an input constant that relates the fuel mass loss to the incident heat flux. Despite their similarities, the heat of gasification and the heat of pyrolysis should not be confused.

- ✓ *Ignition temperature*, in Kelvin, although not representing a critical value for the initiation of pyrolysis, is used to define the initial density of the pyrolysis gases.

- ✓ *Wall temperature,* in Kelvin, could in practice be changed manually during simulation. Such an approach would only be feasible, however, if the transient wall temperature were known in advance.

- ✓ *Critical accumulated heat flux* in J/m^2 is the model criterion for the start of pyrolysis and ignition. Although a numerical value can be calculated from small-scale measurements, such as the Cone Calorimeter, this parameter may need to be optimised to some extent for the material under consideration.

- ✓ *Minimum heat flux* in units of W/m^2 defines the limit below which the solid does not ignite. The parameter can also be considered as representing heat losses through conduction into the solid in which a constant temperature is maintained during simulation. Because of the isothermal boundary condition and since this parameter also has an effect on the accumulated heat flux, and thus on the rate of pyrolysis, certain optimisation may be needed before it is used.

- ✓ *Virgin material density* in kg/m^3 is normally a known quantity.

- ✓ *Char material density* kg/m^3, can be measured in experiments or estimated to approximately 10%-20% of the virgin material density depending on the prevailing heat flux to which the sample has been subjected.

- ✓ *Maximum char depth*, in metric units, limits the time of burning. Its value typically corresponding to the thickness of the combustible material.

- ✓ *Surface emissivity* is usually assigned a constant value of 0.9-1.0.

Gas phase input

SOFIE does not currently support the use of multiple fuels. Information on the specific heat capacity, the heat of formation, etc. is provided in a separate database, numerical values being readily available in several handbooks on thermodynamics.

- ✓ *Heat of combustion* units of Jkg^{-1} is provided in terms of heat of formation in the species database. It is used to convert heat release to mass loss and vice verse. Its numerical value can be obtained from the averaged output from the Cone Calorimeter.

5.4 Cone Calorimeter model, SOFIE

The Cone Calorimeter testing device has proved to be reliable and to provide reproducible test results[77]. It is in use worldwide, large databases concerning a variety of materials having been amassed in almost every fire-testing laboratory. Karlsson[28] employed data from the Cone Calorimeter to derive input to the analytical thermal flame-spread model described in Chapter 3. Furthermore, Yan[71] used the data directly in a CFD-coupled flame-spread model, obtaining close correlation with the experimental data from two enclosed fire scenarios. Rubini and co-workers[20] have presented a material model that they implemented in SOFIE in a manner allowing all the necessary input data to be obtained directly or to be easily derived from a series of Cone Calorimeter tests. One of the main advantages of this methodology is that flame-spread simulations can, potentially, be performed on a variety of materials, even if details concerning the pyrolysis of the material or its thermal properties are largely unknown.

The ignition criterion is based on the critical heat load absorbed by the material being defined as a threshold flux expressed as $\int_0^{t_{ig}} \frac{1}{2}\dot{q}''(t)t^{-1/2}dt$. Under ideal conditions, this ignition threshold flux should be independent of the thermal exposure, a straight line parallel to the abscissa resulting when it is plotted against differing values for the incident heat flux. It should be noted that, unlike the ignition criterion used in the Qaccumulative model, the minimum heat flux is not used to modify the net heat flux to the wall surface.

The local rate of pyrolysis following ignition is identified directly from the heat release rate output obtained in the Cone Calorimeter experiments. Once the ignition criterion has been fulfilled, the rate of pyrolysis follows the heat release profile described by the Cone Calorimeter data, representing the total heat flux to the surface at that time. Regardless of the heat exposure after ignition the rate of pyrolysis is fixed to the prescribed curve derived for the flux prevailing at ignition. This approach involves the assumption that the post-ignition flame flux in the Cone Calorimeter test is similar to that in the simulation scenario and is thus, for example, independent of the sample orientation during testing.

Again, like the Qaccumulative model, this approach suffers from the requirement of isothermal conditions being applied to the transpiring wall surfaces. Since this assumption affects the net heat flux to the surface, which is the driving force in flame spread, the model becomes rather complicated to use.

5.4.1 General description of the input data

Most of the input data to this model can be derived directly from the Cone Calorimeter output. From a user perspective, this is indeed a very attractive feature. Data on the (integrated) heat release rate from three different heat fluxes, each test described using 21 unique points in time are required input. An interpolation procedure known as a spline approximation is used to create a continuous function for the mass loss rate as a function of incident heat flux using the data from the three different heat fluxes and repeating this for each of the 21 data points. Mass loss profiles for ignition heat fluxes other than the three provided directly are estimated by interpolation, resulting in a new set of data points, from which a continuous profile can be obtained by use of a spline approximant. No extrapolation is made beyond the maximum and minimum fluxes from the tests.

A key feature here, similar to what characterises the Qaccumulative model is an input constant called the minimum heat flux below which pyrolysis cannot be sustained. For this model, however, the parameter is used as an independent, second, ignition criterion. In the present version of the code, therefore two conditions must be fulfilled at the boundary cell surface for pyrolysis to proceed, the first concerning the threshold flux and the second the critical minimum heat flux[20].

A similar ignition criterion is discussed by Tewarson[78], who presents a methodology for predicting the ignition of thermally thick materials in which a minimum heat flux is subtracted from the incident flux and a Thermal Response Parameter, TRP, is introduced consequently which diverges only slightly from the threshold flux:

$$t_{\mathrm{ig}}{}^{-1/2} = \frac{2}{\sqrt{\pi}} \frac{\left(\dot{q}''_e - \dot{q}''_{\min}\right)}{\mathrm{TRP}} \qquad [86]$$

Subtracting the incident heat flux from the critical flux for ignition would have been consistent with the definition of critical accumulated heat flux used by the previous, Qaccumulative model. The consequences of modifying the ignition criteria to explicitly include the minimum heat flux in the definition of the threshold flux have not been evaluated in the present study.

The following input data are required.

Solid phase

- ✓ *Accumulated cone data* in units of J/m^2 are calculated from experiments involving three different heat fluxes and stored in a separate data file, with which the CFD code communicates during a simulation.

- ✓ *Threshold flux* in $Ws^{1/2}m^{-2}$, is the ignition criterion the model employs. The value is easily derived from the Cone Calorimeter by taking the incident heat flux times the square root of the time to ignition. This quantity should be approximately the same for any heat flux.

- ✓ *Minimum heat flux* in Wm^{-2} can be viewed as a tuning parameter. Its purpose is to prevent ignition form occurring at locations at which the heat flux is insufficient to sustain ignition but where the limiting threshold flux has been reached nonetheless. The numerical value for the piloted ignition of an untreated wooden material can be shown experimentally to be about 8-12 kWm^{-2}. For prolonged heat exposure, several hours, however, values as low as 4.3 kW/m^2 have been reported[15].

- ✓ *Surface emissivity* is usually assigned a constant value of 0.9-1.0.

Gas phase

SOFIE does not currently support the use of multiple fuels. The information on the specific heat capacity, the heat of formation, etc. are provided in a separate database and are all readily available in several handbooks on thermodynamics.

- ✓ *Heat of combustion* in units of Jkg^{-1} is used to convert heat release to mass loss and vice verse. Its numerical value can be obtained from the averaged output of the Cone Calorimeter.

5.5 Arrhenius based pyrolysis model, FDS

The Fire Dynamics Simulator (FDS) includes a crude model for ignition and surface-flame spread, in which an ignition temperature is assigned to the combustible surface. The basis of the model includes the solution of the general heat transfer equation in one dimension, the rate of pyrolysis being governed by a user prescribed constant which is either a rate of heat release per unit of the surface area or a heat of vaporisation, the latter being identical to the heat of gasification parameter as defined by Equation [85]. A far more advanced model has been implemented into the code, however.

Hostikka and McGrattan[79] have presented a paper on the implementation and validation of a rather advanced physical pyrolysis model as a part of the FDS code. The model originates from earlier work of Atreya[18] and Parker[80].

Assuming there to be no pressure gradients within the solid material, thus ignoring any mass transport and letting water vapour and pyrolysis gases reach the solid surface instantaneously, pyrolysis is converted into a heat transfer problem. The overall governing (heat transfer) equation can be expressed then as

$$\overline{\rho c_p}\frac{\partial T}{\partial t}=\frac{\partial}{\partial x}\left(k_w\frac{\partial T}{\partial x}\right)+\frac{\partial \rho_w}{\partial x}\left[\Delta H_{py}-C_1\left(T-T_0\right)\right]+\frac{\partial \rho_m}{\partial x}\left[\Delta H_{ev}-C_2\left(T-T_0\right)\right] \qquad [87]$$

to which a standard boundary condition is applied at the exposed surface and on the back surface of the material.

In this equation the coefficients C_1 and C_2 represent calculated average values of the specific heat for the wooden material and for moisture, respectively, ρ_w is the total density of the

wood, and ρ_m is the density of the moisture, ΔH_{py} is the heat of pyrolysis treated as being a constant and ΔH_{ev} represents the heat of water evaporation. The overbar in Equation [87] indicates the parameters to be evaluated at the average of the momentary temperature, T, and the initial temperature, T_0. At the evaporation temperature, all the energy available is used for evaporation of moisture but because of the constant pressure assumption, no moisture transport is seen as taking place inside the material. Both moisture and pyrolysis gases reaching the surface immediately since the momentum equations are not solved within the material.

The rate of pyrolysis is estimated using a single-step Arrhenius rate law of the first order, written as $\frac{\partial \rho_w}{\partial t} = -\rho_a A e^{-E_a / RT}$, where A is the pre-exponential factor and E_a is the activation energy. These parameters are probably the most difficult to choose when using a model of this kind. The values found in the literature are not consistent with each other and can differ by one order of magnitude or more.

In the version of the code used in the present study, the pyrolysis gases are assumed to ignite at a particular mass loss rate, 0.0025 kg/s representing the critical value here. The effect of this parameter is considered briefly in Appendix B.

5.5.1 General description of the input data

The complexity of this model is reflected in the input data required, in that, the value of several of the variables may be rather difficult to select with precision. Arrhenius physics has been used in pyrolysis modelling by several researchers, this being common practice in studies of biomass. Nevertheless, very little reliable and practically useful data concerning the additional parameters that the kinetics approach employs are available. Another difficulty in simulating the burning behaviour of wood is that its different components – cellulose, hemicellulose, lignin and other substances within the material – differ in how they decompose. This suggests that several Arrhenius equations would be needed in order to capture the decomposition of the wooden material, and that the use of a single rate equation is overly crude.

The model requires the following input data.[79,81]

Solid phase input

- ✓ *Pre-exponential factor*, A_p, in units of s^{-1} and the *Activation energy*, E_a, $Jmole^{-1}$, are of major importance to the overall performance of the model since they represent the essence of simulating the thermal decomposition of the combustible material. Numerical values have been derived using thermo-gravimetric analysis (TGA). Due to the differences in the behaviour of cellulose, hemicellulose and lignin, several different rate equations may need to be considered as was discussed in section 2.1. If the temperature is sufficiently high, however, the characteristic reaction time will be an order of magnitude or more less than the thermal time scale and the effects of the different rate mechanisms are likely to diminish. The model implemented in FDS is based on a single, overall, rate equation thus requiring only one set of reaction parameters.

- ✓ *Heat of pyrolysis*, in units of Jkg^{-1} should not be confused with the parameter in Yan's model[69] that bears the same name. Here, the heat of pyrolysis is a complement to the decomposition kinetics of the Arrhenius equation, whereas Yan uses it as a quantity controlling the rate of pyrolysis, which meant replacing the chemical kinetics completely by the heat of pyrolysis and the net heat transfer. The numerical value of the measure considered here has traditionally been rather difficult to obtain with any precision, as shown by the fact that researchers have reported widely differing values from large negative values, indicative of an exothermic pyrolysis reaction, to positive, endothermic values which would seem a more reasonable overall result. Several modellers, because of the lack of reliable data, have used a zero value for this parameter[8]. Hostikka and McGrattan[79] employed a value of 125.6 kJ/kg in simulating an interior lining of spruce.

- ✓ *Density* kgm^{-3} of virgin material and the final carbonaceous residue are normally known or are readily estimated.

- ✓ *Moisture content* is defined as the ratio of the water mass to the mass of the wood in a dry condition. Its numerical value can be estimated if the relative humidity and the temperature are known. A decent guess would be one of about 10 percent by volume for an indoor lining and up to 30 percent or more for outdoor products.

- ✓ *Thermal conductivity*, in units of $Wm^{-1}K^{-1}$ for the *virgin solid*, the *residual char* and the *backing material* are treated separately by the model and can be expressed as fourth degree polynomials. Again, this parameter may be rather difficult to obtain as more than approximations, since several factors, such as the quality of the wooden material, its subsequent thermal decomposition and the origin of cracks and fissures may quickly alter the heat transfer conditions. Some guidelines for the numerical values, both for different wooden materials and for the char, are available in the literature.

- ✓ *Specific heat capacity* in $Jkg^{-1}K^{-1}$ units for the virgin wood and the char layer, are required input and can be specified using a fourth-degree polynomial. The specific heat of moisture is usually considered constant about 4.2 kJ/kgK and need not be specified.

- ✓ *Heat of evaporation* in Jkg^{-1} of the moisture is sometimes set equal to the heat of evaporation of free water, i.e. of 2260 kJ/kg. It can be argued, however, that at a moisture content below the fibre saturation point, being about 30 percent of oven dry mass, the water is chemically bound in the wood cavities and should thus be assigned a higher heat of evaporation. Alves and Figueiredo[83] used a polynomial relationship for the heat of evaporation as function of moisture content, as derived from data of Siau[84].

- ✓ *Surface emissivity* of a wooden material can be found in the literature[85]. Its value for wooden surfaces is normally set to 0.9-0.95, although for a sooty surface it would not be unlikely for the emissivity to rise to almost unity. In the code, the surface emissivity varies from a user-defined initial value to a value based on the degree of charring.

Gas phase input

FDS does not currently support the simultaneous combustion of multiple fuels. Thus, the combustion of the fuel in the initial fire and the pyrolysis gases follows the same chemical reaction. The specific heat capacity of the different fuels involved is dealt with separately, however, in calculation of the fluid flow.

- ✓ *Heat of combustion* in units of J/kg, does not distinguish between user-prescribed and pyrolysis fuel mass flux, meaning that the initial fuel must have the same value as the pyrolysis gases (otherwise the product of the mass-loss rate, as provided by the model, and the heat of combustion would be evaluated erroneously). The effective heat of combustion for the pyrolysis gases can be derived from Cone Calorimeter measurements.

- ✓ *Specific heat capacity*, $Jkg^{-1}K^{-1}$, for the pyrolysis gases can be obtained from handbooks on thermodynamics. In this report the data provided by Fredlund[8] has been employed.

6 Sample calculations and evaluation of models

The aim of this chapter is to provide a brief guide to the use of the different flame spread models that have been taken up and to study on the performance of these models in different scenarios. The sensitivity of the output of the CFD simulations with use of the different codes is also analysed under different computational conditions

6.1 The experiments

The Cone Calorimeter and two large-scale flame-spread configurations are considered in evaluating the models through the results being compared with experimental data. The first flame-spread scenario examined concerns upward flame spread on a vertical particleboard panel, the experiments being ones carried out by Blomqvist and van Hees[40]. The second flame-spread scenario is a room fire as described by ISO 9705[31,41], or the Room Corner Test, in which a particleboard lining covers three walls and the ceiling, the door-wall being non-combustible.

Measurements made in the Cone Calorimeter, frequently used to validate the performance of pyrolysis models in a stand-alone mode, as well as to derive or justify the values to be used as input variables for different models employed in full-scale simulations, constitute a third test. The test methods that have been used in this study are presented and discussed below.

6.1.1 Small scale: The Cone Calorimeter

The ISO 5660 test procedure, commonly known as the Cone Calorimeter testing device, shown in Figure 26, has become widely used and is now a part of the equipment in most fire laboratories worldwide. It has been shown to provide good repeatability in testing within a given facility, and reasonable reproducibility in comparing the outcome of testing in different facilities.

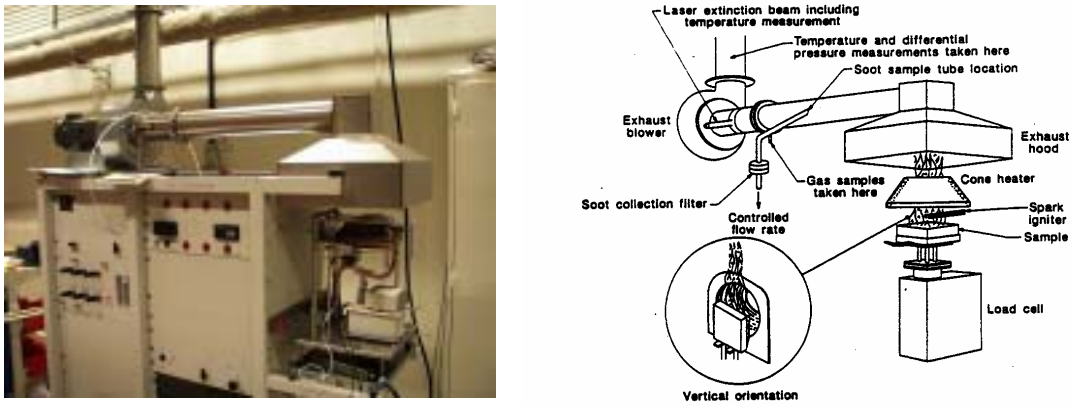

Figure 26. The Cone Calorimeter at Lund University (left) and a schematic view of the apparatus, from ref 28 (right).

The possible errors of measurement using the standardised test procedures have been reported to be 10% or less for the peak heat release rate, the mass loss rate and the specific extinction area and 15% or less for carbon monoxide and calculations of heat of combustion. Simple relationships concerning the repeatability and the reproducibility of different parameters can be found in the literature, see ISO/FDIS5660-1[77] or Babrauskas[86], for example. Even though the standard are sufficiently detailed to enable this level of repeatability to be achieved, however, one should bear in mind the different factors that can affect the outcome both of a test and of the outcome of a simulation based upon the results.

One such factor is the physical scale of the sample tested. The standard size of the specimen is 0.1×0.1 meters, a scale found to perform well for most materials. In examining different materials in a modified Cone Calorimeter, using samples of the dimensions 0.2×0.2 meters, however, Nussbaum and Östman[87] concluded that some materials which failed to ignite in the original test, such as the melamine-faced particleboard at 25 kW/m^2, for example, indeed did ignite when the sample area was increased by a factor of four. The time to ignition was typically found to differ by about 20%, but for wooden materials such as spruce panel or particleboard the discrepancy was closer to 30%. The peak heat release rate per unit area for the wooden materials was shown to be about 20% higher for the larger samples, but the one-minute average heat release rate differed by less then 10%. The results presented by Nussbaum and Östman are corroborated by Babrauskas[88], who refers to tests on PMMA carried out at Factory Mutual, involving both horizontally positioned tests of different-sized samples and vertical wall tests. Thus, it is likely that the time to ignition obtained in the standard test will be longer and the rate of heat release lower than would be the case in a large-scale fire.

Another factor that can be of importance to the modeller is the orientation of the sample. The usual procedure is to keep the sample in a horizontal position, face up. This is in contrast with what would normally be modelled, such as a vertical wall or a combustible ceiling (face down). The effects of sample orientation have been addressed by several researchers, the rate of heat release of a vertically oriented specimen being shown t be notably lower than that of a horizontally positioned sample, likely due to the greater flame depth in the case of a horizontal orientation. The influence of the specimen orientation is illustrated in
Figure 27, presenting results of experiments on Radiata pine performed by Moghtaderi[7473]. Several studies have shown, however, that the time to ignition for a given external heat flux is less sensitive to the orientation of the sample, see references 74 and 89, for example.

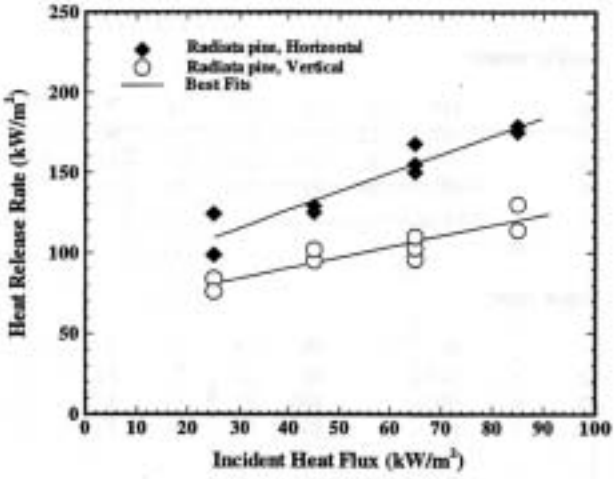

Figure 27 Effects of specimen orientation during a test in the Cone Calorimeter (from ref 74).

For wooden materials, the typical transient heat release curve the Cone Calorimeter provides consists of two peaks. The first peak can be expected under any circumstances when wood is burning, although its appearance may differ somewhat from one test to another, depending on the sampling interval involved. The presence of this first peak can be explained on the basis of an insulating carbonaceous char layer being formed, protecting the as yet unburned wood and leading to a rapid decrease in the heat release rate after this first peak. The presence of the second peak, in turn, indicates the thermal wave to have reached the insulated back side of the sample and heat to have accumulated at the rear end of it, enhancing pyrolysis and increasing the rate of heat release. Thus, the second peak is artificial in a sense, and is highly dependent upon the character of the backing material. Figure 28 illustrates observations made here.

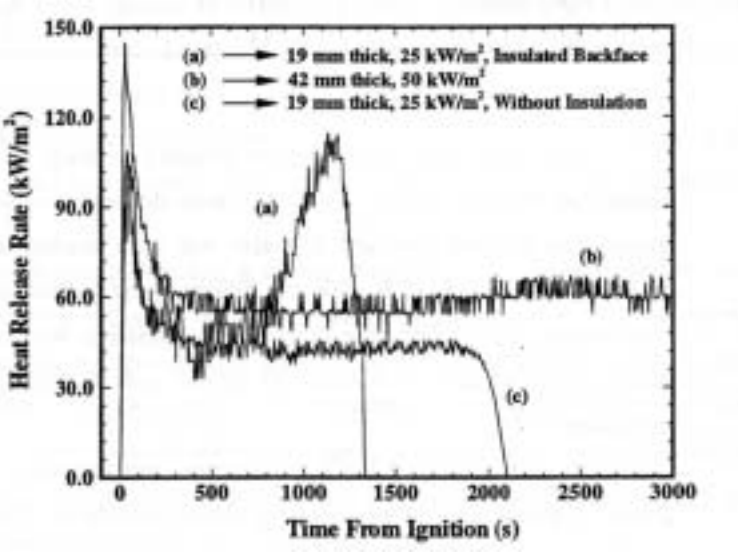

Figure 28. Effects of the thermal boundary conditions on the back face of the sample. The tests were performed with a horizontal orientation (from ref. 74).

The further issue consider is the influence of the flame heat flux to the sample after ignition has occurred. Unlike the heat flux from the cone heater, the heat flux from the flame is by no means homogenously distributed over the surface of the specimen and for most materials it is likely to vary over time, since the rate of heat release from the specimen, and thus the flame

depth, soot concentration and flame emissivity as well, vary. Figure 29 shows the incident heat flux towards the surface of the specimen originating from the flames above it as simulated by the CFD code SMAFS. The average incident flux towards the surface is around 10 kW/m^2, the centre of the fuel surface receiving the highest flux, 20 kW/m^2, whereas the feedback to the edges is about 5 kW/m^2.

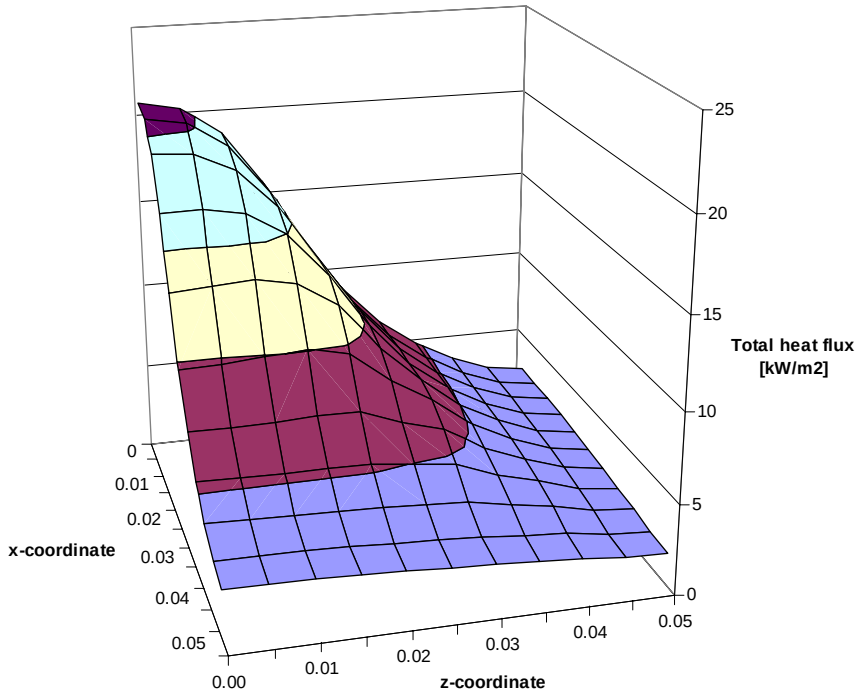

Figure 29. Heat flux towards the sample in a simulation of the Cone Calorimeter. Note that the results have not been modified to reproduce the influx towards a cooled heat flux meter. The DTRM is used, lounging 256 rays from the boundary cells and the presence of soot is prescribed to 3.0% based on the mass inflow of the fuel gas.

To sum up, the modeller should bear in mind that the Cone Calorimeter is not intended primarily as a tool for large-scale modelling purposes. In the forthcoming ISO standard[77] it is stated that the method has the objective of testing "… *the fundamental response of a specimen to specified external irradiance*…". Although this enables comparisons of different materials to be made, it unfortunately does not represent the detailed behaviour they would display in a realistic large-scale scenario.

6.1.2 Intermediate scale: Vertical panel flame spread test

Blomqvist and Van Hees[40] performed a series of tests in which the vertical flame spread on a panel was isolated. Their work was conducted as part of a flame-spread project managed by the Centre for Combustion Science and Technology, CECOST. Three materials were tested: polymethylmetacrylate (PMMA), low-density fibreboard (LDF) and particleboard. In the present report, only the particleboard tests they conducted are studied.

The basic experimental setup adopted was a cable-testing device, IEC 60332-3[90], modified in various ways, such as the ventilation conditions being different and a diffusion-burner flame instead of a premixed one being employed. The sample panel had dimensions of 12×300×3000 (D×W×H) mm. A schematic diagram of the overall test rig is presented in Figure 30.

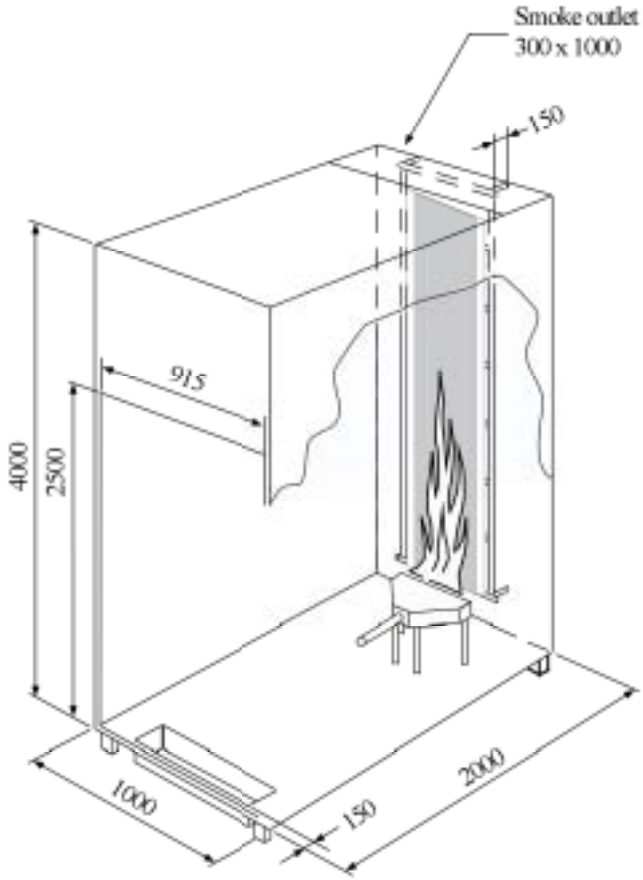

Figure 30 Test rig used for vertical flame spread measurements. The setup is a modified form of a cable testing device (from ref. 40).

Test data available

The measurements included those of the total rate of heat release and of the smoke production rate in a hood above the smoke outlet, and of the total heat flux measured using Schmidt-Boelter gauges at two locations at the centreline of the sample, located 0.75 and 1.25 meters above the rim of the burner, respectively. The pyrolysis front was tracked both by use of measurements of the surface temperature of the sample and visually, using video recordings of the tests.

The fuel was propane and the burner, 257 mm wide and 30 mm high, was located 0.05 meters from the sample surface, providing a constant rate of heat release of 20 kW during the entire test. Due to the unusual outer shell of the burner, it was somewhat difficult to assess whether or not it represented a typical initial fire. Its front side was covered with a perforated sheet having 242 holes, 1.32 mm in diameter, resulting in an average fuel gas velocity of 0.72 m/s through the holes. Since the size of the holes could not be resolved in any practical CFD simulation of the test, the small-scale jets was replaced by a much slower average velocity in

the simulation. Although this lack of detailed resolution may pose problems, it is difficult to assess its influence on the reacting flow further upstream.

For many building materials, including wood and derivatives of wood, this test represents a borderline case in which flame spread is only sustained up to some limiting state, after which burning decreases and eventually stops. Locating this limit in terms of a maximum height of pyrolysis and maximum heat release rate is vital for any flame spread model, since it provides a measure both of the performance of the pyrolysis model and of the heat transfer interaction in the fluid - wall interface.

6.1.3 Large scale: ISO 9705 The Room Corner Test

The Room Corner Test[31], shown in Figure 18, has been used to both quantitatively and qualitatively compare the flame-spread characteristics of different surface-lining materials as full-scale products. Because of the scaling problems and various other drawbacks associated with the Cone Calorimeter the Room Corner Test is superior in its ability to describe the flame spread characteristics of combustible materials. This is also a reason why it was been chosen as a reference scenario for the newly developed Single Burning Item test, SBI[91], which is an intermediate-scale test with a sample size of about 2 m^2.

The Room Corner Test was constructed to promote vertical flame spread and ignition of combustible ceilings by use of a 100 kW (first 10 minutes of the test) and 300 kW (after 10 minutes) corner fire from a square burner measuring 0.17×0.17 m^2. These characteristics yield a non-dimensional heat release rates, evaluated using the correlation $\dot{Q}^* = \dfrac{\dot{Q}}{\rho_0 c_p T_0 D^2 \sqrt{gD}}$, of $\dot{Q}^*_{100\mathrm{kW}} = 5.6$ and $\dot{Q}^*_{300\mathrm{kW}} = 16.9$, respectively, both of which can be considered to be too high to represent a buoyancy-controlled enclosure fire[*], their thus providing somewhat artificial numerical results concerning the rate of flame spread on wall linings.

Test data available
Measurements of the rate of heat release (RHR) and the smoke production rate (SPR) are commonly reported for each test. Time to flashover, defined by a limit RHR of 1000 kW or the occurrence of flames emerging from the door, is likewise reported or, in the cases in which a flashover does not occur, the peak RHR during testing is noted.

In some reports, originating mainly from early work on method development and standardisation, several key parameters are accessible. Two such sources are reports from the Swedish National Testing and Research Institute, SP Report 1986:45[41] and SP Report 1998:11[92]. The first also provides data on gas temperatures in the front corner, wall surface temperatures, total heat flux to the floor, convective heat flux and mass flow through the opening, visual estimation of transient flame spread (burning area) and the properties of the fire gas.

[*] By comparison, consider a heptane pool fire, 1.0 meter in diameter. The mass loss rate is about 0.067 kg/m^2s and the effective heat of combustion 41.2 MJ/kg, resulting in a non-dimensional heat release rate of 2.5.

6.2 Calculation results from calibration simulations

The aim of this section is to evaluate the consistency of predictions of the wall flow conditions using CFD methodologies. The geometry and the basic conditions used for simulation in this section are the same as in the experimental series of Blomqvist and van Hees, Figure 30, however, the sample material is made non-combustible by deactivating the pyrolysis models within the CFD codes.

A number of simulations were performed in order to evaluate the influence of different input data, such as grid dependencies, length of time step and wall characteristics, on predictions of wall heat fluxes, wall surface, and gas temperatures, etc. Since simulation of the turbulent reacting flow provides the input for the pyrolysis models, it is of great importance that the dependencies and uncertainties of the general CFD codes be documented and be distinguished from those inherent in the pyrolysis model itself.

Unfortunately, no experimental data concerning non-combustible panels are available. Instead, simulations are compared with each other to assess their predictive sensitivity to different simulation conditions. The default conditions are thus of little importance, as long as they are used consistently. Note that all the graphs without a time dependency are taken from the simulation time 60 seconds.

6.2.1 RANS code performance

Most of the calibration simulations have been made using the Reynolds Average based CFD code SOFIE. The results are presented and discussed below.

Often, some maximum values for normalised residuals are used to define a converged solution. Using this as the only criteria for convergence may be questionable, however, since the numerical values are not comparable between different codes (or, indeed, simulations). Sometimes, if one does not take adequate account of the grid distribution (for example in using large mesh-size ratios between neighbouring cells, or highly skewed, flat cells), the solution residuals normally remain constant at a rather high value. This implies that the solution is still oscillating somewhere in the flow field.

In evaluating simulations using the implicit time marching scheme the approach employed in this study has been to complement the normalised residual criteria by monitoring important flow variables at key locations, preferably where gradients are expected, plotting these values against the number of iterations made, thus defining a converged solution and at the same time avoiding their being an excessive number of iterations.

Dimensionless distance, y^+

The importance of the dimensionless distance between a wall-adjacent node and the wall surface, y^+, was discussed in section 4.2.3. For the wall flow to be correctly reproduced by use of the wall function method, it is generally recommended that the first fluid cell, the one closest to the wall surface, be placed within the fully turbulent region, or $y^+>30$[*]. Some

[*] The interested reader can find many sources of information on the www, for example the discussion forums at www.cfd-online.com.

researchers would argue, however, that it is perfectly all right to go below this value and thus switch to the laminar wall functions once $y^+ \approx 10$ (for smooth walls). Whatever choice is made could be expected to affect the prediction of the convective flux.

One problem associated with the buoyancy-controlled reacting flow is the significant variation of y^+ in height. This is illustrated in Figure 31, in which the graph shows the variation in y^+, close to the centreline of the panel, with height. Just above the burner, in the lower part in the graph, the turbulent kinetic energy is low, resulting in a very small y^+. Higher above the burner, the turbulent kinetic energy becomes large, y^+ increasing rapidly as one goes upwards, although, the value does not extend beyond the fully turbulent log-law zone, as defined in Figure 23.

In the simulations of the vertical-panel test, achieving a value of y^+ below 30 at all points on the sample was not possible, regardless the size of the grid resolution close to the wall. This could affect the predictions of convective heat flux, although it could be difficult to estimate to what extent.

In Figure 31 it is clear that the numerical definitions of y^+ are not fully consistent. This is possibly due to the assumption of local equilibrium, see section 4.2.3. If not stated otherwise the y^+ numbers in this report have been calculated using Equations [49], [50] and [52].

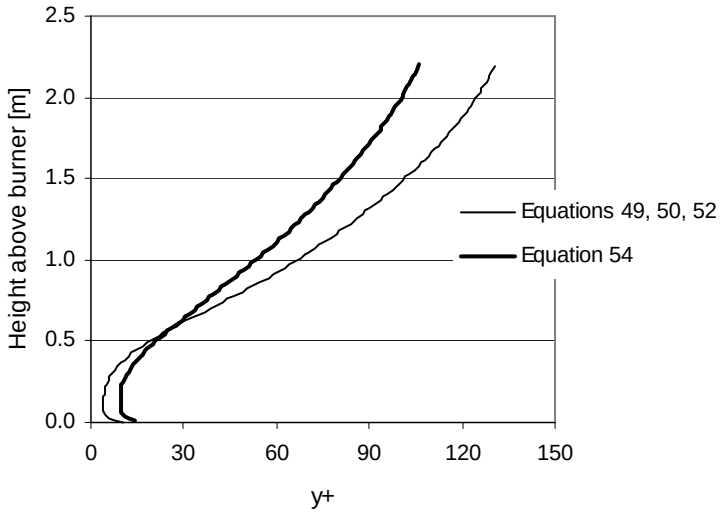

Figure 31. Variation in y^+ with height, as evaluated in the wall-adjacent cells close to the centreline of the sample.

Variations in y^+ across the wall plume at two different locations above the burner are shown in Figure 32.

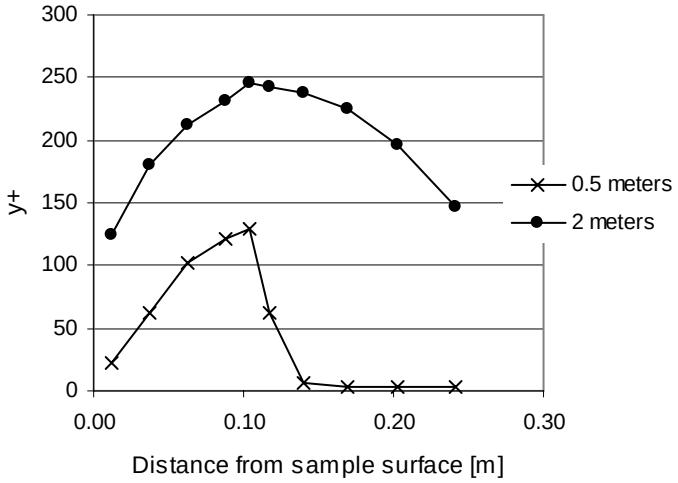

Figure 32. Variations in y^+ across the wall plume at two different vertical locations at the centreline, about 0.5 and 2 meters above the burner, respectively. One can note that the turbulent kinetic energy is rather low and that the entire plume falls within the fully turbulent layer, see Figure 23.

In the pages that follow, various graphs are presented to provide a basic idea of how differing computational conditions affect such variables as wall heat flux and surface temperature. Most of the simulations are performed using the CFD code SOFIE, although comparisons with the other codes have also been made. The following default settings are employed:

Table 7. Default values using SOFIE

Radiation	DTRM, 64 rays, WSGG approximation
Fuel	Propane, soot = 2.7% by mass of fuel inflow[1]
Numerical scheme	Hybrid (generally first order accurate)
Turbulence model	Standard k-ε with buoyancy
Combustion model	Eddy Dissipation Concept
Time step	1 second
Ambient temperature	298 K

[1] The soot fraction originally chosen was 4.8% by mass, a value selected rather arbitrarily, not aimed at reflecting directly the values found in the literature. Since a small bug discovered later in the SOFIE source code was found to have the effect of the soot content being represented as a fraction of the volume flow rather than of the mass flow, the value originally selected is here corrected by the fuel density.

Node dependence

Ideally, the numerical solution in any CFD simulation should go towards the exact solution of the governing, partial differential equations. This is the essence in the concept referred to as consistency. In the problem at hand, however, more acute questions are those of the performance of the different model equations and of their relevance to the problem. The different submodels may vary in their suitability so that some of them have an unwanted influence on the results. One such model is the turbulence model, which uses a wall-function approximation to avoid the need of the entire boundary layer being resolved. Another such model is the submodel governing the combustion. It may come as no surprise, therefore, that the results of making the wall-adjacent cell smaller only partly support there being node independence, as shown in Figure 33 and Figure 34 below.

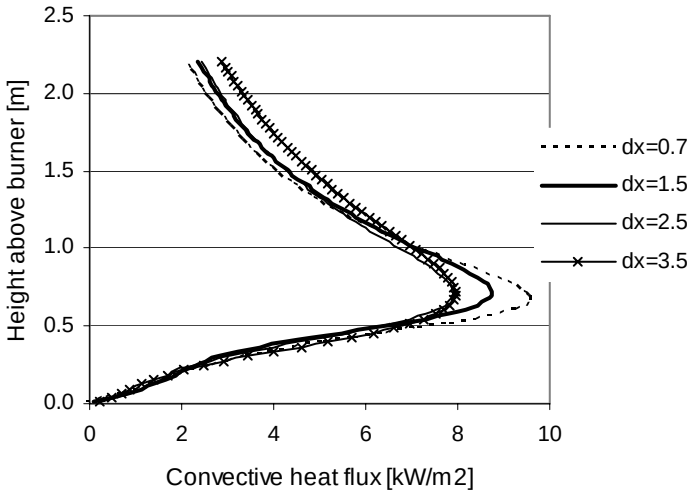

Figure 33. Convective heat flux to the sample surface as a function of height above the burner rim for different grid resolutions. The symbol dx represent the size, in centimetres, of the wall-adjacent node in the direction normal to the surface. The grid sizes in the plane parallel to the sample are about 2.5 cm.

The convective heat flux for the 2.5 cm and 3.5 cm cells, from the burner rim and to about 1.0 meter above it, clearly match rather well, whereas for the 0.7 cm and 1.5 cm cells, a certain difference is evident. Above this interval the simulation using a 3.5 cm wall-adjacent cell size deviates slightly, whereas the other results converge. The predictions for very low y^+ also differ in no appreciable way from one another, suggesting the equilibrium wall functions to perform well, or equally bad, irrespective of the grid resolution.

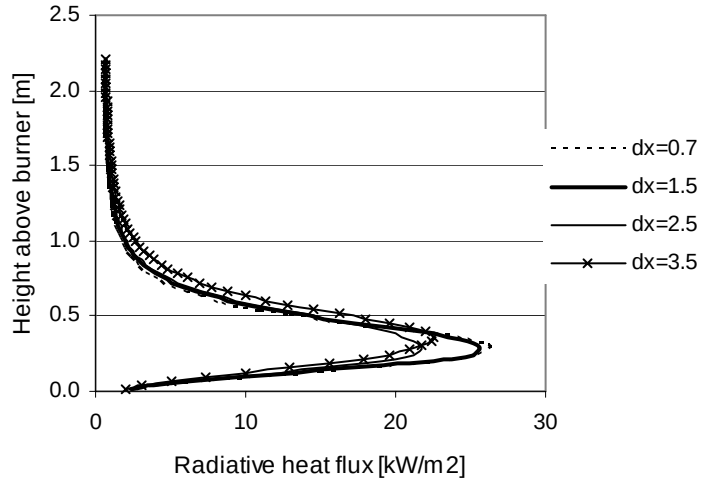

Figure 34. Heat flux due to thermal radiation as a function of the height above the burner. The dx values (in cm) represent size, in the direction normal to the surface, of the cell closest to the sample.

Thermal radiation represents about 2/3 of the total heat flux. Because of its strong dependence on temperature the numerical value can be expected to show a certain grid dependence. The results for dx=0.7 cm and dx=1.5 cm are nearly identical and above the flame all the lines are

rather closely packed. However, the maximum radiation flux from the flame, predicted using dx=3.5 cm and dx=2.5 cm, is noticeably lower than using the other two grid resolutions.

In Figure 35 the horizontal temperature distribution across the fire plume is shown at 0.5 meters above the burner for the different grid resolutions. It can be noted that the relative differences are very small.

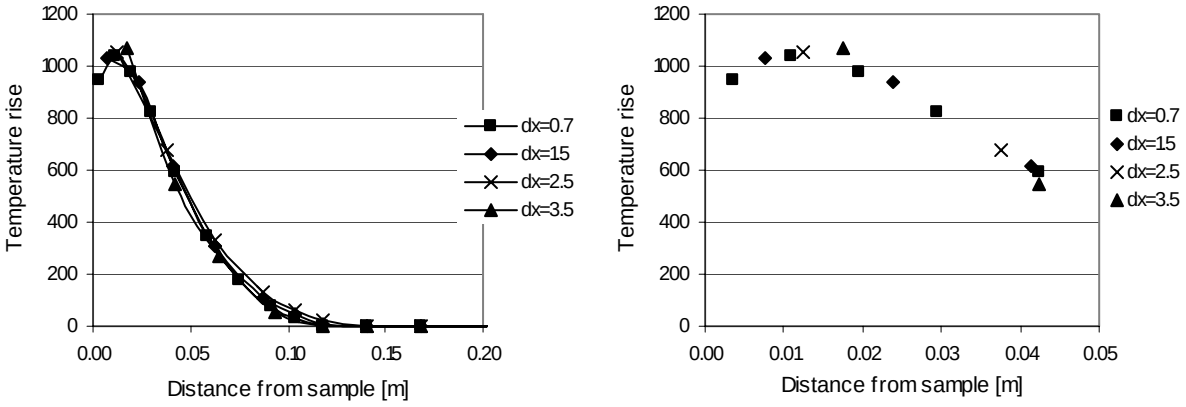

Figure 35. Temperature distribution normal to the sample surface at a location 0.5 meters above the burner edge. The graph at the right is a magnification of the left hand graph.

Further upstream in the gas plume the relative differences are greater, as can be seen in Figure 36. All the predictions of the plume width agree well, regardless of the grid resolution but the temperature in the cells adjacent to the wall differ from one simulation to the other. This suggests that the entrainment of air into the plume is differently predicted.

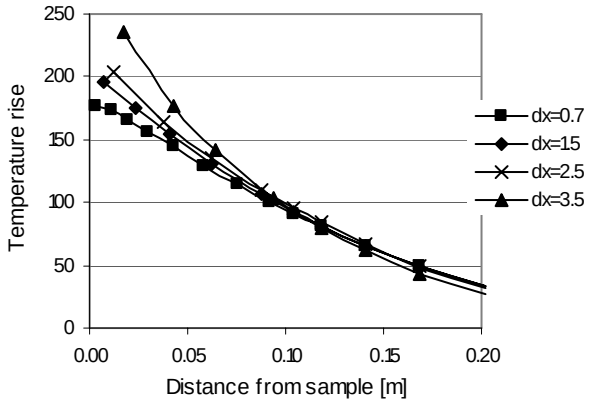

Figure 36. Temperature distribution in the direction normal to the sample surface, data extracted at about 2 meters above the burner edge.

The dependence on the grid resolution in the plane parallel to the sample surface is shown in Figure 37, two different aspect ratios are tested, the cells in the direction normal to the surface being 1.5 cm in size. A small change in the results can be seen, the maximum total difference (the sum of incident radiation and convection) being about 6 %.

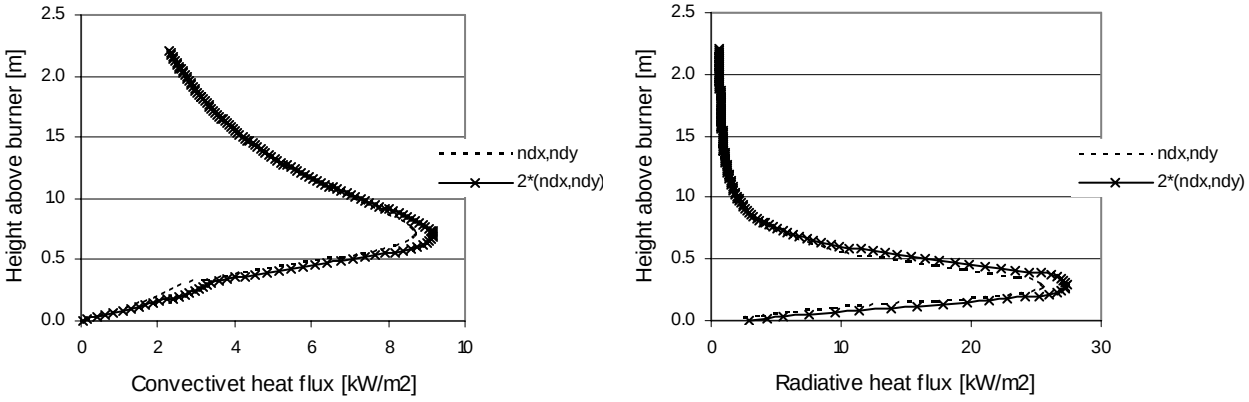

Figure 37. Dependence of the results on grid resolution in the two directions parallel to the sample surface. Results of the original simulations, termed ndx,ndy, for which there is a grid aspect ratio of about 2, are compared with those of a simulation in which the number of cells in the two directions parallel to the sample surface is twice as large.

Time step

Much in the same way as for the node dependence, a converged solution should, strictly speaking, be independent of the length of the time step (as long as the numerical scheme is stable). In Figure 38 it can be seen that the convective heat transfer is not affected at all by the time step being changed from 0.5 seconds to 2 seconds. The maximum incident radiative flux for the 2-second time step differs slightly from the solutions using the 0.5- and 1-second time steps.

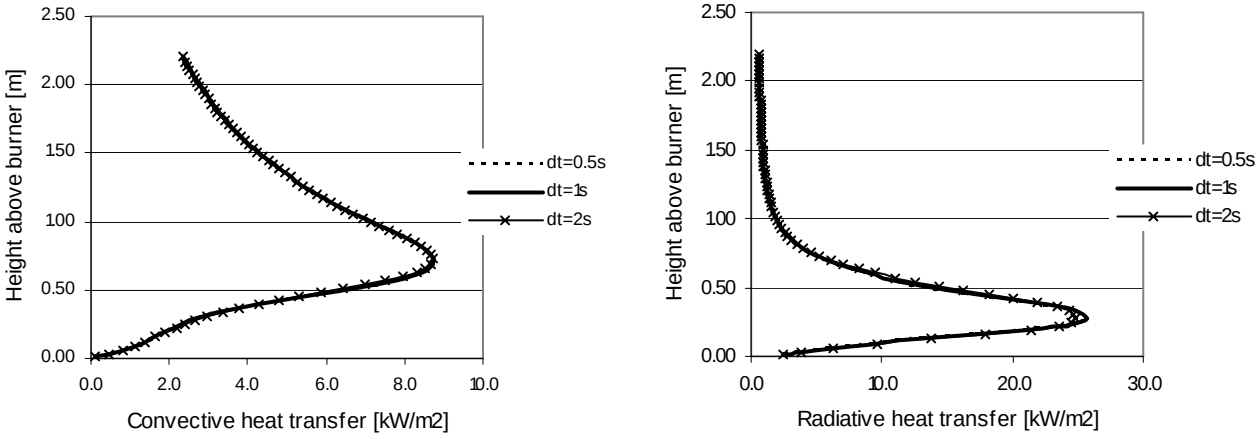

Figure 38. Dependence of the solution on the time step.

Radiation ray number

The number of rays that are launched from the cell surfaces at the boundaries (most importantly from the sample surface) was not expected to generate any noticeable differences. This is connected with the two-dimensional character of the scenario, which makes determining of the major influences rather unproblematical, even when a moderate number of rays are employed by the radiation model. In Figure 39 the incident heat flux due to radiation is shown for two different grid resolutions, there being found to be only a slight dependence

on the number of rays, although it can be noted that a finer grid resolution between the burner and sample surface improves the convergence.

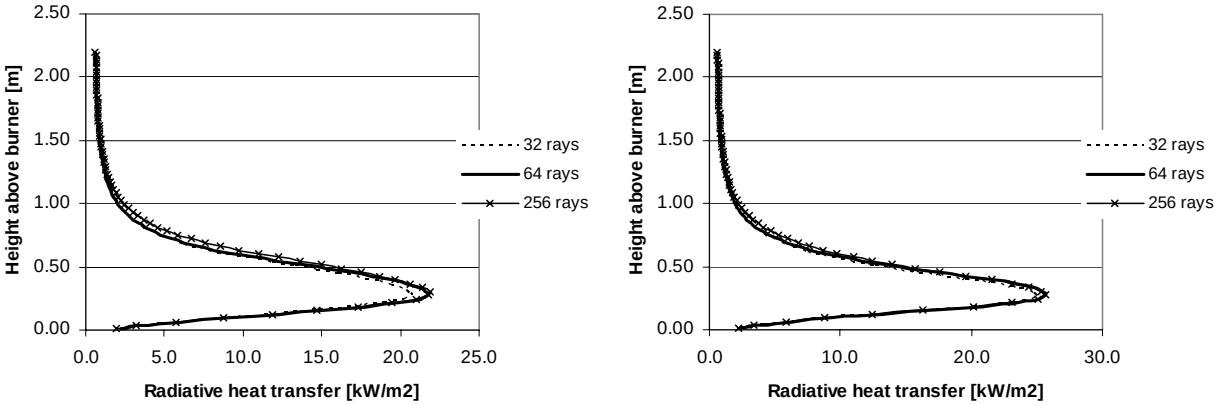

Figure 39. Influence of the number of radiation "rays" launched from the surface cells of the sample using the discrete transfer radiation model. The wall-adjacent cell size normal to the sample is 2.5 cm in the graph at the left and 1.5 cm in that at the right.

Wall conditions

The wall temperatures that SOFIE provides may be somewhat inaccurate, this is due to that Sofie solves the heat transfer within solids using the same grid as used for the fluid flow, which results in a rather poor resolution of the conductive heat transfer problem. The evaluations presented in this section based on use of Sofie alone are only for comparative purposes.

Currently, the transpiring wall condition used by Sofie needs to be complemented by an isothermal wall boundary. Accordingly, a constant temperature needs to be assigned* to the wall surfaces. This alters the net heat transfer conditions at the sample surface as shown in Figure 40.

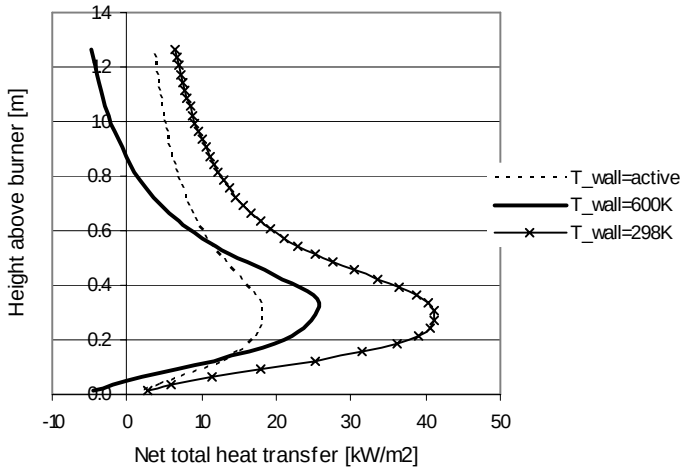

Figure 40. Net total heat flux to the sample surface as a function of height above the burner. T_wall=active implies that the heat transfer equation is solved within the material.

* Although this can, be changed during the simulation, the benefits of such a procedure must be considered rather uncertain and ad hoc.

Using a constant temperature of 298 K, the net heat transfer is severely overpredicted as compared to the "active wall" calculations. Using an isothermal temperature close to the ignition temperature of wood results in a situation in which the wall (above the flame) heats the gas and not the other way around.

Numerical approach

In the finite volume approach, a balance of the physical quantities is made for the entire control volume, ensuring that the physical law is satisfied over a finite region rather than only at a point as the grid size goes to zero. The amount of work the calculations require puts an effective restraint, however, on the complexity of the numerical scheme used to propagate flows and disturbances throughout the domain.

A hint of how well a numerical scheme approximates the exact solution of the original continuous, partial differential equation is given by its "order of accuracy". The default scheme in Sofie is the hybrid scheme, which is a combination of the upwind and the central differencing schemes. The hybrid scheme is, generally, first order accurate in space meaning that its truncation error depends directly on cell size, Δx.

To evaluate the influence of the choice of numerical approach, predictions obtained using the hybrid scheme were compared with solutions obtained using a TVD scheme of second-order accuracy based on van Leer[50]. Figure 41 shows the results on incident fluxes from such a comparison. Although the predictions confirm the maximum values, the distribution of the second-order scheme is shifted upstream in space. When the hybrid, first-order accurate, scheme is employed, the plume width is broader as can be seen from Figure 42. This can be expected since the truncation error for first-order schemes tends to reduce all gradients in the solution, due to what is often referred to as numerical dissipation.

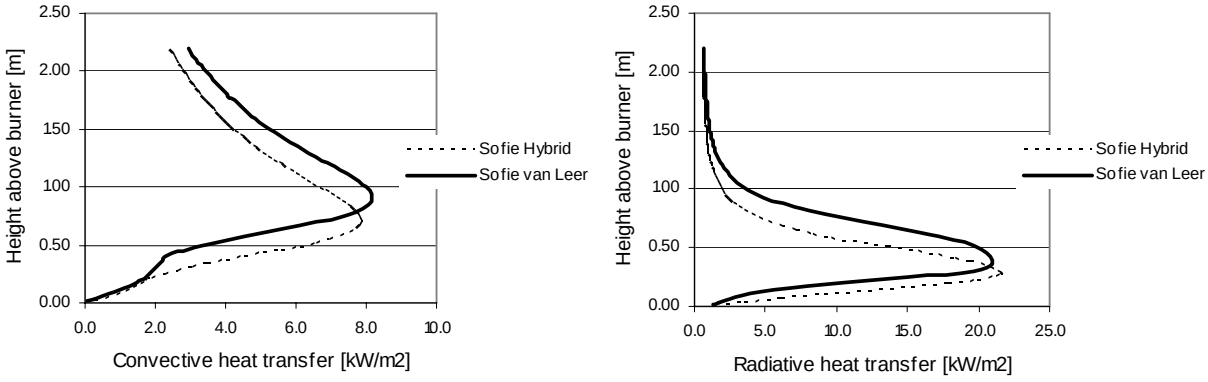

Figure 41. Influence of the numerical scheme on predictions of incident convective and radiative heat fluxes. The grid size of the wall-adjacent node, in the direction normal to the sample, is 1.5 cm.

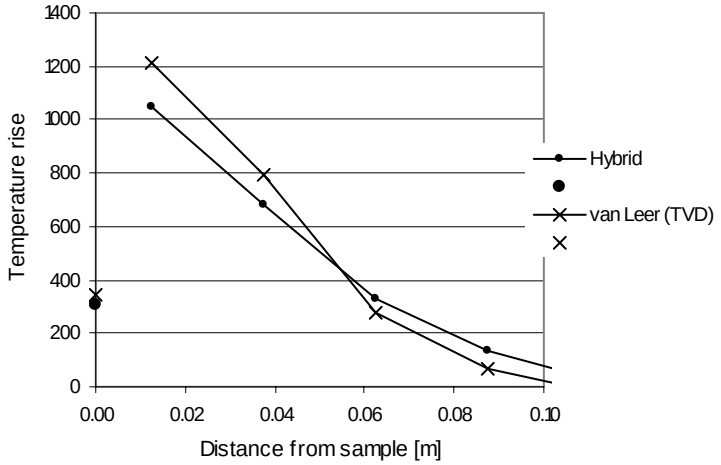

Figure 42. Temperature distribution in the direction normal to the sample surface at a location 0.5 meter above the burner edge. The values located at single points on the ordinate are wall surface temperatures.

By way of comparison, Figure 43 shows the node dependence in using the numerical scheme based on van Leer. As in the simulations using the hybrid scheme, the node convergence appears to be good, except for the heat flux predictions in the region behind the main flame. As in Figure 35, the gas temperature converges very well in the number of nodes.

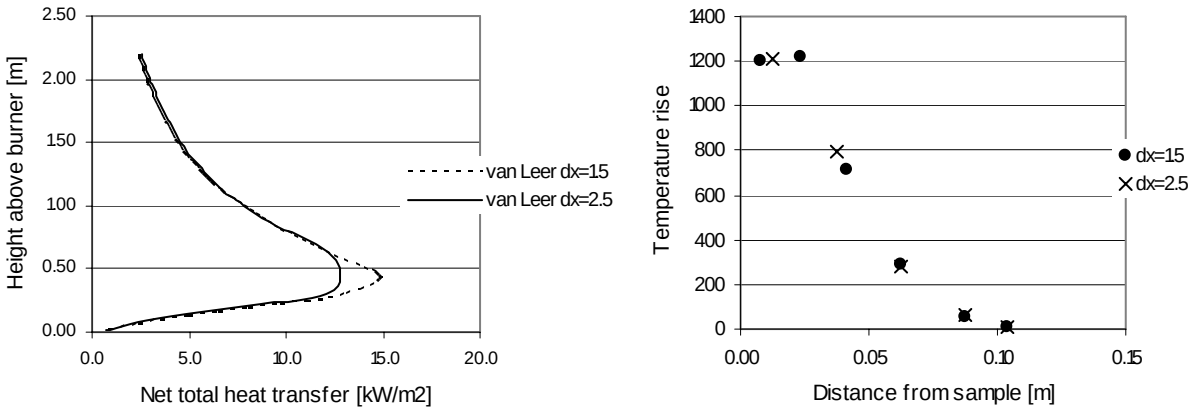

Figure 43. Node dependencies when using the second order accurate TVD numerical scheme based on van Leer and wall-adjacent nodes sizes in the direction normal to the surface of 1.5 cm and 2.5 cm respectively. To the left is the net total heat flux, which is a parameter used directly in flame spread modelling, and to the right the gas temperature in the direction normal to the sample at a location about 0.5 meters above the burner edge.

Turbulence model

The k-ω model which follows with the current version of Sofie (v. 3.3) was used in an attempt to resolve the boundary layer. Since the implementation of the model was not completely known at the time these simulations were made, the numerical results may not be fully representative, although the qualitative trends obtained in a first study of this sort appear informative.

Two different grid resolutions were employed 0.07 cm and 0.1 cm, respectively, in the normal direction from the sample surface. The maximum grid aspect ratio over the sample was about 25 for the first case and about 17 in the second. The sensitivity of the first simulation was

studied by increasing the number of nodes, resulting in an aspect ratio of 14. The results are given in Figure 44 and Figure 45. Again, because of the uncertainties in the model implementation as well as the behaviour of the combustion model at the "laminar" layer close to the wall, etc., the graphs should only be viewed as providing qualitative information. It should also be noted that the maximum height on the ordinate has been changed.

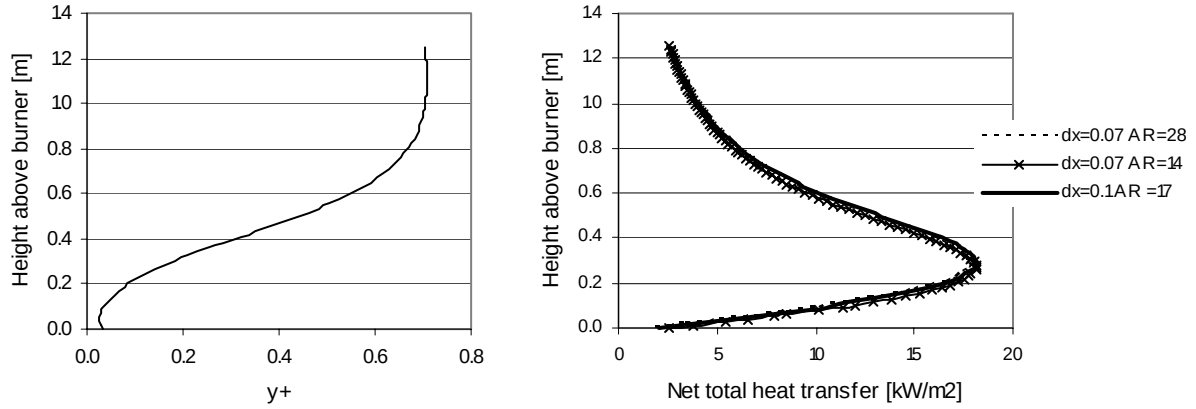

Figure 44. Resulting y^+ for a wall-adjacent node size of dx=0.07 cm (left) and the total net heat flux as a function of height above burner (right). AR=Aspect Ratio, dx is the size (cm) of the wall-adjacent cell in the normal direction from the sample surface.

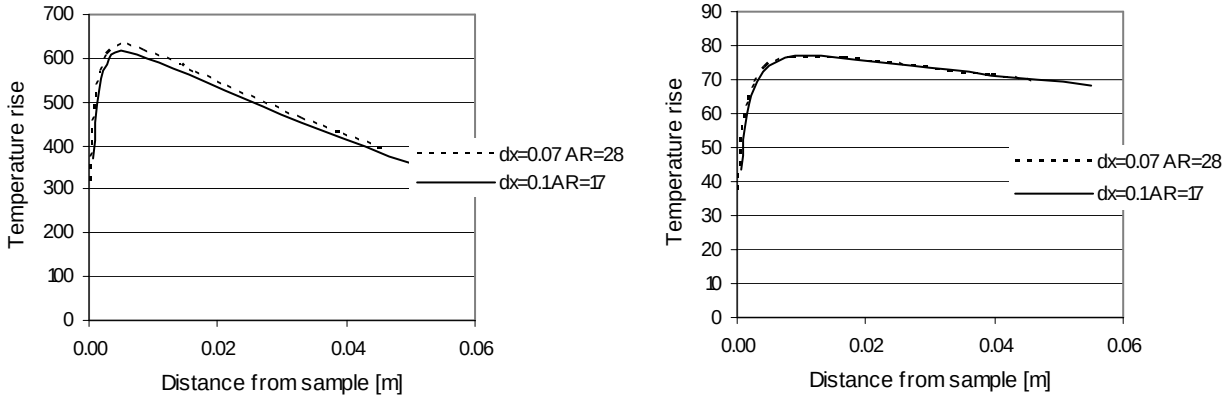

Figure 45. Temperature distribution in a direction normal to the sample surface at a distance 0.5 and 2 meters above the burner edge. The agreements are close. AR=Aspect Ratio, dx is the size (cm) of the wall-adjacent cell in the normal direction from the sample surface.

CFD code

Both SOFIE and SMAFS were originally developed to solve the Reynolds averaged Navier Stokes equations. In order to be able to compare the flame spread models within the codes, it is important that the differences in heat transfer predictions be known. Figure 46 and Figure 47 shows a number of simulations using the different CFD codes. SMAFS uses the Power Law Differential Scheme (PLDS), which is first order accurate and the Modak model for evaluating the radiation emitting medium.

The data may have been taken from slightly different locations (likely less than 1 cm apart) due to differences in the handling of coordinates in the two codes, but nevertheless, the shape of the flame is clearly predicted differently. The reason to this is not known*.

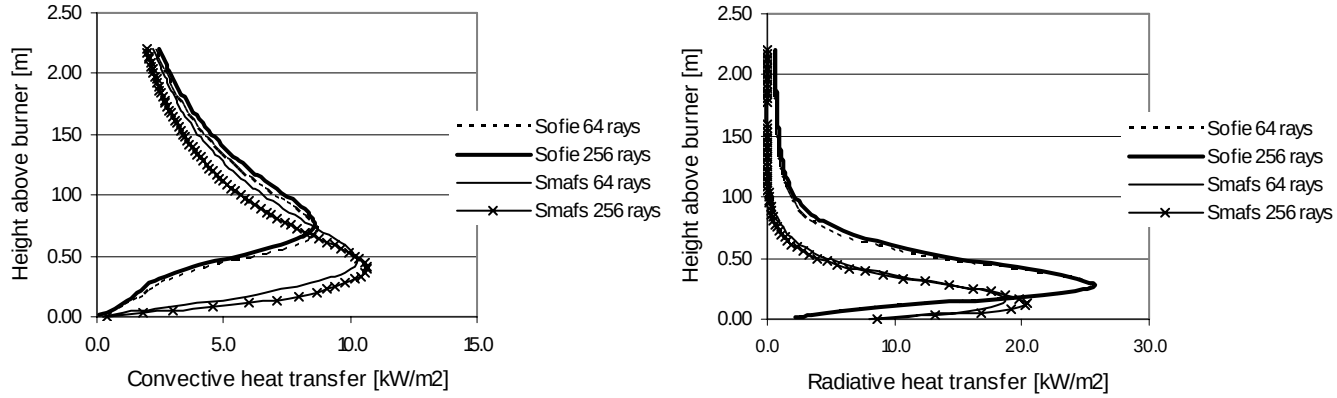

Figure 46. Incident convective and radiative heat transfer as a function of height above the burner edge. The size of the wall-adjacent control volume is 1.5 cm in the direction normal to the surface.

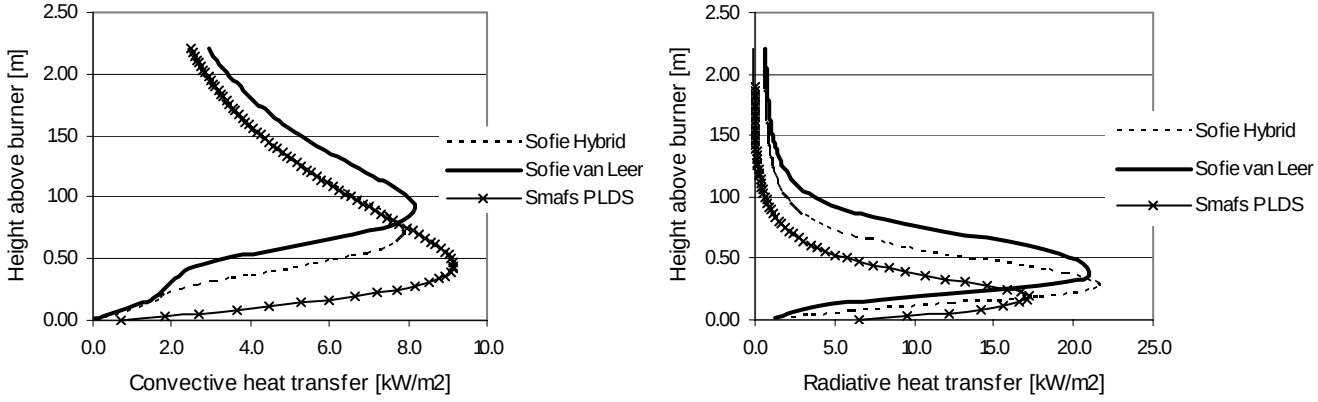

Figure 47. Incident convective and radiative heat transfer as function of height above the burner edge. The size of the wall-adjacent control volume is 2.5 cm in the direction normal to the surface.

6.2.2 FDS performance

Various comparative simulations were made in FDS for studying the effect of the grid resolution on the results. The results are given below. Three different grids were employed, one using fewer grid nodes but applying a stretch to obtain a comparable grid size in the near field of the flame (about half a meter from the sample in the normal direction). The maximum aspect ratios within the computational domain were 1.7, 1.4 and 2.6, respectively.

* It should be emphasised that the inputs of the two simulations differ in terms of the soot content prescribed, the fraction of soot in the SMAFS simulations being 4.8 percent by mass and that in the SOFIE simulations 2.7 percent by mass, which can be shown to have an effect on the final results.

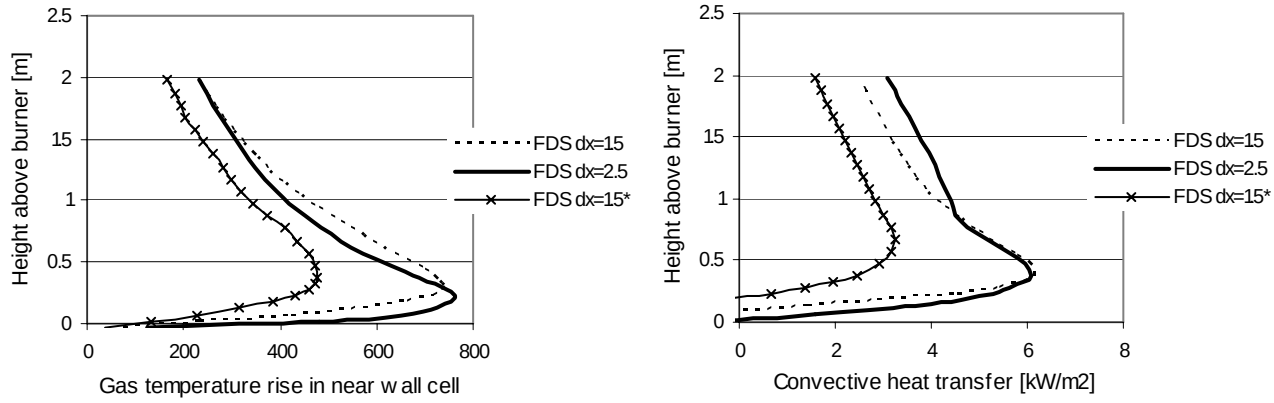

Figure 48. Rise in gas temperature over the ambient (left) and convective heat flux to the sample surface as a function of height (right). The symbol dx denote wall-adjacent grid size in cm, the star (*) signifying that the grid has been stretched to arrive at the resulting grid size.

The convective heat flux profiles appear reasonable in shape, showing the values to be slightly lower than the earlier results of the RANS models. Stretching the grid affected the results markedly. A node dependence is apparent, though not sufficient to have an influence on the flame spread calculations.

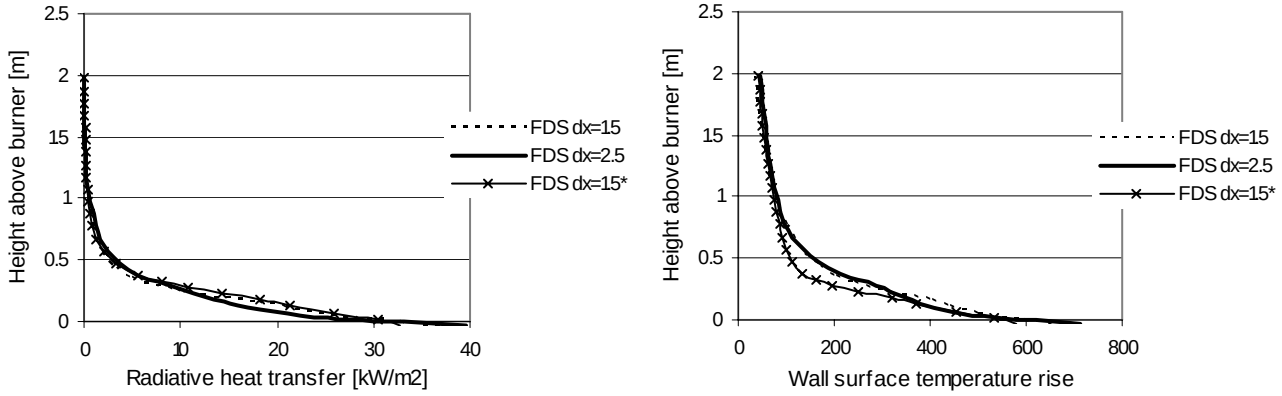

Figure 49. Radiative heat flux (left) and surface temperature rise above ambient (right) as a function of height above the burner edge. The dx denote wall-adjacent grid size in cm, the star (*) signifying that the grid has been stretched to arrive at the resulting grid size.

The prediction of the incident radiation heat flux makes little sense, however, its maximum occurring at the same level as the bulk of the burner, which contradicts the gas temperature profile shown in Figure 48. The radiation flux dominates the heat transfer to the sample, the surface temperature thus showing a similar distribution.

Figure 50 shows the temperature distributions over the fire plume at two different heights above the burner. Again, the results of the simulation using a stretched grid differ in shape and value. The plume width is not consistently predicted but close to the wall the two non-stretched-grid simulations agree well at both locations in the plume suggesting consistent predictions of the entrainment of air.

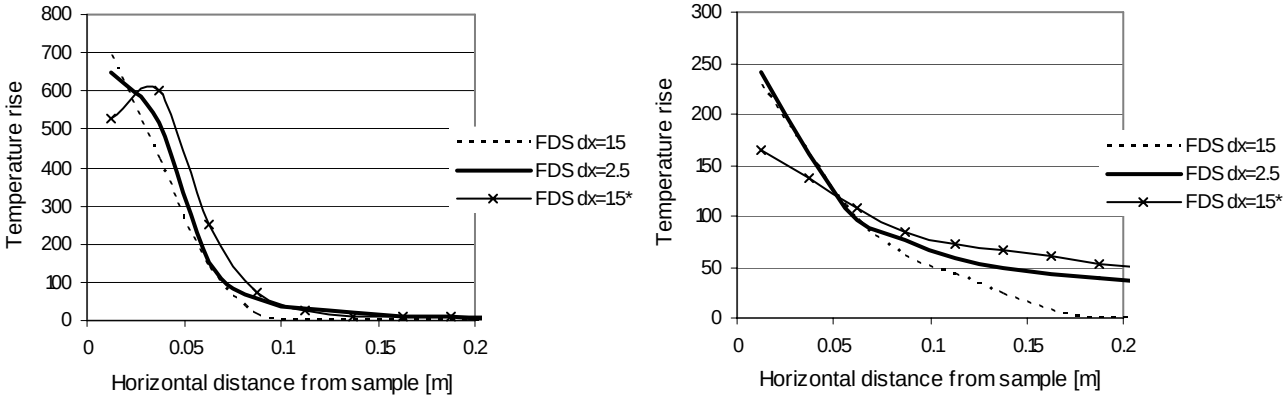

Figure 50. Horizontal temperature profiles over the fire plume at a location 0.5 meters (left) and 2 meters (right) above the burner edge, respectively. The symbol dx denotes the wall-adjacent grid size in cm, the star (*) signifying that the grid has been stretched to arrive at the resulting grid size.

6.3 Results of the CFD based flame-spread calculations

The models considered in this chapter are all concerned with how different materials respond to a given net thermal heat flux. Since general pyrolysis or material models are involved the required input data is not believed to change much from one configuration to another or from one scenario to another. Accordingly, once the mandatory set of material properties for a certain material has been derived these are expected to be valid for all configurations.

Values in the literature concerning the thermal properties of practical building materials are often in short supply, particularly concerning parameters dependent upon temperature or moisture content such as wood and char conductivity, specific heat capacity, coefficients of chemical kinetics and heat of pyrolysis. The modeller is normally referred to small-scale experiments, such as the Cone Calorimeter, for deriving the set of model parameters that represent the best fit to the measurements, or for justifying the choice of a particular input data. However, such experiments utilise rather artificial boundary conditions, ones not generally appropriate for use in more authentic room-fire scenarios. It may thus be advisable to consult relevant literature, at least so as to determine whether the parameter chosen has a value within a plausible range. In addition, one may need to take account of the known weaknesses of the Cone Calorimeter.

Since the Cone Calorimeter constitutes the most practical choice here, the general problem arises of all the drawbacks associated with this test becoming inherent in the input data optimised according to the test and hence in the final flame spread calculations as well. Analysing the relative importance of these errors is beyond the scope of this dissertation. In the simulations presented in this study the experimental results based on the use of the Cone Calorimeter have been employed, despite the potential errors this involves.

A true comparison of the different pyrolysis models is only possible in a stand-alone mode in which all the fluxes are controlled by the user. This is because of the different CFD codes sometimes providing fundamentally different input conditions used in calculating the course of flame spread, as was shown in the previous section.

The Cone Calorimeter data used in this chapter was obtained from reference 93, which pertain to the board materials used in the Blomqvist-van Hees tests. In the present study, only the particleboard tests have been assessed.

6.3.1 Yan pyrolysis model

Development of the Yan pyrolysis model was based upon consideration of the heat transport into a solid material. The thermal response of the material is modelled using a constant heat of pyrolysis applied on an extremely fine moving subgrid. Since the nature of pyrolysis has been significantly simplified in the model, the relevant input data need to be derived using Cone Calorimeter experiments and cannot generally be obtained from the literature.

Cone calorimeter

Thus, to derive the required input data, the model was used in a stand-alone mode, the calculation results being compared with measurements obtained at three different heat fluxes in Cone Calorimeter experiments, a best fit to the heat release rate being obtained by use of an iterative procedure. The final input parameters chosen are given in Table 8. Lumped parameters were employed. This demonstrates the difficulties with the lack of input data but it is also due to the model not providing sensible results when the values suggested by Fredlund[8], for example, were employed.

Comparisons of the experimental results with results of the model, using input data as referred to below, are shown in Figure 51.

Table 8 Input to a particleboard corresponding to a best fit to Cone Calorimeter measurements.

Pyrolysis temperature	= 593 K
Specific heat capacity	= 2.7 kJ/kg
Thermal conductivity	= 0.30 W/mK
Density of virgin solid	= 570 kg/m^3
Density of residual char	= 57 kg/m^3
Heat of pyrolysis	= 1.10 MJ/kg
Heat of combustion	= 14 MJ/kg
Heat flux from flames	= min(0.1*RHR,20) kW/m^2 (only used in stand alone mode)

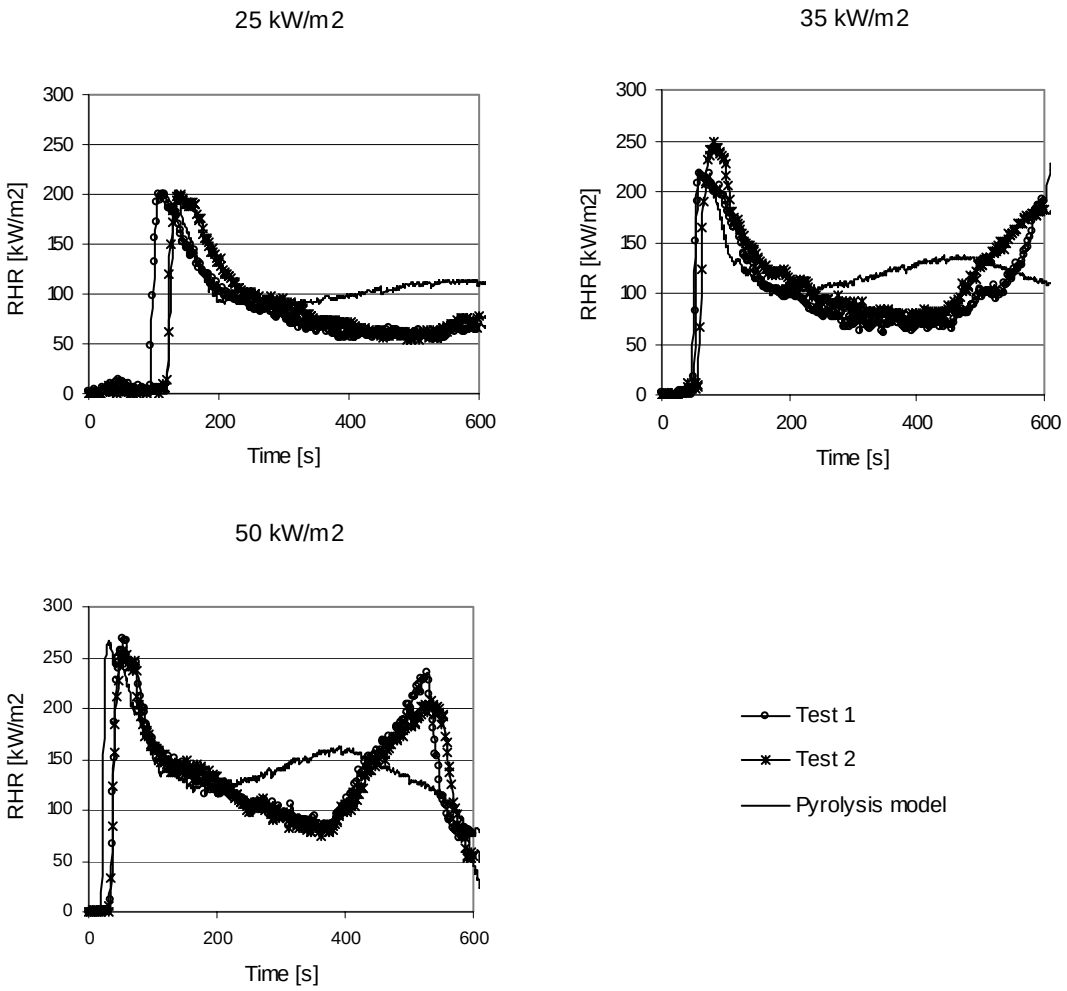

Figure 51. Results for the pyrolysis model using the input data as shown in Table 8.

Any of the result in Figure 51 above about 200 seconds (or where the gradient changes direction) is directly controlled by the thermal properties of the backing material or, more correctly by the thermal boundary conditions on the rear surface of the sample. Figure 52 provides a qualitative illustration of this dependency.

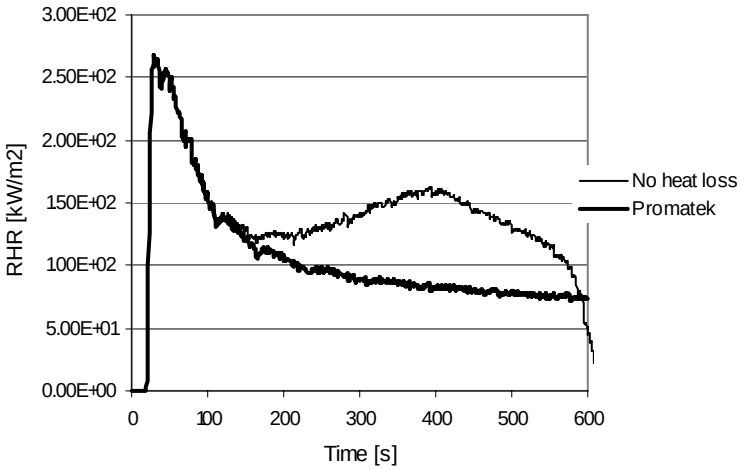

Figure 52. Model predictions for differing boundary conditions at the rear surface. The original setting basically assumes a very well isolated backing material which reflects the conditions in the Cone Calorimeter. The curve designated as Promatek use a Promatek H* backing, which is sufficiently deep to prevent the thermal wave from penetrating through its rear surface.

Vertical flame spread test

Although it may look uncomplicated at first glance, the upward flame spread test by Blomqvist and van Hees represents a rather complex scenario. The major difficulties involved are the prediction of the limit at which the flame spread stops and the heat release rate starts to decline, eventually causing the panel fire to self-extinguish.

Figure 53 presents a comparison between the experimental total rate of heat release and predictions from three simulations using different grid resolutions. The grid sensitivity is noticeable, no node convergence is detectible. The size of the grid in the plane parallel to the sample was constant 2.5 cm.

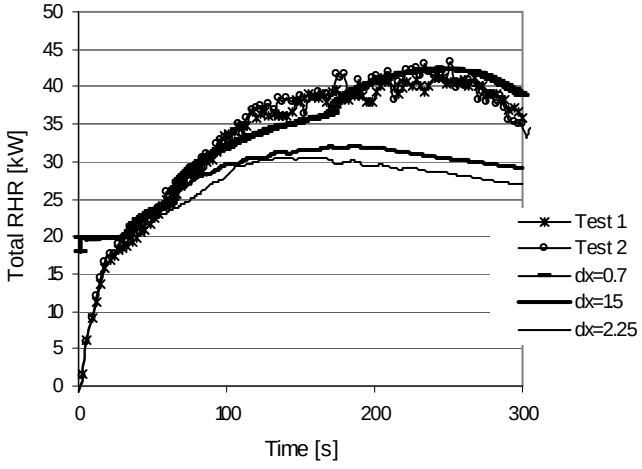

Figure 53. Predicted and measured rate of heat release. The symbol dx denote wall-adjacent grid size measured in cm. A constant soot mass fraction inflow was used, corresponding to 0.024 for burner propane and 0.015 for the pyrolysis gases.

* A fiber-reinforced calcium silicate board.

The original calculations by Yan[71] used propane diluted with carbon dioxide and water vapour to represent the pyrolysis gases. Since the CFD code allows multiple reactions, this simplification is not necessary. Consequently, the predictions in Figure 53 all used pyrolysis gas properties according to data suggested by Fredlund[8].

Figure 54 shows the best fit prediction from Figure 53, using dx=0.7 cm close to the sample surface and the pyrolysis gas properties suggested by Fredlund, comparing the results with those of an equivalent simulation using diluted propane to represent the combustible pyrolysis gas. The predicted total heat release rate is noticeably lower in the simulation using the data according to Fredlund but the overall shapes of the predicted RHR curves are quite similar.

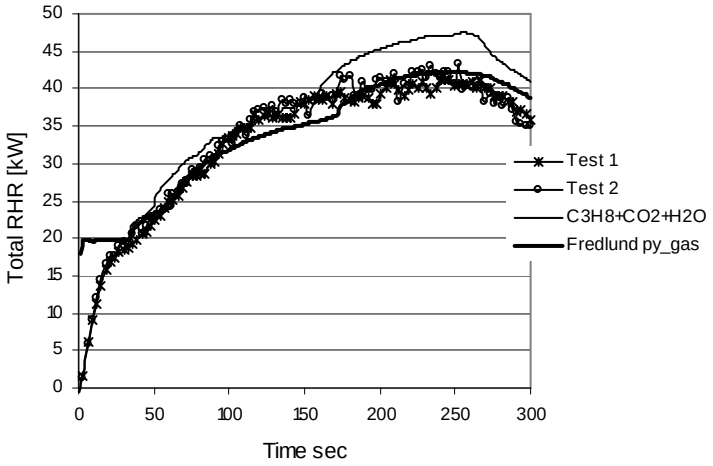

Figure 54. Influence of the composition of the pyrolysis gas. The input data is chosen in accordance with Table 8 and the wall-adjacent grid size is 0.7 cm in the direction normal to the sample.

The total heat flux to the sample surface is measured at two different locations on the vertical centreline of the sample, 0.75 and 1.25 meters, respectively, above the top of the burner. The measurements were performed using water-cooled Schmidt-Boelter flux meters[39], which has been taken into account by modifying the predictions to represent the flux towards a 25°C probe. A comparison of the measured and the predicted values is presented in Figure 55.

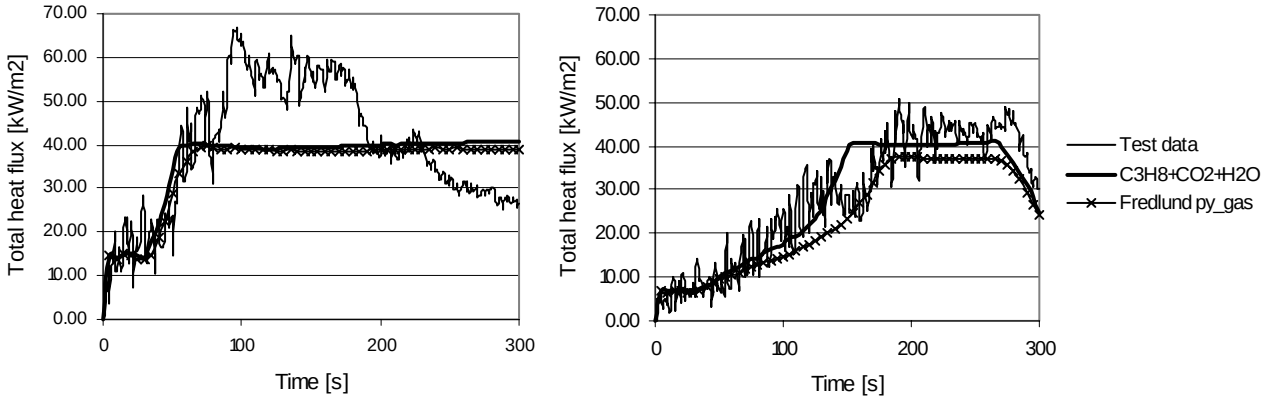

Figure 55. Total heat flux to a water-cooled probe 0.75 meters (right) and 1.25 meters (left) above the burner edge. The calculated values have been modified to apply to a probe temperature of 25 °C.

The experimental results as obtained by a flux gauge 0.75 meters above the burner are well predicted by both simulations during the time until the pyrolysis front reaches the location of the flux meter, after about 60-90 seconds. At that instant, the prediction finds an equilibrium at about 40 kW/m^2, the measured values ceases to rise then for only a short period of time, after which the data increases rapidly to about 60 kW/m^2. It can be thought that the measurement device is disturbed by the presence of soot on its outer surface, affecting the result from about 90 seconds upwards. The prediction based on the use of Fredlunds pyrolysis gas is slightly lower than that based on the use of diluted propane for representing the pyrolysis gas.

At a position 1.25 meters above the burner, the comparison is close. If the presence of a soot layer affects the gauge there 0.5 meters below, it is likely that these results are also affected. One explanation of this measurement appearing less affected by soot could be that the soot yield from the burning of wood is lower than the value for propane by a factor of two and that the soot content in the plume decreases with height. At this location, the prediction using Fredlunds pyrolysis gas is noticeably lower than the other calculation, the shape also being somewhat shifted in time. This coincides with the differences in the heat release rate predictions, shown in Figure 54.

In comparing Figure 54 and Figure 55 one can note that the simulation which shows the best correlation to the total rate of heat release is the one that underpredicts the incident heat flux. Put differently, the simulation showing the best agreement with the total heat flux is the one which overpredicts the resulting rate of heat release. Although the heat flux exposure is not completely clear, the conclusion from a qualitative point of view must be that there is a discrepancy, very likely in the input data in Table 8 and possibly also in the pyrolysis model itself.

The movement of the pyrolysis front is illustrated in Figure 56, where the average and the centreline predictions are presented and compared with visual observations from the video recordings and measurements using the 0.13 mm thermocouple. The average value is derived from the total area of burning, the centreline prediction corresponding to local ignition of the sample. The prediction is based on the simulation using diluted propane as pyrolysis gas and a wall-adjacent cell size of 0.7 cm in the direction normal to the sample.

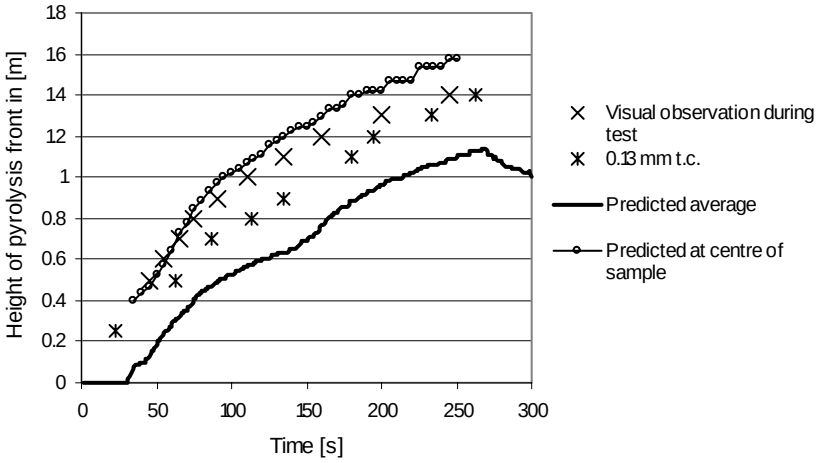

Figure 56. Predicted movement of the pyrolysis front as compared with test observations and measurements. Note that the step profile at the end of the centreline prediction is not a measure of the cell size but simply reflects the limited number of output points chosen in processing the data. The flame spread reaches a maximum at about 250 seconds, after which self-extinguishing of the panel starts.

It can be instructive to study a plot of the local heat release rate for the sample. Figure 57 illustrate the process of ignition and self-extinction at two points on the centreline of the panel. It should be considered together with Figure 55 and Figure 56. It may also be instructive to compare these results with the predictions of the Cone Calorimeter experiments in Figure 51. Such a comparison suggests the direct use of the experimental data in flame spread modelling to be questionable.

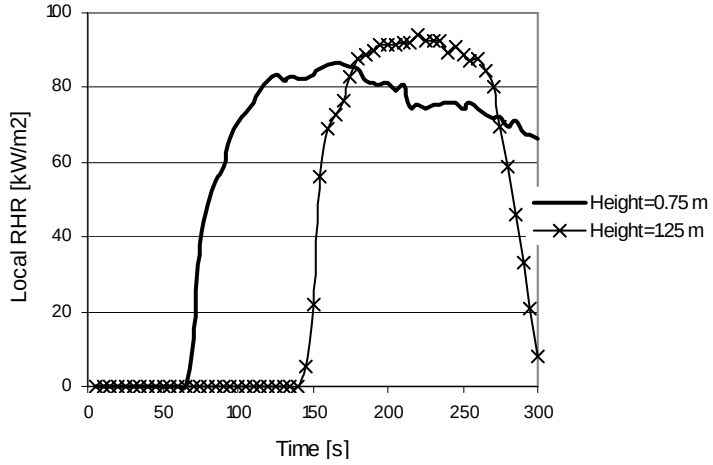

Figure 57. Local rate of heat release at two locations on the vertical centreline of the sample. The height is measured from the top edge of the burner.

The soot formation and its appearance in the combustion products have been greatly simplified by prescribing a constant soot fraction in connection with the fuel mass flux. The effect of the choice of this constant on the predicted RHR is shown in Figure 58.

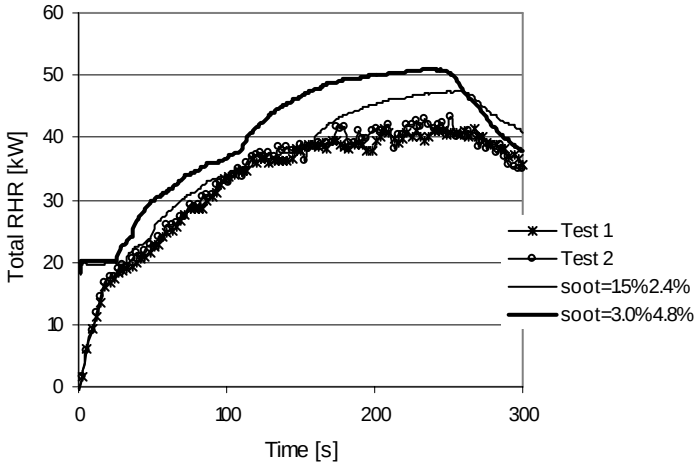

Figure 58. Effect of the prescribed soot content in the combustible gases on RHR predictions. The pyrolysis gases are modelled as being diluted propane with a prescribed soot concentration of 1.5 % and 3.0 %, respectively, the soot contribution from the propane burner being 2.4 % and 4.8 % of the fuel mass flow.

Room Corner Test

A set of input data corresponding to a best fit to the Cone Calorimeter data was derived from the results discussed above. Parameter values were primarily chosen within what was thought to be reasonable physical limits. On the basis of CFD simulations, it was concluded that the numerical results suffer from a clear node dependency but that a wall-adjacent node size, in the direction normal to the sample, of 0.7 cm yields predictions that agree well with the heat flux measurements and the resulting rate of heat release in the vertical flame spread test.

Ideally, with use of the same input and the same computational assumptions, any scenario should be fairly well predicted.

Figure 59 shows, however, that the heat release rates in the Room Corner Test cannot be fully described by results of the simulation. It should be pointed out that the test from which the data used for comparison purposes here was obtained from reference 41 and performed some 20 years ago. Thus, the particleboard used in that test may not fully conform to the one used by Blomqvist and van Hees. Further, in the vertical flame spread test the grid sizes in the directions parallel to the sample were about 2.5 cm. This resolution was not computationally possible in the simulations of the Room Corner Test. Instead, the average size of the nodes was 6.5 cm×4.5 cm×4.5 cm.

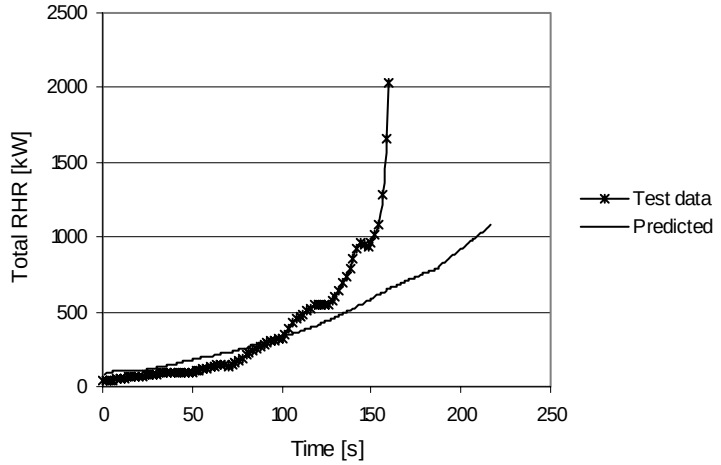

Figure 59. Total rate of heat release in the Room Corner Test. The input data is the same as used in Figure 53, with pyrolysis gas according to Fredlund being employed.

In Figure 60 the effects of changing the soot mass fraction from 1.5% to 3.0% for the pyrolysis gases and 2.4% to 4.8% for the propane in the initial burner are shown.

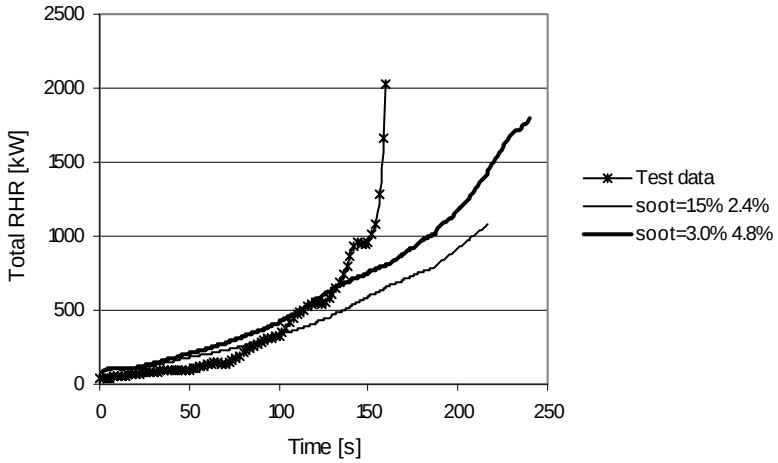

Figure 60. Influence of the prescribed soot mass fraction in the fuel flow on RHR predictions.

The stand-alone calculations indicated fairly well how the pyrolysis model performs at different heat fluxes. From Figure 51 it is clear that the time to ignition is not perfectly consistent but that the predictions could otherwise be made to agree rather well with the experimental data. Thus the really crucial part appears to be the prediction of the gas phase.

6.3.2 SOFIE Qaccumulative model

The Qaccumulative model in SOFIE is rather simple and straightforward. Its performance may be clouded, however, by the inherent need of isothermal conditions being assumed on the transpiring walls to which the model is applied. Since this is a model having purely an

empirical basis, little input data is available in the literature and, even if it should be found, may not be applicable to use directly in the model.

The simulations in this section were performed using a wooden-like fuel with the chemical formula $CH_{1.5}O_{0.75}$. Since this molecule has a density of about 1 at ambient temperature, the bug concerning the prescribed soot mass fraction being translated as volume fraction by the code has no meaning as long as the temperature of the gases are about 293 K. In the cases using a higher temperature, the prescribed soot fraction must, however, be corrected by gas density.

Cone Calorimeter

The Qaccumulative model was fitted into a simple Fortran90 program for evaluating its performance in a stand-alone mode. In the numerical experiments, the model was found to be unable to provide consistent predictions regarding the time to ignition when compared with experimental data obtained using different cone fluxes. In addition, it was not clear how the curves should be fitted to the experimental data, since the RHR plateau was also not consistently correlated with the experimental data. There is also a question of what isothermal temperature to use for the combustible sample surfaces. Accordingly, two main sets of input data differing in the wall temperatures involved were identified, the first using ambient temperature and the second using an assumed ignition temperature of the sample material. The choices of required input data were based on correspondence of results of the model to Cone Calorimeter data.

Table 9 Input to the particleboard using an isothermal wall temperature of 293 K (20 °C).

Critical accumulated energy	= 1.35 MJ/kg
Initial heat of gasification	= 1.80 MJ/kg
Minimum heat flux	= 5.0 kW/m^2 or 7.5 kW/m^2 or 10.0 kW/m^2
Ignition temperature (density)	= 593 K (320 °C)
Heat of combustion	= 14 MJ/kg
Heat flux from flames	= min(0.1*RHR,20) kW/m^2 (only used in stand alone mode)

Table 10 Input to the particleboard using an isothermal wall temperature of 593 K (320 °C)

Critical accumulated energy	= 0.8 MJ/kg
Initial heat of gasification	= 1.10 MJ/kg or 1.30 MJ/kg or 1.70 MJ/kg
Minimum heat flux	= 5.0 kW/m^2
Ignition temperature (density)	= 593 K (320 °C)
Heat of combustion	= 14 MJ/kg
Heat flux from flames	= min(0.1*RHR,20) kW/m^2 (only used in stand alone mode)

Figure 61 and Figure 62 present a comparison of model stand-alone predictions with experimental results using parameters for wall temperatures of 293 K and 593 K, as given in Tables 9 and 10. It should be emphasised that the physical "correctness" of the choice of minimum heat flux parameter can be questioned. The values given in this context should thus be viewed as being part of the "tuning" of the model rather than representing physical quantities.

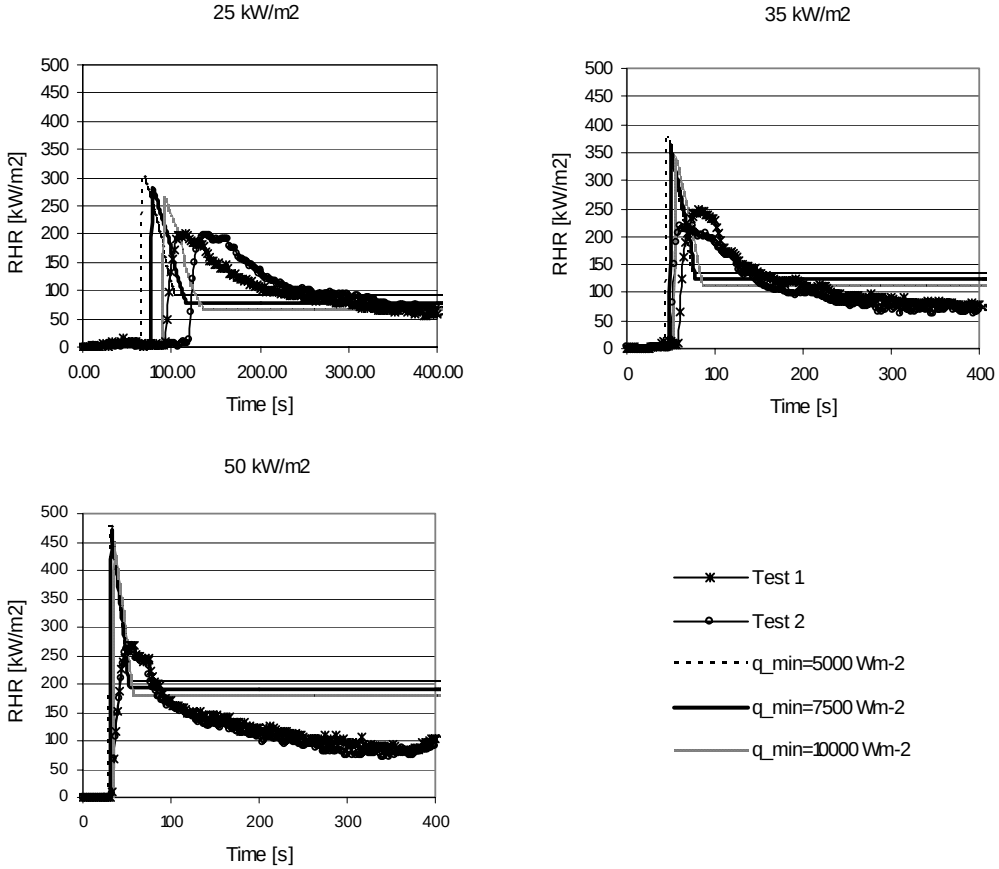

Figure 61. Comparison with Cone Calorimeter RHR results using the input presented in Table 9.

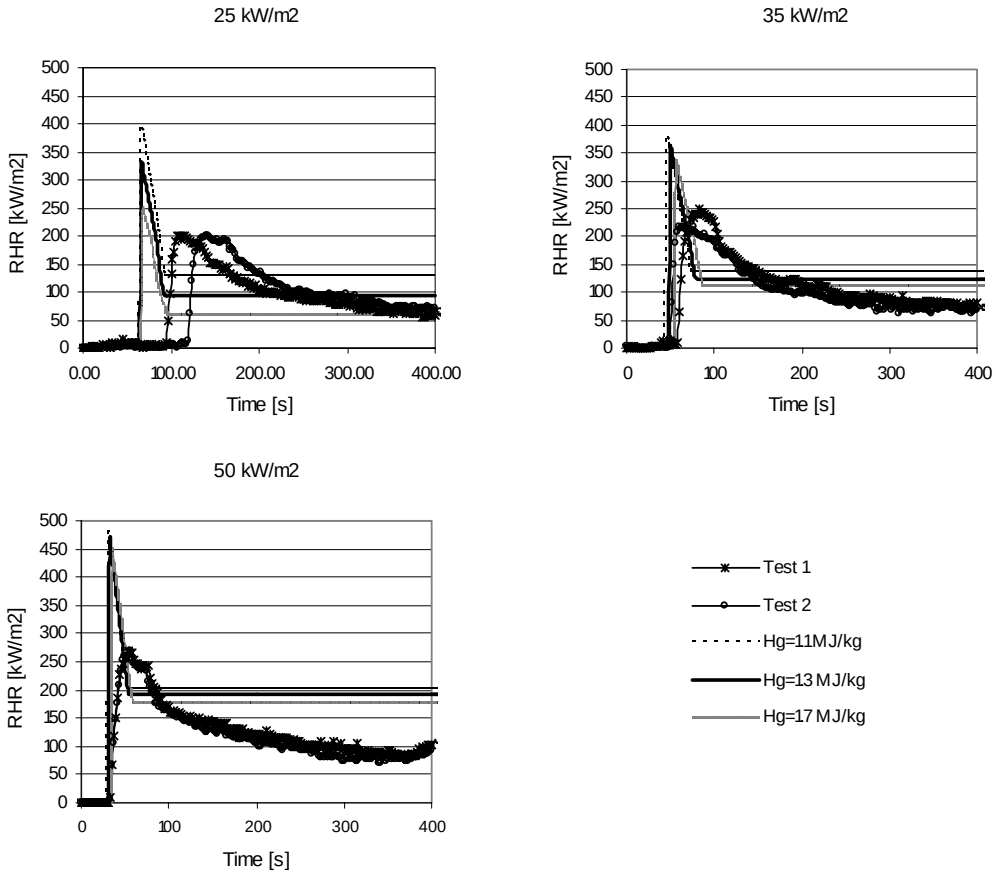

Figure 62. Comparison with Cone Calorimeter RHR results using the input as presented in Table 10.

By adding program routines for conductive heat transfer through the material, the effect of applying isothermal boundary conditions to the transpiring surfaces in the simulations could be assessed. Solving the heat transfer equation results in a transient surface temperature rather than a user-prescribed isothermal surface boundary condition. It should come as no surprise that this approach generates much better predictions then the one described above. The results are presented in Appendix C.

Vertical flame spread test

Simulations were made using the different input options shown in Tables 9 and 10. In the calculations presented in Figure 63, the sample surface is kept at 293 K and the grid size close to the wall is 1.5 cm, with an aspect ratio of 1.7 in both directions in the sample plane. The results correlate well with the stand-alone representations, showing a direct dependency on the minimum heat flux (model-) parameter, q_{min}, with a best prediction obtained using q_{min}=7500 W/m^2.

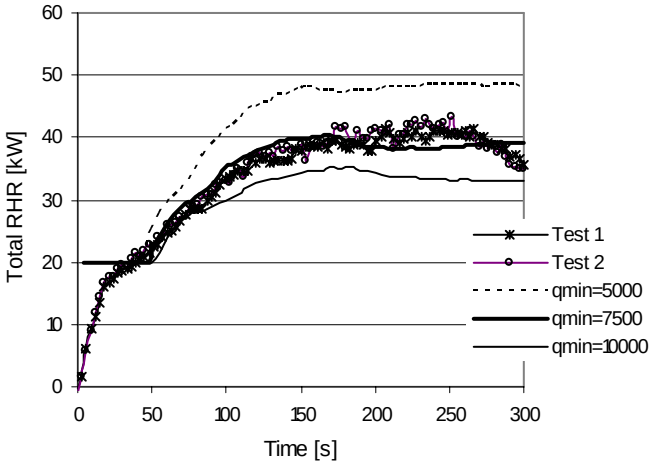

Figure 63 Comparison of experimental and the predicted results using the input data shown in Table 9, the wall-adjacent cell size, in the direction normal to the sample, being 1.5 cm.

Comparisons of the predicted total incident heat transfer for the best scenario in the figure above (the one using q_{min}=7500 W/m^2) with measurements at two locations above the burner on the centreline of the sample are plotted in Figure 64. The predictions are close until the pyrolysis front reaches the height of the probe, after which the heat flux is underpredicted. The influence of soot on the measurement device may be a factor here, although it is difficult to quantify.

Since the sample surface is already cool, being kept at ambient temperature, there was no need to modify the predictions to take the cooling of the measurement probe into account. One should bear in mind, however, that the model input is in terms of net heat flux and not incident flux as plotted in the figure.

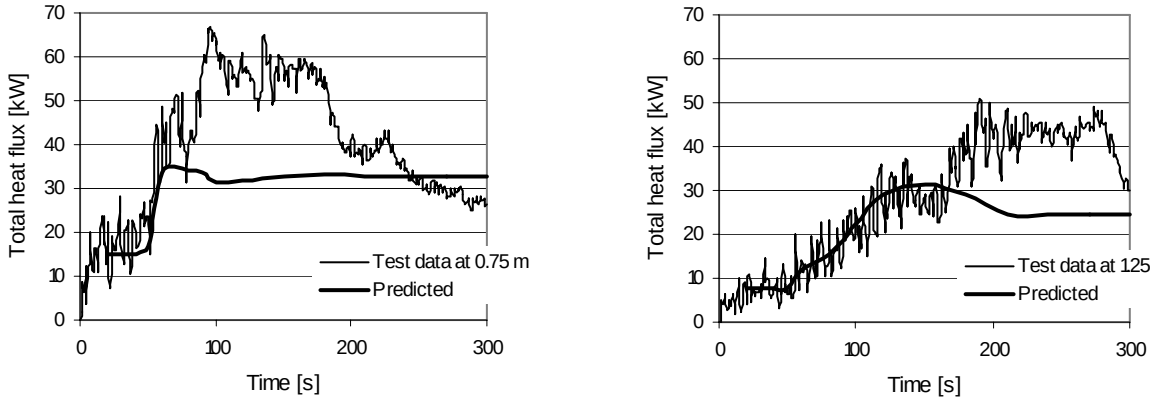

Figure 64. Comparison of computed and measured incident heat flux at two locations, 0.75 meters and 1.25 meters above the burner edge, respectively, along the centreline of the sample.

Figure 65 shows the node dependency using data taken from Table 9 and a q_{min} of 7500 W/m^2. It is clear that node convergence cannot be claimed, there in fact being almost a linear node size dependency.

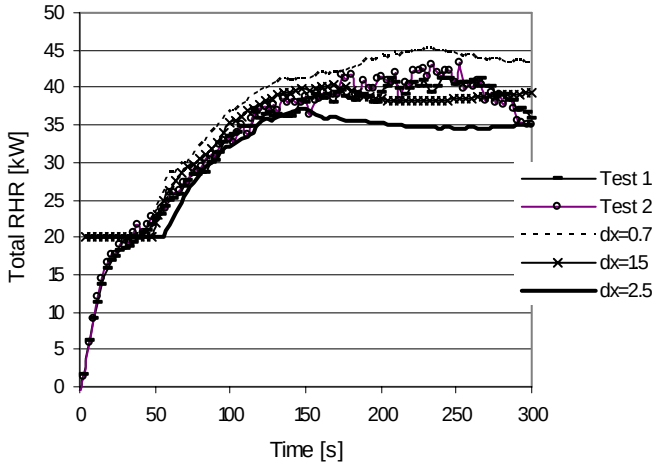

Figure 65. Effect of wall-adjacent cell size on the prediction of heat release rate using the best fit as shown in Figure 63. The grid sizes in the plane parallel to the sample are 0.026 meter large.

Figure 66 shows comparison of the measured and the predicted rate of heat release, using an isothermal wall temperature of 593 K and input data taken from Table 10. As was indicated in the stand-alone calculations, there is a direct dependency on the initial heat of gasification, H_g. On the basis of this graph, the best initial value seems to be between those of the two simulations, at about 1.2 MJ/kg.

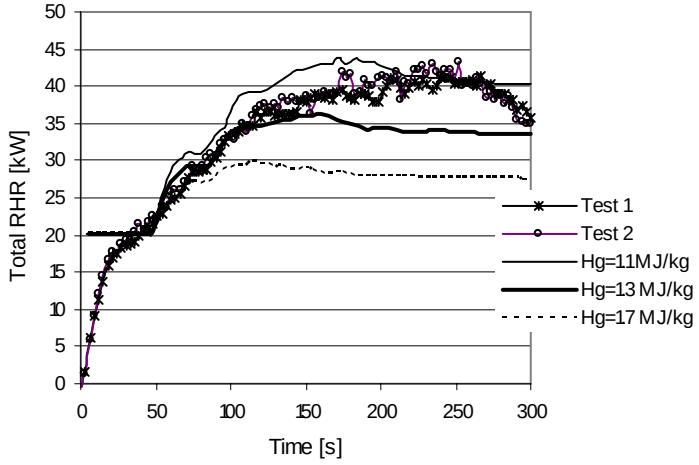

Figure 66. Comparison of the experimental and the predicted results using input data shown in Table 10 and with a wall-adjacent cell size in the direction normal to the sample of 1.5 cm.

In Figure 67 the predicted total incident heat flux from the simulation using $H_{g,initial}$=1.1 MJ/kg is compared with measurements at 0.75 meters and 1.25 meters above the burner. The computed values are modified to account for the cold measuring device, a temperature of 293 K being assumed. At the 1.25 meter location, the incident flux is slightly overpredicted which is consistent with the rate of heat release shown in Figure 66. It is important to note, however, that the calculations do not use the incident flux but the net flux, which is more likely to be erroneously predicted as a result of the isothermal sample surface.

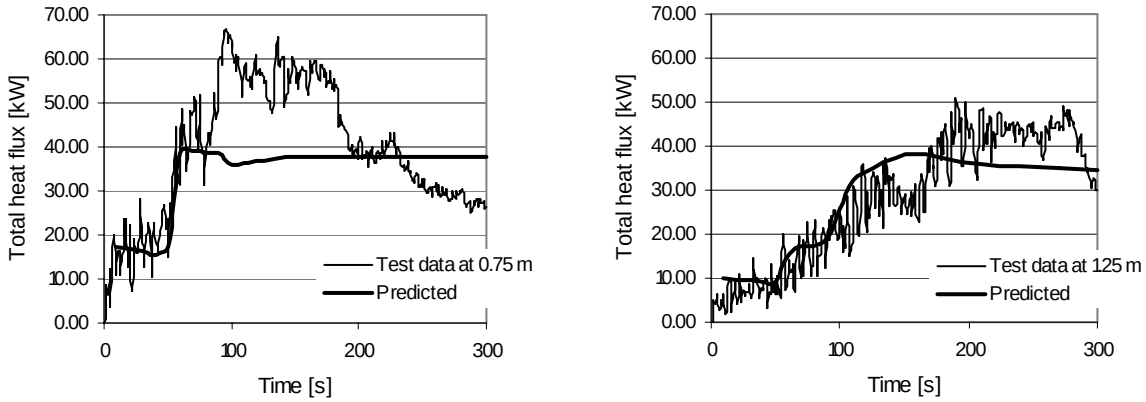

Figure 67. Computed and measured incident heat flux.

Room Corner Test

In order to evaluate the generality in the model predictions, simulations of the Room Corner Test were made using the parameters that provided the best agreement with results of the vertical flame spread test. The results of two simulations, the one using T_{wall}=293 K and the other using T_{wall}=593 K, are compared with the measured heat release rate as shown in Figure 68. The close agreements obtained in the vertical test are not repeated here.

The results of using a wall temperature of 593 K differ considerably for those from the 293 K simulation. This can be expected, since the walls themselves contribute to the heating of the room.

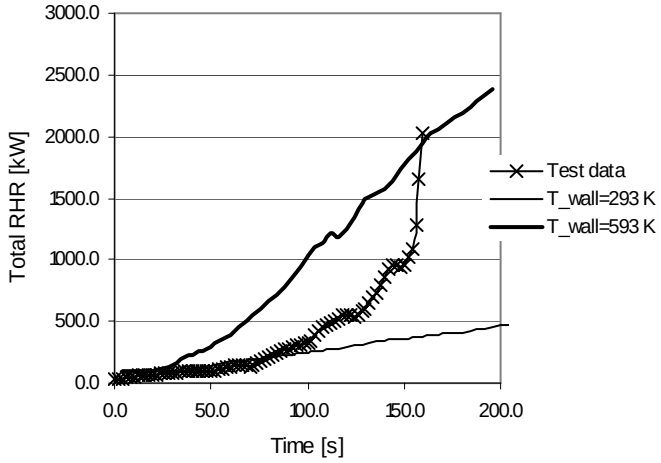

Figure 68. Computed and measured rate of heat release in the Room Corner Test.

6.3.3 SOFIE Cone Calorimeter model

The Cone Calorimeter model in SOFIE is not a pyrolysis model in itself since, rather than simulating the pyrolysis process, it uses an interpolation scheme based on the results of the Cone Calorimeter for describing the rate of heat release at different heat fluxes.

To evaluate the model at specific heat fluxes, it was extracted from the SOFIE source code and was fitted into a small stand-alone Fortran90 program. Again, the prediction of time to ignition suffers from the use of an isothermal boundary condition on the sample surface. Once the ignition criterion has been fulfilled, the rate of heat release is taken directly from the Cone Calorimeter output (or from an interpolation of experimental data), locking itself to the RHR profile described by the net incident heat flux at the time of ignition. The assumption here is that the net flux in the experiment, including the additional heat flux from the flames, is valid in most scenarios. Since the experimental data used in this study are from horizontal face-upwards tests, it can be questioned, however, whether the input is directly applicable. Also, from the plot of the local rate of heat release using the pyrolysis model by Yan, the transient RHR were shown to have a quite different behaviour as compared with the Cone Calorimeter result.

Cone Calorimeter

To describe the rate of heat release from the Cone Calorimeter, the interpolation scheme use 21 time-integrated RHR points for each of three heat fluxes from the Cone Calorimeter. Two different sets of input data were employed, the one derived for an isothermal sample temperature of 293 K and the other for a sample temperature of 593 K. The values are given in Table 11. The value for the threshold flux may not be directly derivable from the Cone Calorimeter, since such values represent the result of transient heating and thus include different surface heat losses than for the isothermal boundary used in the simulation.

Figure 69 shows the input curves corresponding to an isothermal wall temperature of 293 K used in this study, as based on the data points and the interpolation scheme employed by the model. The data file was constructed using average values from all the experimental results available for the specific cone heat flux, the effect of this approach is especially evident at the first peak. Also, the calculations were made for an isothermal surface including only a surface emissivity and not surface cooling or re-radiation, so that the heat flux does not exactly represent the same flux as that it was derived from. The corresponding comparison for an isothermal of 593 K is found in Appendix D.

Table 11 Input data for the particleboard

	T_{wall} = 293 K	T_{wall} = 593 K
Threshold flux	= 246 $kWs^{1/2}m^{-2}$	= 197 $kWs^{1/2}m^{-2}$
Minimum heat flux	= 10.0 kW/m^2	= 10.0 kW/m^2
Heat of combustion	= 14 MJ/kg	= 14 MJ/kg

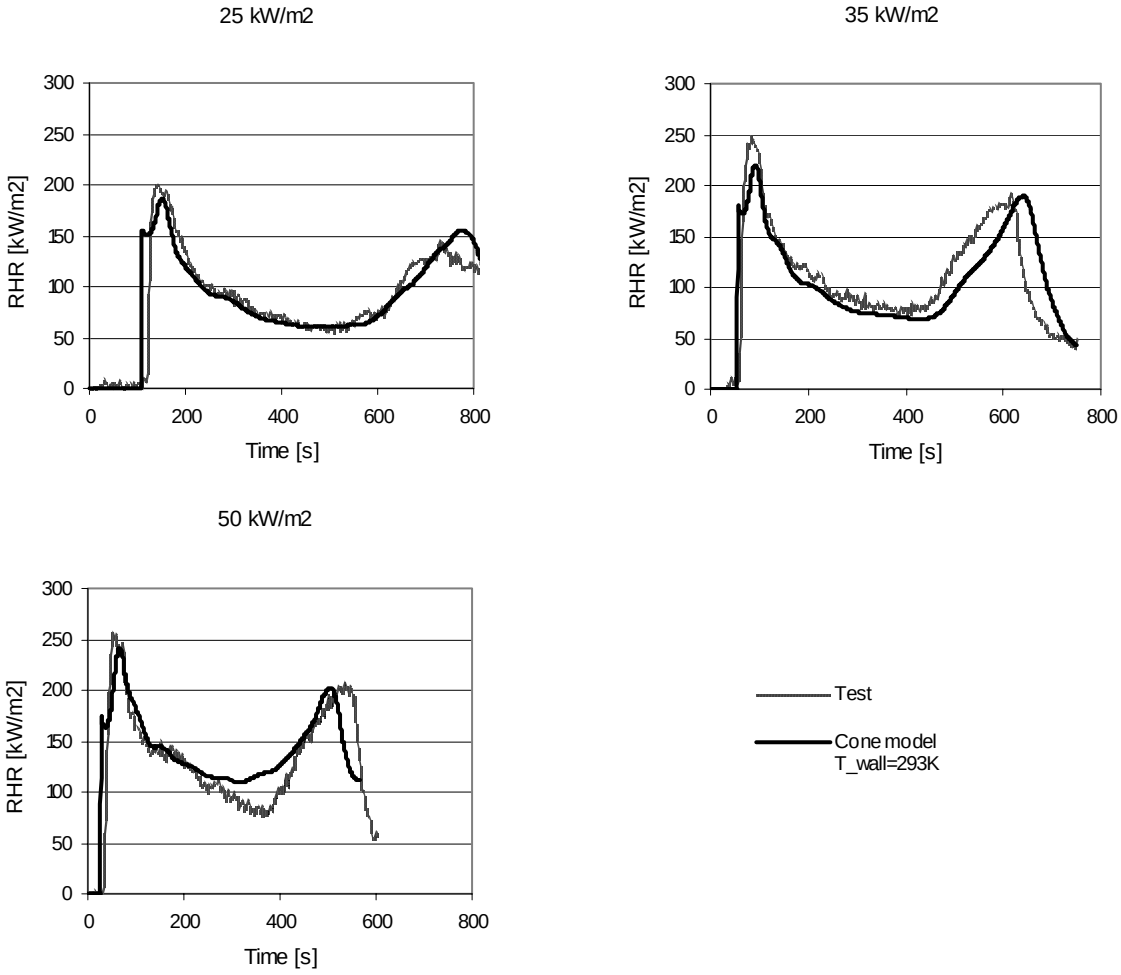

Figure 69 Comparison of experimental data and Cone Calorimeter stand-alone model predictions for an isothermal wall temperature of 293 K using input shown in Table 11.

Vertical flame spread test

In Figure 70 the measured rate of heat release is compared with computations using three different sizes of the wall-adjacent cell in the direction normal to the sample surface, the grid size in the vertical plane being 2.6 cm and the wall temperature being 293 K. A clear node dependence can be observed, the time to ignition, however, being quite alike for the scenarios using 0.7 cm and 1.5 cm grid normal to the sample surface.

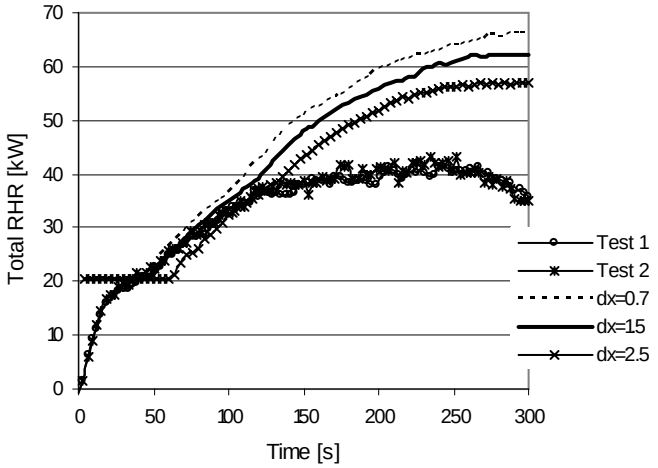

Figure 70. Predictions using three different computational grids. The wall temperature is 293 K.

In Figure 71 computations using both 293 K and 593 K wall surface temperatures are compared with experimental data. From the results, it appears likely that the stand-alone simulation of the heated wall (for a Cone Calorimeter comparison see Appendix D) did not do as well as the one for the cold surface.

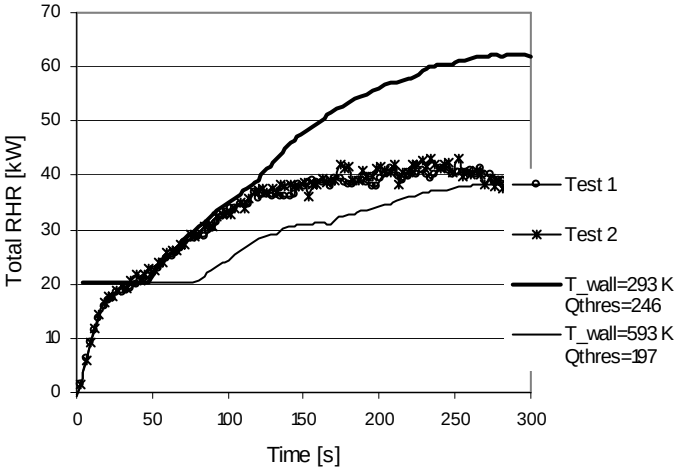

Figure 71. Computed rate of heat release using different isothermal temperatures on the surface of the sample as compared to experimental results.

The local rate of heat release is given directly by the Cone Calorimeter data. Again, comparing it with the predicted local RHR from the pyrolysis model by Yan, Figure 57, the correctness of this assumption can be questioned.

Room Corner Test

Using a geometry and grid resolution similar to that used in the simulations employing the Qaccumulative model, computations of flame spread in the Room Corner Test were made using input from the different wall temperatures. The grid size close to the walls was 1.5 cm and the model inputs were those shown in Table 11. The results are presented in Figure 72.

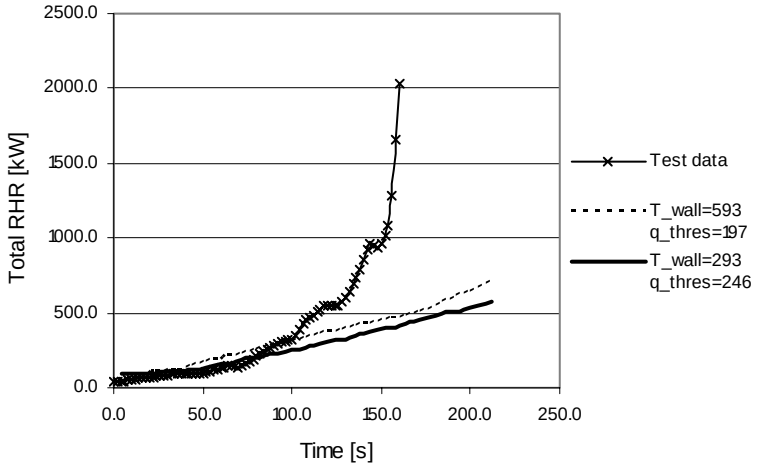

Figure 72. Measured and computed rate of heat release using different strategies in the Cone Calorimeter model.

In this scenario, the simulation using an isothermal wall at 593 K gives somewhat higher values. The effect is not as high as in the simulations using the Qaccumulative model, which may be explained on basis of the model "locking" the rate of pyrolysis to the heat flux at the time of ignition.

6.3.4 FDS Pyrolysis model

The pyrolysis model incorporated into FDS is the most advanced model considered here in the sense of its including the reaction kinetics of pyrolysis in the form of an Arrhenius equation. This can be regarded as the most reasonable thing to do, the drawback, however, being that the required input data is in short supply or suffering from significant uncertainties.

Most of the simulations in this section were made during late summer of 2002 using version fds2p2 with a compilation date in June. No simulation has been made using later versions of the code.

Cone Calorimeter
Because of the limited access to unambiguous measurements of the Arrhenius parameters and of the heat of pyrolysis, the reasonable alternative appears to be to turn to small-scale experiments, in particular the Cone Calorimeter, for deriving or justifying a set of input parameters. Figure 73 and Figure 74 shows the model results obtained in using a best-fit set of input data, as given in Table 12, and making a comparison with the experimental results.

Table 12 Input to the particleboard corresponding to a best fit to the Cone Calorimeter measurements.

Pre-exponential factor, A_p	= 150 s^{-1}
Activation energy, E_a	= 52 kJ/mole
Specific heat capacity (unburned)	= (1430+0.355*Temperature in K) J/kg
Specific heat capacity (char)	= (150+3.7*Temperature in K) J/kg
Thermal conductivity	= (0.05+4.0E-4*Temperature in K) W/mK
Density of virgin solid	= 600 kg/m^3
Density of residual char	= 60 kg/m^3
Heat of pyrolysis	= 150 kJ/kg
Heat of combustion	= 14 MJ/kg
Heat flux from flames	= min(0.1*RHR,20) kW/m^2 (only used in stand-alone mode)

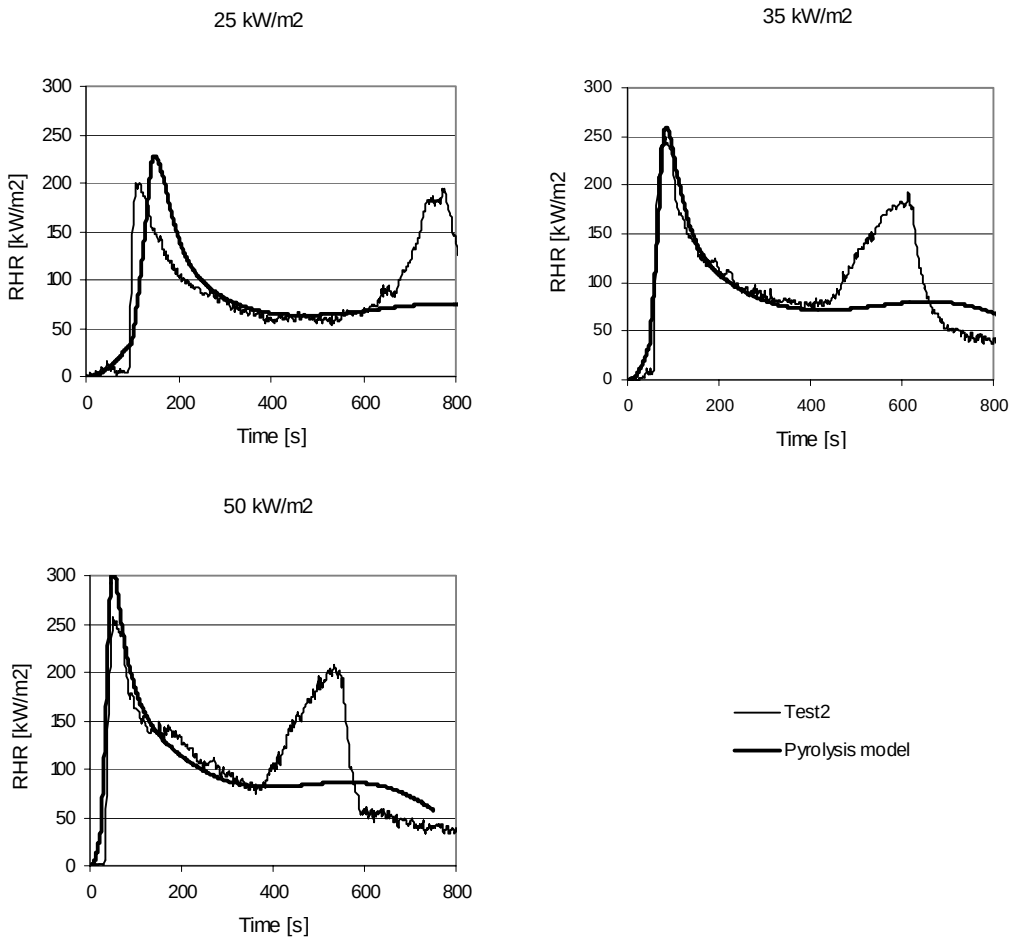

Figure 73. Predicted rate of heat release compared with experimental data.

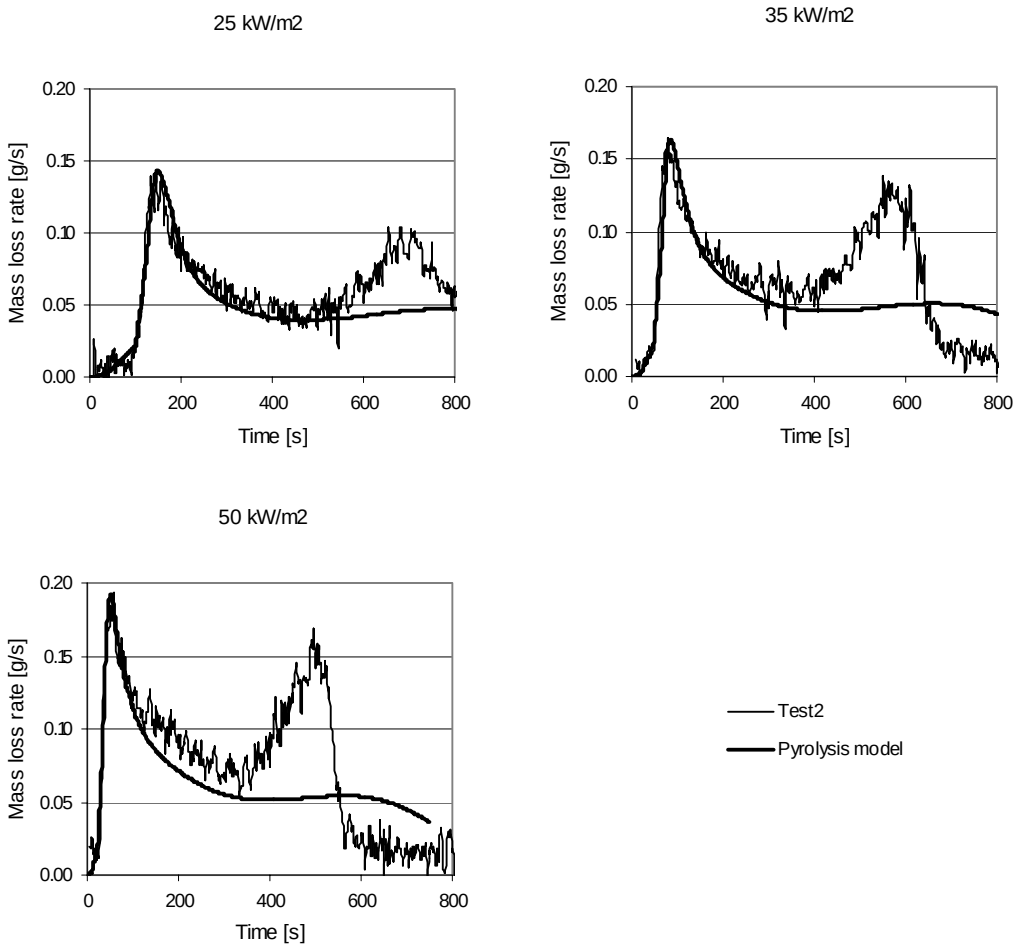

Figure 74. Predicted mass loss rate compared with experimental data.

The second peak in the experimental data can be readily obtained by modifying the heat transfer conditions on the rear face of the material. In the predictions above, conditions corresponding to the properties of Promatek H board were used which is consistent with the experimental configuration in the vertical panel tests by Blomqvist and van Hees.

The results of the pyrolysis model show close agreement with measurements for all three incident fluxes. The time to ignition was also consistently predicted, which is the reason for only one test being shown in the graphs, the one used to define the best fit.

Vertical flame spread test

The simulations of the vertical flame spread test show significant node dependencies. In Figure 75, results for three different grid resolutions are presented. The simulations 1.5 cm and 2.5 cm have a uniform grid in the direction normal to the surface, whereas the 0.7 cm grid is stretched, generating this small node size close to the sample.

All the simulations were made using input data taken from Table 12 and a wooden-like fuel having additional properties as described by Fredlund[8].

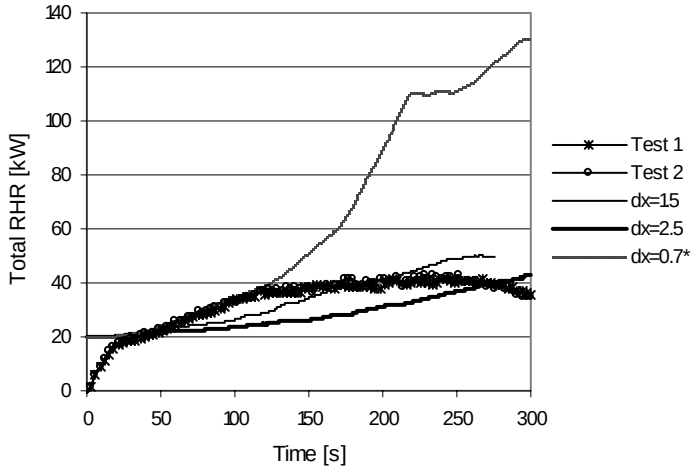

Figure 75. Comparison of measured and predicted heat release rate using different grid resolutions. The numbers designated as dx are the grid sizes in the direction normal to the sample surface, * indicating that the grid has been stretched to obtain the resulting wall-adjacent cell size. The grid in the plane parallel to the sample is unchanged, giving a maximum aspect ratio of AR(dx=1.5)=2.0, AR(dx=2.5)=1.2, AR(dx=0.7*)=4.3.

Whereas the time to ignition is similar in the calculations, irrespective of the grid resolution, there are clear differences between them regarding the predictions of the rate of flame spread. This can be thought to be connected with differences in the predicted gas temperatures, which have a strong influence on the radiative heat transfer.

Figure 76 shows a comparison of the measured and the predicted total heat flux at two points on the centreline of the sample. The predicted value has been corrected to represent the flux to a water-cooled measurement probe, ambient temperature being assumed. It is clear that the heat flux is underpredicted, although the agreement 1.25 meters above the burner is rather good. Both the fact that the heat flux is underpredicted and a comparison with the results shown in Figure 75 suggest there to be some error in the derivation of the input data. Also, the use of the wood reaction instead of propane to describe the burner may have some effect on this.

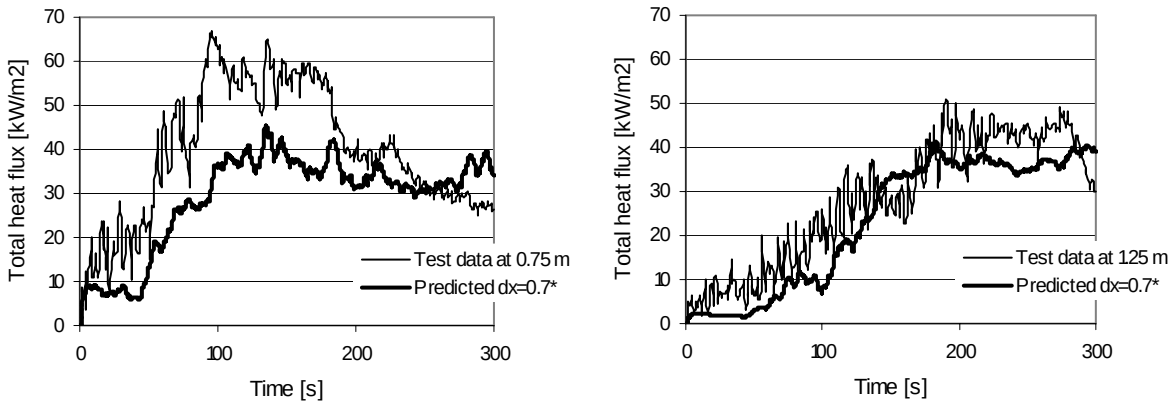

Figure 76. Total heat flux to a cold probe at two different locations above the burner. The predicted results have been averaged over 6 seconds.

Room Corner Test

A Room Corner Test scenario was simulated using different grid resolutions, the results are shown in Figure 77. The grids represent different resolutions of the initial burner of 5, 3 and 2 cells, respectively. There is a clear node dependency, although the grid resolution in the vertical coordinate appears more sensitive than the resolutions in the coordinates in the horizontal plane. This is confirmed in Figure 78, in which two simulations are shown in which the grid resolution in the horizontal plane is kept constant but that in the vertical direction (dz) is varied.

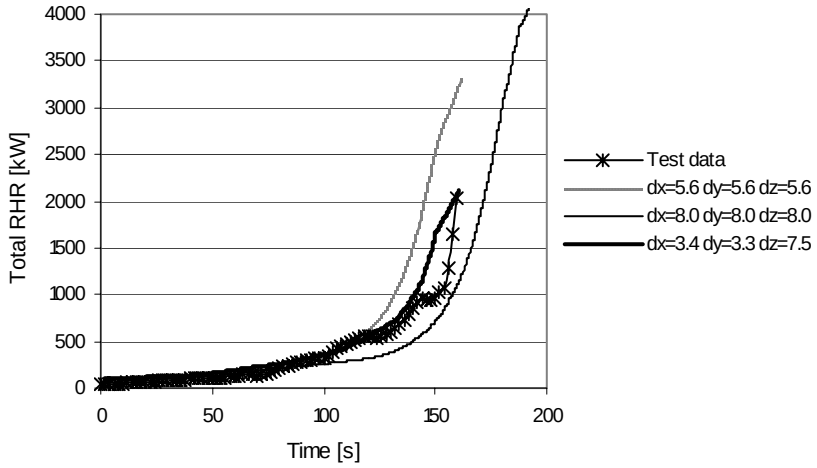

Figure 77. Comparison of total rate of heat release in the Room Corner Test, dx and dy being the node size in cm in the horizontal plane, and dz being the size in cm in the vertical direction.

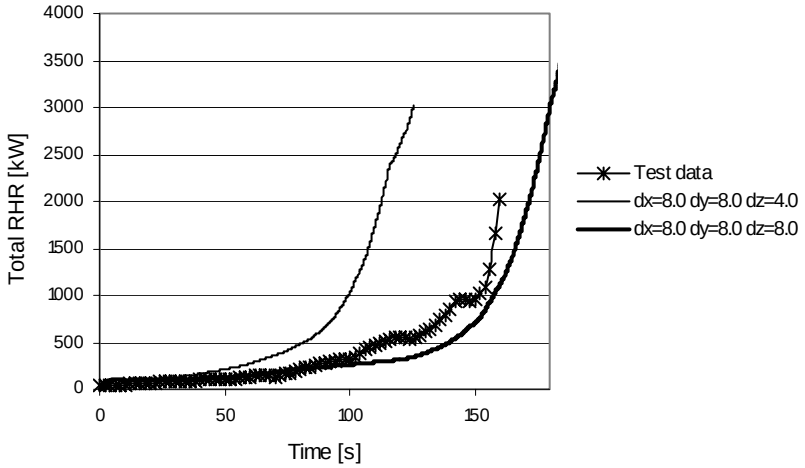

Figure 78. Sensitivity analysis of grid size in the vertical (z) direction, the symbols dx, dy and dz denoting grid sizes in cm.

6.4 Conclusions and practical considerations

Since the CFD codes solve the governing transport equations on a relatively fine mesh, allowing the use of variable exchange coefficients and providing information regarding the local values of the dependent variables, it provides the possibility of evaluating very complex

phenomena, such as combustion, heat transfer and flame spread. Unfortunately, certain key issues are still too complex to be fitted into a comprehensive and general model. This section basically close Chapters 4-6, involving the use of computational fluid dynamics in the computation of flame spread and fire growth.

Turbulence modelling has been a favourite subject for decades, considerable amounts of resources, in terms both of manpower and of money, having been spent in efforts to understand and predict the seemingly chaotic phenomena involved to a satisfactory degree. This has led to a large number of turbulence models which can be placed along a continuum in terms of complexity and sophistication, from simple linear eddy viscosity models, used in most of today's large-scale simulations, to DNS, which in view of the computer resources available, is virtually impossible to use for anything except small-scale simple flows involving a Reynolds number of less then say 1000. Thus, due to the limitations in computational power, any large-scale simulation of a fire is referred to the use of Reynolds averaged simulation or, in some cases, LES. One can note that the standard high-Re k-ε model used in the present study was first suggested some thirty years ago.

The behaviour of turbulent reacting flows close to walls pose considerable computational problems due to their anisotropy and their steep velocity and scalar gradients in the boundary layer. The common approach in most commercial and research CFD codes is to use some kind of semi-empirical wall functions, which are algebraic relationships applied as boundary conditions in control volumes closest to the wall, this replacing the integration of the governing equations through the boundary layer. The wall function approach is generally considered to require a cell size corresponding to a y^+ value of 30 or more in the wall-adjacent node. Close to the source of a buoyant diffusion flame, this is not always possible to achieve, due to the low turbulence rate there. Despite this, the convective heat flux may not be the most important heat transfer mechanism involved, thermal radiation being more likely to dominate most scenarios. In the simulations performed using a fictitious non-combustible sample board, that a clear node dependency in the heat flux predictions was only observed in the area just behind the flame, where radiative heat transfer dominates. The implication of this could be that the major errors originate from the combustion model and from an insufficient resolution of the flame, and perhaps as well from an overly crude soot-modelling approach. The influence of local errors on the convective heat flux appears, therefore, to be of secondary importance to the accuracy of the overall results.

The Eddy Dissipation Concept for combustion modelling has proved to give satisfactory results in general smoke movement simulations. However, its performance in predictions of the flame and the flame near field are not as easy to demonstrate. In flame-spread calculations, using a relatively small grid size in the nodes close to the wall raises the question of the validity of the model in boundary layer flows. Research is continuing on alternative combustion models. The flamelet approach is perhaps the most reasonable substitute in the near future.

The results presented in this chapter leave a lot to wish for. No overall model was able to consistently predict the flame spread and the fire growth, the models instead showing clear dependencies on the scenario as well as on computational strategies. Comparisons of computed and measured incident heat flux suggest that the input data derived from best-fit correlations to the Cone Calorimeter results were not optimally chosen. This was no complete surprise, however, since there is reason to believe that the test procedure suffers from scaling problems. In addition, the best-fit data was derived using simply a guessed value on the

transient heat flux from the flame to the sample. The fact that this could have an effect is shown in Appendices A and B.

Despite the complexity of the pyrolysis process in wood, as was discussed in section 2.1, the first order single step Arrhenius function used by the model in FDS showed the potential of quite correctly and consistently predicting the heat release rate stand-alone as compared with measurements using the Cone Calorimeter. Also, the pyrolysis model of Yan provided rather good approximations to test data. However, it should be borne in mind that the Cone Calorimeter represents a somewhat artificial scenario, the sample being momentarily exposed to a high level of heat flux, which is only likely to be found in the very vicinity of the initial fire. The large variation in the results relating to the different computational assumptions and strategies nevertheless suggests that the problem is more an issue of the performance of CFD predictions than of modelling the rate of pyrolysis at some given net heat flux.

7. Conclusions and recommendations for further work

Presentation of various conclusions that have been drawn and a discussion of certain practical matters regarding different computational strategies for flame-spread and fire-growth modelling are to be found in sections 3.5 and 6.4. The reader is referred to these portions of the text for a more comprehensive analysis of these matters, a brief summary of them being provided here.

7.1 Conclusions

The use of Fire Safety Engineering, FSE, in performance-based building regulations places demands on the validity and performance of models that are employed in the design work. In using fire models to evaluate smoke movement and tenability conditions in buildings, the fire source needs to be prescribed by the user. If a building has combustible linings, the choice of fire source can be complicated since no standard or natural model for flame spread and fire growth, i.e. the movement of the burning area and the increase in heat release rate, is available. Thus far, the introduction of performance-based regulations has been of only limited value to practicing architects and engineers who want to use wooden building materials for both the interior and the exterior part of the buildings, the only way forward having been and still being full-scale testing.

Early work on flame-spread modelling aimed at deriving comprehensive, yet rather simple, analytical stand-alone relationships to describe the process occurring in some limited scenarios. The idea of fairly simple algebraic flame-spread and fire-growth models useful in an engineering context experienced something of a revival with the advent of performance-based building regulations and Fire Safety Engineering, FSE. The model of this sort in Chapter 3 was found to be highly dependent on its tuning parameters, although it was found to agree rather well with experimental data from the scenario for which it was designed, that of the Room Corner Test. Using another configuration, on the other hand, the results were found to be considerable less accurate, although the flame-spread velocity could be computed with certain degree of accuracy, though only after the results were known.

Flame-spread routines linked with the solution of equations describing fire and smoke transport have been implemented in several models of both the CFD and zone-model type. Few if any of these have been employed successfully, however, outside their research environment. None of the models considered in the dissertation show scenario consistency in predicting the rate of heat release. Using the same computational strategies in two different sets of geometrical relationships provided qualitative and quantitative results that differed from the test results. Also, there was considerable variation in the choice of input data and in grid resolution for the various models, the most consistent model being the CFD code SMAFS, which included the pyrolysis model developed by Yan, although it was unable to predict flashover in the Room Corner Test. The pyrolysis model contained in FDS provided excellent curve fit to the Cone Calorimeter data, although the input derived from this procedure may well suffer from the assumptions made concerning flame heat flux, for example, as well as being influenced by the drawbacks related to the Cone Calorimeter. In modelling the full-scale tests, the predictions made were found to be highly sensitive to changes in the computational conditions.

7.2 Recommendations for future work

Computational Fluid Dynamics
CFD modelling has become an integrated part of Fire Safety Engineering. Despite its application being thus far limited to the investigation of smoke movement within buildings, it is generally believed to represent a highly flexible and accurate tool. Computations and measurements for smoke transport and gas temperatures have consistently been shown to agree well, and the reproducibility has been good as well as the possibility of obtaining results independent of small changes in the basic user-prescribed computational conditions such as time step and grid resolution. There are indeed situations, however, in which the predictions are less satisfactory. Until adequate validation has been ensured, considerably caution in employing a new model in design work is in order.

The currently available CFD codes suffer from several weaknesses, one of these being the very core of CFD, the turbulence model. The most widely used turbulence-closure model, that used mainly in this study, is the k-ε model, which is known to have certain difficulties in predicting buoyancy-controlled, wall-bound reacting flows in particular. Alternative turbulence models do exist and their application is only a matter of time and of computer resources. The semi-empirical wall functions that complement the k-ε model in its application in regions close to walls are likewise known to have limitations. The fact that few research projects on wall functions have been presented in recent decades suggests, however, there to not be much to expect in terms of their further development. On the basis of the present study, it can be regarded as unlikely that the limitations of the wall functions currently employed affect computational results to a degree that would justify the amount of work such development would require.

Because of its direct dependency on k and ε, the Eddy Dissipation Concept used for combustion modelling inherits the uncertainties present in the attempt to solve problems connected with the turbulent flow field. A reasonable alternative to EDC seems to be the flamelet approach, which uses libraries of state relationships between different dependent variables, such as enthalpy or chemical species, and the mixture fraction. Statistical fluctuations in the mixture fraction is represented either by use of a probability density function (PDF) or by LES. One drawback, however, is that few flamelet libraries are readily available. Also, LES is not yet a realistic option in large scale scenarios. Further development and use of the flamelet approach in fire modelling represents an important area for research.

Few generally accepted and widely used methods for representing the concentration of soot in a flame and the fire gases are presently available. One widely used approach is to prescribe some constant soot fraction relative to the flow of fuel into the domain, although the value chosen may not be more than a crude assumption. The addition of a more physically oriented soot modelling approach and better insight into the effects of the present simplifications are needed.

Flame spread and pyrolysis modelling
The future of flame-spread modelling is undoubtedly closely connected with the use of Arrhenius rate functions. In order to couple the pyrolysis model to CFD, however, it is necessary to complement the computations with some criterion for ignition. Although most pyrolysis models make use of a critical ignition temperature, the present use of a constant value for it is quite artificial since the true criterion would vary with the incident heat flux[94].

Even though a number of ignition criteria that could be more suitable are cited by Kanury[14], further research efforts here seem clearly needed.

One drawback to using chemical kinetics to model pyrolysis is the persistent lack of experimentally unambiguous Arrhenius parameters and heat of pyrolysis measures. Recent detailed investigations suggest that use of separate rate laws for the decomposition of major components of wooden materials may be necessary. Similarly, one may need to distinguish governing mechanisms based on heat transfer and those based on the kinetics of the pyrolysis process.[11,82] Much work on this remains to be done.

It can be asked to what extent it is reasonable to make the pyrolysis model more sophisticated, since it is the CFD code that is likely to place the most stringent constraints on the final computations. However, if one can make a CFD calculation in which the chemistry of combustion is largely decoupled from the uncertainties in predictions of the turbulent flow, such as in using the flamelet approach, there may be relatively little to gain in making overly crude assumptions in the pyrolysis model. Important factors, however, being the computational expense added by the model as well as the availability of input data. Further work is required using more physically oriented pyrolysis models coupled to state of the art CFD.

The Cone Calorimeter is a standardised and widely used apparatus for testing of the ignition and thermal response of combustible materials at different external heat fluxes. Although it may thus have considerable potential in aiding engineering computations of flame spread, various uncertainties remain that need to be investigated thoroughly. One of the most important tasks involved is to investigate the flame contribution to the incident heat flux towards the sample, including the effect of the size, transient development and distribution of this flame flux. Detailed information regarding those matters is needed when a pyrolysis model is to be evaluated in a stand-alone mode. In addition, there is a need of determining more precisely the effects of scaling on values obtained in the Cone Calorimeter and how this can best be taken into account in computations concerning large-scale flame-spread scenarios.

References

1. Boverkets Byggregler BBR, Boverket, september 2002.
2. de Ris J., Spread of laminar diffusion flame, 12th Symposium (International) on Combustion, The Combustion Institute, p241, 1969.
3. Fernandez-Pello A C., Flame spread modelling, Combustion Science and Technology 39, pp 119-134, 1984.
4. Williams F A., Mechanisms of flame spread, 16th Symposium (International) on Combustion, The Combustion Institute, p1281-1294, 1976.
5. Grant G., Drysdale D., Numerical modelling of early flame spread in warehouse fires, Fire Safety Journal, vol 24, No 3, pp 247-278, 1995.
6. Dinwoodie J. M., Wood-Nature's Cellular, Polymeric Fibre-Composite, The Institute of Metals, ISBN 0-901462-35-7, 1989.
7. Rubini P. A., Course Lecture Notes, 2001
8. Fredlund B., A Model for Heat and Mass Transfer in Timber Structures During Fires, PhD Thesis, Dept. of Fire Safety Engineering, Lund University, Lund, 1988.
9. Parker W. J., LeVan S. L., Kinetic Properties of the Components of Douglas-Fir and the Heat of Combustion of their Volatile Pyrolysis Products, Wood and Fiber Science 21(3), pp 289-305, 1989.
10. LeVan, Susan L. Thermal Degradation, Schniewind, Arno P., ed. Concise Encyclopedia of Wood and Wood-Based Materials. 1st edition. Elmsford, NY: Pergamon Press: 271-273. 1989. *http://www.fpl.fs.fed.us/documnts/pdf1989/levan89a.pdf*
11. Leckner B., Hansson K-M, Tullin C., Borodulya A. V., Dikalenko V. I., Palchonok G. I., Kinetics of fluidized bed combustion of wood pellets, Proceedings of the 15th International Conference on Fluidized Bed Combustion, Savannah, Georgia, May 16-19, 1999.
12. White Robert H., Shaffer E. L., Transient Moisture Gradient in Fire-Exposed Wood Slab, Wood and Fiber, 13(1), pp 17-38, 1981.
13. Brehob E. G., Kulkarni A. K., Experimental measurements of upward flame spread on a vertical wall with external radiation, Fire Safety Journal, 31, pp 181-200, 1998.
14. Kanury A. M., Flaming ignition of solid fuels, The SFPE Handbook of Fire Protection Engineering, 2nd Edition, Section 2 Chapter 13, 1995.
15. Babrauskas V., Ignition of Wood – A Review of the State of the Art, Proceedings from the 10th Interflam conference, Edinburgh, 2001.
16. Yan Z., Holmstedt G., CFD and experimental studies of room fire growth on wall lining materials, Fire Safety Journal, 27, pp 201-238, 1996.
17. Kung, H. C., A Mathematical Model of Wood Pyrolysis, Combustion and Flame, 18, pp 185-195, 1972.
18. Atreya A., Pyrolysis, ignition and fire spread on horizontal surfaces of wood, Division of Applied Sciences, Harvard University, Cambridge MA, March 1984.
19. Aksit I.M., Mackie P., and Rubini P A, Coupled radiative heat transfer and flame spread simulation in a compartment, Presented at the 3rd International Seminar on Fire and Explosion Hazards, 10-14th April 2000, Lake Windermere, UK.
20. Aksit I.M., Moss J.B., and Rubini P A, CFD Simulation of Cable Tray Fires, Proceedings from the 9th Interflam conference, pp 1129-1140, 2001.
21. Andersson M., McKeever C., Pehrson R., Barnett J., An Experimental Study of Upward Flame Spread on Cellulosic Materials, Proceedings from Interflam Seventh International Fire Science and Engineering Conference 1996, pp 169-178.

22. Quintere J., Surface Flame Spread, The SFPE Handbook of Fire Protection Engineering, 2nd Edition, 1995.
23. Di Blasi, C, Modeling and simulation of combustion processes of charring and non-charring solid fuels, Prog. Energy Combust. Sci., Vol 19, pp 71-104, 1993.
24. ISO 5660, Fire Tests – Reaction to Fire – Rate Heat Release from Building Products, International Standards Organisation, Geneva, Switzerland, 1991.
25. ISO DP 5658, Fire Tests – Reaction to Fire – Surface Spread of Flame of Building Products – Part I, Vertical Specimen, International Standards Organisation, Geneva, Switzerland, 1986.
26. ASTM E 1321-90, Standard Test Method for Determining Material Ignition and Flame Spread Properties, Annual Book of ASTM Standards, ASTM, Philadelphia, 1990.
27. Saito K., Quintiere J G., Williams F A., Upward Turbulent Flame Spread, Proceedings from the First International Symposium on Fire Safety Science, Hemisphere Publishing, New York, 1984.
28. Karlsson B., Modelling Fire Growth on Combustible Lining Materials in Enclosures, PhD Thesis, Dept. of Fire Safety Engineering, Lund University, Lund, 1992.
29. Thomas P., On Concurrent Upward Surface Spread of Flame, Fire Safety Journal, 22, pp 89-99, 1994.
30. Thomas P., Karlsson B., On upward flame spread on thick fuels, SE-LUTVDG/TVBB-3058, Lund University, Lund, 1990.
31. ISO 9705, Fire Tests – Reaction to Fire – Full-Scale Room Fire Test for Surface Products, International Standards Organization, Geneva, 1991.
32. Baroudi D., Kokkala M., Analysis of upward flame spread- Project 5 of hte EUREFIC fire research programme, VTT Fire Technology Laboratory, VTT Publications 89, 1992.
33. Kokkala M., Baroudi D., Parker W J., Thimes – A computer program for upward flame calculations, Software written by D Baroudi, VTT Building Technology/Fire Technology, Finland.
34. Karlsson B., Models for Calculating Flame Spread on Wall Lining Materials and the Resulting Heat Release Rate in a Room, Fire Safety Journal, 23, pp 365-386, 1994.
35. Lee C H., Investigation of a Model for Upward Flame Spread: Transient Ignitior and Burning Rate Effects, NIST-GCR-97-726, 1997.
36. Özisik N M., Heat conduction, ISBN 0-471-05481-X, John Wiley & Sons, 1980.
37. Quintere J., Harkleroad M., New Concepts for Measuring Flame Spread Properties, NBS, CFR, Gaithersburg, MD, 1984.
38. North, G. A., An Analytical Model for Vertical Flame Spread on Solids-An initial investigation, Master thesis, May 1999, New Zealand.
39. Karlsson B., Calculation of Heat Release Rate in the Room Corner Test, Fire Safety Journal, 20, pp93-113, 1993.
40. Blomqvist P., Van Hees P., Upward Flame Spread Experiments – a preparatory study, SP AR 2001:32, Borås, 2001.
41. Sundström B., Full Scale Fire Testing of Surface Material, Technical Report, SP-RAPP 1986:45, Borås, 1986.
42. Hasemi Y, Tokunaga T, Some experimental aspects of turbulent diffusion flames and buoyant plumes from fire sources against a wall and in a corner of walls, Combustion Science and Technology, Vol 40, pp 1-17, 1984.
43. Patankar S. V., Numerical Heat Transfer and Fluid Flow, Series in computational methods in mechanics and thermal science, Taylor & Francis, ISBN 0-89116-522-3 1980.

44. Jones, W. P., Launder B. E., The Prediction of Laminization with a Two-Equation Model of Turbulence, International Journal of Heat and Mass Transfer, Vol 15, pp 301-314, 1972.
45. Versteeg H. K., Malalasekera W., An Introduction to Computational Fluid Dynamics – The Finite Volume Method, Longman Scientific & Technical, Loughborough, 1995.
46. Rodi W, Turbulence models and their application in hydraulics – A state of the art review, SBF Report 80/T/125, University of Karlsruhe, 1980.
47. Markatos N. C., Malin M. R., Cox G., Mathematical Modelling of Buoyancy-Induced Smoke Flow in Enclosures. International Journal of Heat Mass Transfer, 25, pp 63-75, 1982.
48. Yan Z. Holmstedt G, A two equation model turbulence model and its application to a buoyant diffusion flame, International Journal of Heat and Mass Transfer, Vol 42, pp 1305-1315, 1999.
49. Zhenghua Yan, Smoke Movement and Flame Spread Version 5 (SMAFS), Lund University, Personal communication 2001/2002.
50. Rubini P. A., SOFIE (Simulation Of Fires In Enclosures) Version 3.0, School of Mechanical Engineering, Cranfield University, England, 1999.
51. Knight D., Sakell L., Recent Advances in DNS and LES, Proceedings if the Second AFOSR Conference, New Brunswick, U.S.A., June 7-9, 1999.
52. Gullbrand J., Large Eddy Simulation of Turbulent Flows in Combustor Related Geometries, Doctoral Thesis, Department of Heat and Power Engineering, Lund Institute of Technology, 1999.
53. McGrattan K. B., et al, Fire Dynamics Simulator (Version 2) – User's Guide, National Institute of Standards and Technology, NISTIR 6784, 2001.
54. Smagorinsky J., General Circulation Experiments with the Primitive Equations, Monthly Weather Review, Vol 91, no.3, pp 99-164, 1963.
55. McGrattan K. B., et al., Fire Dynamics Simulator (Version 2) – Technical Reference Guide, National Institute of Standards and Technology, NISTIR 6783, 2001.
56. Wilcox, D. C., Turbulence Modelling in CFD, DCW Industries Inc, 2001.
57. Tannehill J. C., Andersson D. A., Pletcher R. H., Computational Fluid Mechanics and Heat Transfer, 2nd Edition, Taylor and Francis, 1997.
58. Spalding D. B., Genmix – A General Computer Program for Two Dimensional Parabolic Phenomena, Pergamon Press, 1977.
59. Jansson S., Turbulence Modelling of Flows Related to Wall-Cooling Applications, PhD thesis, Dept. Thermo and Fluid Dynamics, Göteborg, 1994.
60. Norris L. H., Reynolds W. C., Turbulent Channel Flow with a Moving Wavy Boundary, Rept No.FM-10, Dept Mech. Eng., Stanford University, 1975.
61. Lam C. K. G., Bremhorst K. A., Modified Form of the k-ε Model for Predicting Wall Turbulence, Journal of Fluids Engineering, 103, pp 456-460, 1981.
62. Duwig C., Studies of Gas Turbines Combustion Chambers: use of new fuels and development of new tools, PhD thesis, Division of Fluid Mechanics, Department of Heat and Power Engineering, Lund, 2003.
63. Spalding D. B., Mixing and Chemical Reaction in Steady Confined Turbulent Flames, Thirteenth Symposium (International) on Combustion, The Combustion Institute, Pittsburgh, PA, pp 649-657, 1971.
64. Magnussen, B.F., The Eddy Dissipation Concept, subtask 3.1.C, Presented at Task Leaders Meeting, Lund, 1995.
65. Chomiak J., Turbulent Reacting Flows, Graduate Course Book, Third Edition, Dept. of Thermo and Fluid Dynamics, Chalmers University of Technology, 2000

66. Lookwood, F.C., Shaw, N.G., Eighteenth Symposium (International) on Combustion, The Combustion Institute, Pittsburgh, 1981, pp 1405-1414.
67. Modak A. T., Radiation from Products of Combustion, FMRC No. OAOE6.BU-6, Technical Report, Factory Mutual Corporation, 1978.
68. Grosshandler W. L., RADCAL: A Narrow Band Model for Radiation Calculations in a Combustion Environment, National Institute of Standards and Technology, NIST Technical Note 1402, 1993.
69. Yan, Z., Numerical Modelling of Turbulent Combustion and Flame Spread, PhD Thesis, Lund University, Lund, 1999.
70. Aksit M.,Mackie P. and Rubini P. A., Coupled Radiative Heat Transfer and Flame Spread Simulation in a Compartment, Fire and Explosions Hazards, Proceedings of the Third International Seminar, pp343-353, Lancashire, 2000.
71. Yan, Z., Holmstedt G., CFD and Experimental Studies of Room Fire Growth on Wall Lining Materials, Fire Safety Journal, 27, pp 201-238, 1996.
72. Yan, Z., Holmstedt G., CFD Simulation of Upward Flame Spread over Fuel Surface, *Fire Safety Science*, Proceedings of the Fifth International Symposium, Melbourne, 1997.
73. Simpson W., TenWolde A., Wood Handbook – Wood as an Engineering Material, Chapter 3, Physical Properties and Moisture Relations of Wood, Forest Products Laboratory, General Technical Report FPL-GTR 113, Wisconsin.
74. Moghtaderi B., Combustion Characteristics of Solid Fuels Under Fire Conditions, PhD thesis, Department of Mechanical and Mechatronic Engineering, The University of Sidney, Australia, 1996.
75. Tien C. L., Lee K. Y., Stretton A. J., Radiation Heat Transfer, The SFPE Handbook of Fire Protection Engineering, Section 1/Chapter 4, 2nd Edition, 1995.
76. Sibulkin M., Heat of Gasification for Pyrolysis of Charring Materials, Fire Safety Science, Proceedings of the First International Symposium, pp 391-400, 1985
77. ISO/FDIS 5660-1, Fire Tests – Reaction to fire – Heat release, smoke production and mass loss rate: Part 1: Heat release (cone calorimeter method), Final Draft
78. Tewarson A., Generation of Heat and Chemical Compounds in Fires, SFPE Handbook of Fire Protection Engineering, 2nd edition, National Fire Protection Association, Quincy, MA, 1995.
79. Hostikka S., McGrattan K., Large Eddy Simulation of Wood Combustion, Proceedings from the 10th Interflam conference, Edinburgh, 2001.
80. Parker W. J., Prediction of the Heat Release Rate of Douglas Fir, Fire Safety Science, Proceedings of the Second International Symposium, pp 337-346.
81. Simo Hostikka, VTT Building and Transport, Personal communication, October 2001.
82. Svenson J., Pettersson J., Kinetics for the Thermal Decomposition of Polymers and Construction Materials, Centre for Combustion Science and Technology, Fourth Seminar, Lund, 2001.
83. Alves S. S., Figueiredo J. L., A Model for Pyrolysis of Wet Wood, Chemical Engineering Science, Vol 44, No 12, pp 2861-2869, 1989.
84. Siau J. F., Transport Processes in Wood, Springer-Verlag, Berlin, 1984.
85. Siegel R., Howell J. R., Thermal Radiation Heat Transfer, Second Edition, McGraw-Hill, ISBN 0-07-057316-6, 1981.
86. Babrauskas V., The Cone Calorimeter, Heat Release in Fires, Editors: Babrauskas V., Grayson S. J., Elsevier Applied Science, ISBN 1-85166-794-6, 1992.
87. Nussbaum R. M., B. A.-L. Östman, Larger Specimens for Determining Rate of Heat Release in the Cone Calorimeter, Fire and Materials, vol. 10, No. 3 & 4, pp 151-160, 1986.

88. Babrauskas V., On the Rate of Heat Release in the Cone Calorimeter, Letter to the Editor, Fire and Materials, vol 11, No. 4, p 204, 1987.
89. Thuresson P., EUREFIC – Cone Calorimeter Test Results, Project 4 of the EUREFIC fire research programme, SP REPORT 1991:24, Swedish National Testing and Research Institute, Fire Technology, 1991.
90. Technical report, CEI IEC 60332-3, Tests on electric cables under fire conditions Part 3: Tests on bunched wires or cables, Second edition, 1992.
91. SBI, Reaction to fire tests for building products - Building products excluding floorings exposed to the thermal attack by a Single Burning Item, EN 13823:2002.
92. Sundström B., van Hees P., Thuresson P., Results and Analysis from Fire Tests of Building Products in ISO 9705, the Room/Corner Test, The SBI Research Programme, SP REPORT 1998:11, Borås.
93. Andersson J, Persson F., Computer supported simulation of pyrolysis – A theoretical and experimental study concerning fire in construction materials, Master thesis, 01-08, Dept Chemical Engineering, Chalmers Lindholmen University College.
94. Göransson U, Omrane A, CECOST flame spread group, Lund, Personal communication, 2003.

Appendix A Parameter analysis of the pyrolysis model by Yan.

Note that in the graphs below all but the two first have the same axis. The incident external heat flux is 75 kW/m^2.

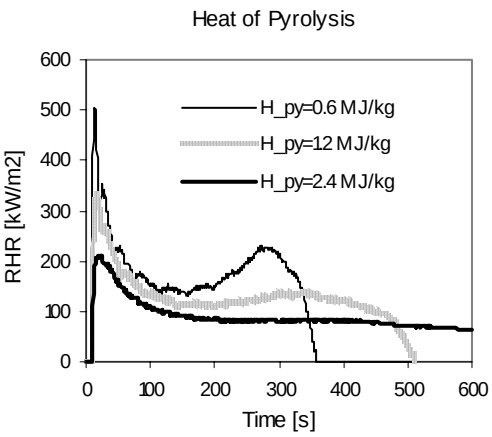

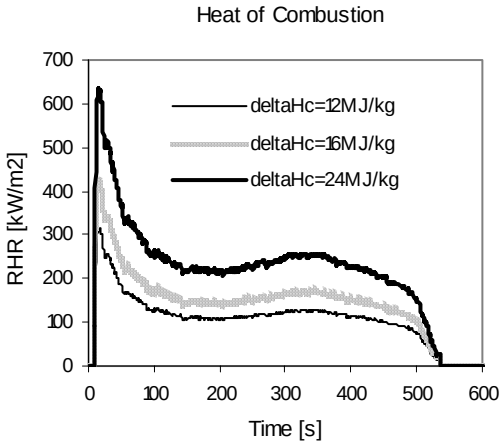

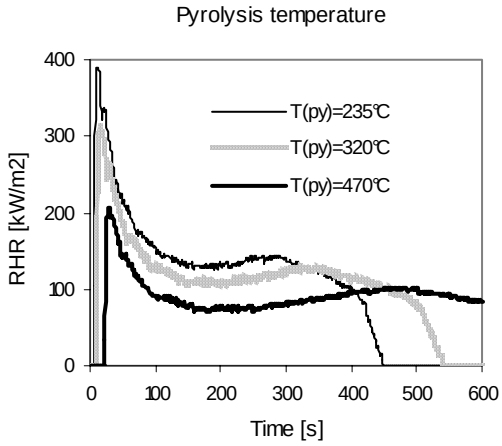

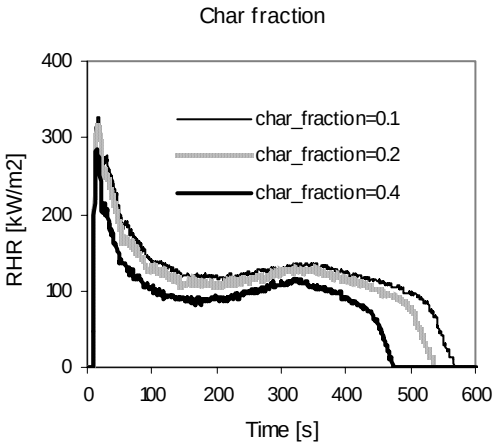

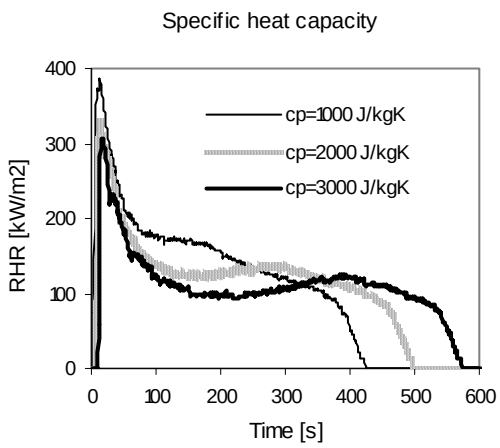

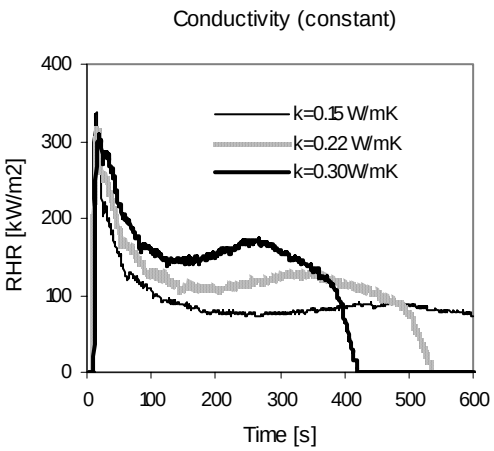

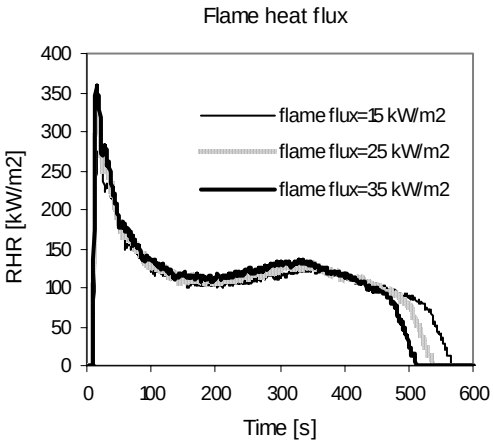
Flame heat flux
RHR [kW/m2]
Time [s]
flame flux=15 kW/m2
flame flux=25 kW/m2
flame flux=35 kW/m2
0
50
100
150
200
250
300
350
400
0
100
200
300
400
500
600

Appendix B Parameter analysis of the pyrolysis model used in FDS.

Note that, in the graphs below, the first one has a different y-axis and the last a different x-axis. The incident external flux is 50 kW/m^2.

Activation energy

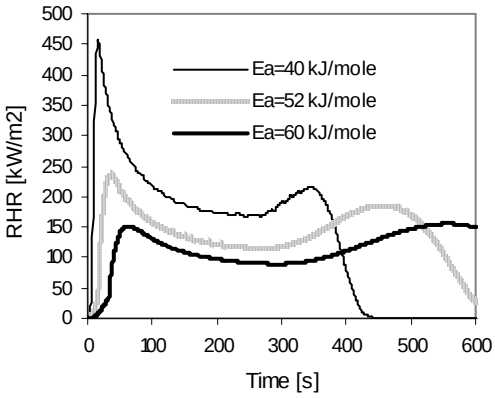

Pre-exponential factor

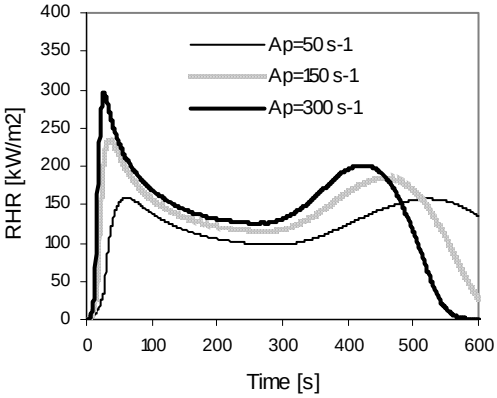

Heat of pyrolysis

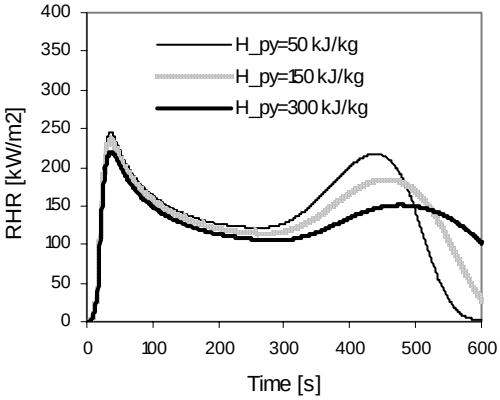

Heat of combustion

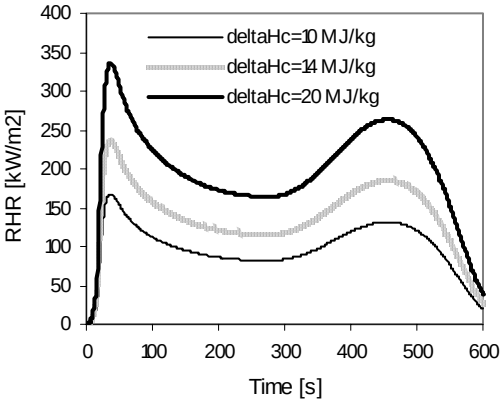

Specific heat capacity (constant)

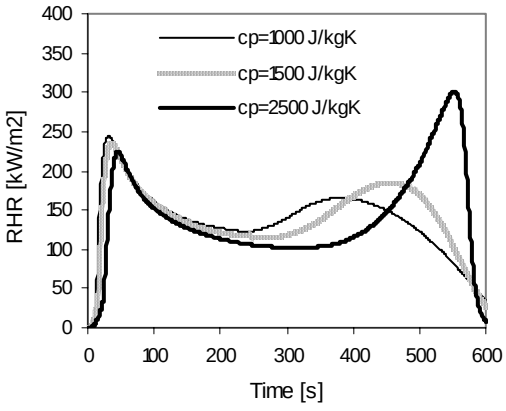

Heat conductivity (constant)

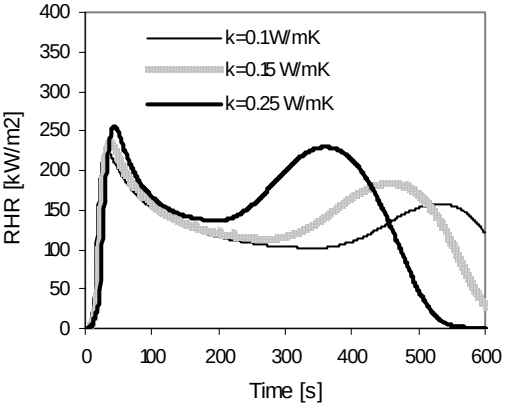

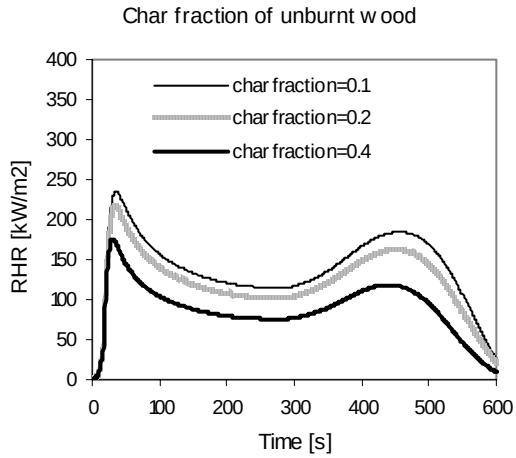
Char fraction of unburnt wood
char fraction=0.1
char fraction=0.2
char fraction=0.4
RHR [kW/m2]
Time [s]
0
50
100
150
200
250
300
350
400
0
100
200
300
400
500
600

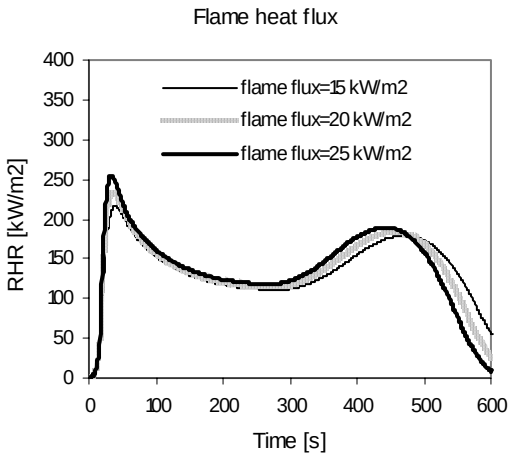
Flame heat flux
flame flux=15 kW/m2
flame flux=20 kW/m2
flame flux=25 kW/m2
RHR [kW/m2]
Time [s]
0
50
100
150
200
250
300
350
400
0
100
200
300
400
500
600

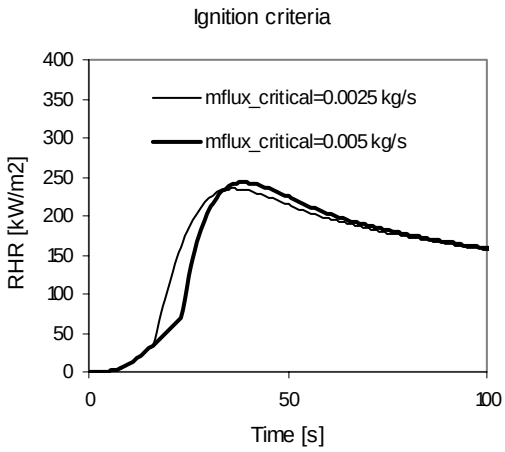
Ignition criteria
mflux_critical=0.0025 kg/s
mflux_critical=0.005 kg/s
RHR [kW/m2]
Time [s]
0
50
100
150
200
250
300
350
400
0
50
100

Appendix C Using transient heating with the Qaccumulative model.

Best fit to Cone Calorimeter data using the Qaccumulative material model as stand-alone solving the heat transfer equation to avoid isothermal boundary condition.

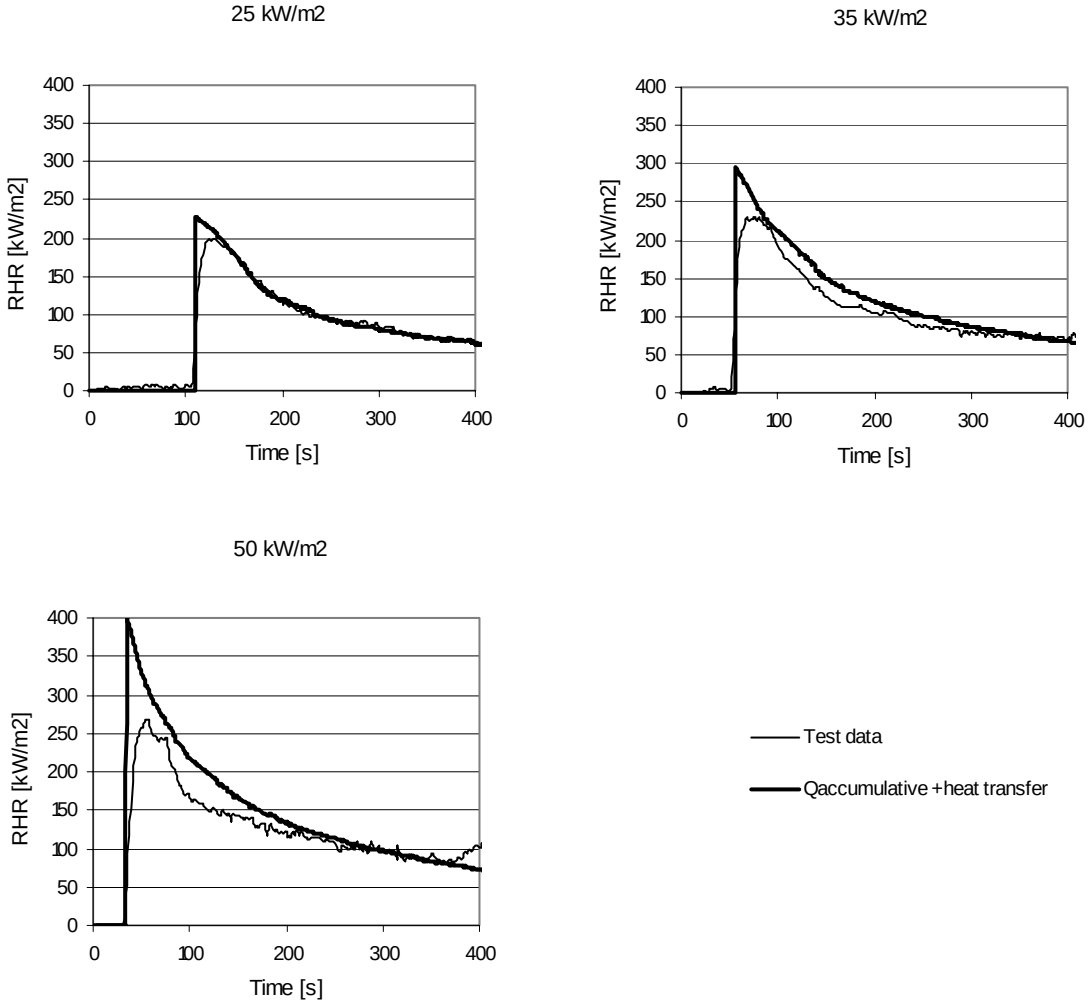

Appendix D Stand alone predictions from the Cone model in Sofie using sample temperature of 593 K.